UNIVERSIDADE DE LISBOA
FACULDADE DE CIÊNCIAS
DEPARTAMENTO DE FÍSICA

Heating of head tissues during TTFields therapy: a computational study

Nichal Gentilal

Mestrado Integrado em Engenharia Biomédica e Biofísica
Perfil em Radiações em Diagnóstico e Terapia

Dissertação orientada por:
Prof. Pedro Cavaleiro Miranda

2018

"If I have seen further than others,
it is by standing upon the shoulders of giants"
Sir Isaac Newton

Acknowledgments

A realização deste trabalho não seria possível sem o apoio de várias pessoas que, de uma maneira ou de outra, de forma direta ou indireta, contribuíram para que me desse uma satisfação enorme fazer este projeto.

Obrigado à minha família, pelo apoio constante, por terem acreditado sempre em mim e pela força que me transmitiram.

Obrigado a todos os que me são próximos, pelos conselhos, pelos momentos de descontração e simplesmente por estarem lá.

Obrigado às minhas colegas de gabinete, pelas ideias partilhadas, pela simpatia com que me receberam e por me ajudarem quando precisava.

Obrigado ao Instituto de Biofísica e Engenharia Biomédica e a todos os que dele fazem parte, por desde o meu primeiro ano de faculdade me permitirem chegar mais longe e mais alto.

Por último, um Grande Obrigado ao meu orientador professor Pedro Cavaleiro Miranda. Por me ter ajudado em cada etapa deste projeto, por me ter dado a liberdade para escolher o passo seguinte e por me apoiar desde o primeiro dia e me motivar a querer ser melhor.

Quando o esforço não recompensava, compensavam-no vocês.

Abstract

Glioblastoma Multiforme (GBM) is one of the deadliest brain diseases that is characterized by a rapid progression and a short survival time. The expected life time is only 15 months with optimal treatment and the current standard of care includes one technique that was first reported 15 years ago, named Tumour Treating Fields (TTFields). This non-invasive approach relies on injecting an alternate current in electrodes placed on the scalp with an optimal frequency of 200 kHz to produce an electric field with a minimal therapeutic intensity of 1 V/cm at the tumour site. A field with these properties was shown in in-vitro studies to have an anti-mitotic effect capable of reducing the growth rate of the tumoural cells. This led to the creation of what is now a Food and Drug Administration (FDA) approved device named Optune®. These fields are applied injecting an alternating current with 900 mA amplitude per array in two perpendicular directions alternately (Left-Right and Anterior-Posterior), with a switching time of one second. Additionally, clinical trials showed that a daily usage of at least 18 hours can significantly enhance treatment outcomes. Apart from skin dermatitis underneath the regions where the electrodes are placed, there are no other major changes reported in the literature that can be considered as side-effects of this technique. However, it is a known fact that biological tissues heating occurs due to the Joule effect. This problem is addressed by shutting down the fields in both directions when a transducer reaches 41^{o}C which consequently leads to GBM not being treated at all. The aim of this project is to study this on/off process and evaluate the thermal damage to the healthy tissues while, at the same time, suggesting ways to improve how Optune® works.

To accomplish these goals, a realistic head model already built by our research group based on Magnetic Resonance Imaging (MRI) data, was used. This model consists of six different biological tissues (scalp, skull, CerebroSpinal Fluid (CSF), grey matter, white matter and eyeballs), the transducers arrays that mimic Optune® and a virtual lesion that intends to represent a GBM. The computational studies were done using COMSOL Multiphysics after performing validation tests to ensure the reliability of its results. This software uses the finite element method to calculate the electric potential and the temperature within each tissue as a function of space and time.

The results obtained show that due to the thermal constraints and under normal conditions, Optune® is only being used to treat the tumour around one-third of the time (6 hours). However, we show that it is possible to increase this time if the room temperature is lowered, if the injected current is controlled at the transducer level instead of at the array level and if just the array that has the electrode that reaches 41^{o}C is shut down instead of both arrays. Additionally, considering a hypothetical situation where Optune® works with half the injected current in each transducer but with both configurations applied simultaneously instead of alternately, we concluded that the device is more time on and might be a good alternative to enhance treatment outcomes. All

the simulations surpassed the thresholds defined by the international agencies for the Specific Absorption Rate (SAR) values for a MRI diagnostic, which was expected considering that the time that the electric fields are applied should be maximized to treat this disease. Additionally, thermal damage evaluated using the Cumulative number of Equivalent Minutes at 43^{o}C (CEM 43^{o}C) showed that only minor and acute changes are expected at the skin level, while the thresholds for the skull, CSF and the eyeballs were not reached for one treatment day. For the brain, some changes such as increased Blood-Brain Barrier (BBB) permeability, a variation of the cerebral blood flow and an alteration of the Gamma-AminoButyric Acid (GABA), glycine and glutamate concentrations may occur.

The conclusions here drawn consider that the metrics chosen can be used in TTFields without any major change to the thresholds from which they were developed for. Although this might not be completely true, the main points here achieved should be seen as a principle of proof that Joule heating in TTFields can be harmful and lead to some changes, especially in the brain, that may lower the quality of life of GBM patients. One important question that remains to be answered is if these results proved to be true, can the benefits of this technique really compensate the side-effects considering the low survival rate? To increase the validaty of these results this data should be compared with what is seen in clinical trials. We hope that these conclusions can be helpful to improve this technique and to increase the awareness of the thermal damage during TTFields therapy.

Keywords: Glioblastoma; Joule heating; Realistic head model; Thermal damage; Tumour Treating Fields;

Resumo

Glioblastoma Multiforme (GBM) é um dos tipos de tumores cerebrais mais malignos e mais comuns em pessoas com idade superior a 65 anos com uma taxa de incidência de 10 em cada 100 000 pessoas. Apesar de ser uma doença idiopática, existem estudos que já conseguiram demonstrar que existe uma relação entre a sua ocorrência e a exposição a radiações ionizantes, enquanto outros fatores como a genética, raça e lesões na cabeça não demonstraram ser percursores para o seu aparecimento. Ao longo do tempo, vários métodos de tratamento foram sugeridos e aplicados sem que no entanto houvesse uma melhoria significativa dos resultados. Atualmente, o tratamento desta doença começa com uma cirurgia de modo a remover o máximo de volume do tumor possível, seguindo-se terapia com radiação e quimioterapia. Esta última pode ser aplicada juntamente com os *Tumour Treating Fields* (TTFields).

Os TTFields consistem na aplicação de um campo elétrico através de elétrodos colocados sobre o escalpe. Estudos *in-vitro* demonstraram que campos com determinadas propriedades capazes de induzir uma magnitude mínima de 1 V/cm no tumor conseguem afetar a mitose das células cancerígenas sem aumentar a toxicidade nas células saudáveis que não se encontram em divisão celular. Esta interferência é explicada por dois fenómenos distintos. Durante a metafase, a polimerização dos filamentos de tubulina leva à formação dos microtúbulos que são responsáveis por separar os cromatídeos-irmãos em direção a polos opostos da célula. O campo elétrico aplicado leva a que as sub-unidades de tubulina se reorientem consoante o campo externo aplicado e consequentemente comprometam a ação dos microtúbulos e a correta divisão celular. O segundo mecanismo ocorre já durante a fase final da divisão, durante a citocinese, quando a célula está prestes a separar-se em duas. Nesta altura, devido à forma da célula e à elevada quantidade de iões e dipolos que esta possui, existe uma acumulação de carga na região de separação das células quando um campo elétrico externo é aplicado levando a que a célula-mãe se rompa e não complete corretamente a divisão celular. Esta técnica já provou também ser mais eficaz quando as células tumorais têm a mesma orientação espacial do campo elétrico externo, o que explica ser vantajoso injetar a corrente em mais que uma direção.

O Optune®, desenvolvido pela Novocure™, é o aparelho aprovado pela *Food and Drug Administration* (FDA, EUA) que é usado para implementar clinicamente esta técnica. A sua utilização consiste na injeção de uma corrente alternada com uma frequência de 200 kHz e 900 mA de amplitude em duas direções perpendiculares (Anterior-Posterior e Esquerda-Direita) de forma alternada, com um período de troca de um segundo, durante cerca de 18 horas por dia, todos os dias. Até agora, o problema mais significativo descrito na literatura derivado de uma utilização tão elevada é dermatite por debaixo do local onde os elétrodos são colocados, sendo esta facilmente ultrapassada com a utilização de corticoesteróides e mudanças periódicas dos transdutores. Não obstante, existem outras limitações desta terapia como por exemplo o aquecimento dos tecidos biológicos da cabeça devido ao efeito de Joule. Para evitar a ocorrência de queimaduras, o Optune® desliga sempre que algum elétrodo atinge os 41ºC. O impacto deste

processo de ligar e desligar leva a que os efeitos do tratamento sejam imprevisíveis uma vez que quando o aparelho se encontra desligado a mitose das células tumorais não é afetada. Assim, o objetivo deste projeto passa por, numa primeira fase, modelar o funcionamento do Optune® e, de forma paralela, sugerir modos de aumentar o tempo de aplicação dos campos elétricos.

Com o intuito de atingir os objetivos propostos foi usado um modelo realista de uma cabeça, previamente desenvolvido pelo nosso grupo de investigação através de imagens de ressonância magnética. Este modelo encontra-se segmentado em diferentes tecidos biológicos que compreendem o escalpe, crânio, líquido cefalorraquidiano (CSF), olhos e substâncias branca e cinzenta. Foi ainda criada uma lesão virtual representativa de um glioblastoma e foram colocados os elétrodos sobre o escalpe de modo a que representassem da forma mais realista possível o Optune®. Todas as simulações computacionais foram feitas usando o software COMSOL Multiphysics após validação dos seus resultados com modelos mais simples. As equações implementadas foram resolvidas com base no método dos elementos finitos que permitem calcular o campo elétrico e a temperatura em cada tecido em função da posição e do tempo.

Os resultados obtidos mostraram que sob condições normais, os TTFields são aplicados apenas durante um terço (6h) do tempo mínimo diário recomendado devido às restrições térmicas. No entanto, foi possível demonstrar que este valor pode ser aumentado se for maximizado o tempo que o doente se encontra em ambientes frios, se se usarem controladores de corrente ao nível dos elétrodos ao invés de ao nível dos *arrays* e se apenas a configuração da qual faz o parte o elétrodo que aquece mais for desligada em vez de ambas as configurações. Foi ainda realizada uma simulação em que metade da corrente era injetada em cada transdutor, mas ambas as configurações funcionavam de forma simultânea em vez de alternada. Os resultados demonstraram um aumento do tempo de aplicação dos campos elétricos e indicaram que esta solução pode melhorar a eficácia do tratamento. Todas as simulações feitas ultrapassam os limites definidos pelas agências internacionais para o *Specific Absorption Rate* (SAR), o que já era esperado uma vez que os campos elétricos são a base do tratamento e consequentemente o seu tempo de aplicação deve ser maximizado. Por outro lado, os valores obtidos para o *Cumulative number of Equivalent Minutes at 43ºC* (CEM 43ºC) considerando um dia de tratamento indicam que o aquecimento poderá causar alterações apenas ao nível do escalpe e do cérebro (matérias branca e cinzenta). Relativamente ao primeiro, são esperados apenas pequenos problemas que podem ser facilmente tratados. As mudanças que mais preocupações podem causar são ao nível do cérebro onde os resultados obtidos indicam que a permeabilidade da barreira cérebro-sangue (BBB) pode aumentar, o fluxo sanguíneo no cérebro pode variar e que é possível que hajam alterações ao nível de neurotransmissores como o ácido gama-aminobutírico (GABA), glicina e glutamato.

Apesar da veracidade destas conclusões ter ainda que ser confirmada com dados experimentais e o seu efeito analisado de forma mais detalhada, estes estudos permitem concluir que o efeito de Joule é significativo nesta terapia, algo que ainda não foi reportado por nenhum outro grupo de investigação. Se estes resultados se confirmarem verdadeiros levantam-se ainda outras questões nomeadamente se o benefício obtido justifica o dano causado tendo em conta a baixa expetativa de vida destes pacientes. Nós esperamos que estes resultados permitam alertar os grupos que trabalham na área dos TTFields que este efeito deve ser tido em conta durante o planeamento e que as sugestões apresentadas possam, de algum modo, ajudar no desenvolvimento desta técnica.

Palavras-chave: Dano térmico; Efeito de Joule; Glioblastoma; Modelo realista da cabeça; *Tumour Treating Fields*;

Contents

List of Figures

List of Tables

List of Abbreviations

AP ..... **A**nterior-**P**osterior

ATV ..... **A**bove-**T**hreshold **V**olume

BBB ..... **B**lood-**B**rain **B**arrier

CEM 43ºC .... **C**umulative number of **E**quivalent **M**inutes at **43ºC**

CSF ..... **C**erebrospinal **F**luid

DoF ..... **D**egrees **o**f **F**reedom

FDA ..... **F**ood and **D**rug **A**dministration

FEA ..... **F**inite **E**lement **A**nalysis

GABA ..... **G**amma-**A**mino**b**utyric **A**cid

GBM ..... **G**lio**b**lastoma **M**ultiforme

GM ..... **G**rey **M**atter

IEC ..... **I**nternational **E**lectrotechnical **C**ommission

LR ..... **L**eft-**R**ight

MRI ..... **M**agnetic **R**esonance **I**maging

MSE ..... **M**ost **S**ignificant **E**lectrode

RMS ..... **R**oot **M**ean **S**quare

SAR ..... **S**pecific **A**bsorption **R**ate

tCS ..... **t**ranscranial **C**urrent **S**timulation

tDCS ..... **t**ranscranial **D**irect **C**urrent **S**timulation

TMS ..... **T**ranscranial **M**agnetic **S**timulation

TTFields ..... **T**umour **T**reating **F**ields

WM ..... **W**hite **M**atter

Motivation and project outline

In general, the people who suffer from Glioblastoma Multiforme do not have a good quality of life and are subjected to different kind of treatments whose side-effects can be very painful, not only for them but also for their relatives that have to go through all this experience without much they can do. Despite all the efforts that have been put into studying a cure for this disease the outcomes have not improved significantly throughout the years and these patients remain with a very low expected survival time.

Thus, it is necessary to study different approaches that can help them or at least try to investigate how to improve their life while being treated. In particular, Tumour Treating Fields is a technique with a lot of potential, despite the fact that it can also have some side-effects that were yet not reported in the literature, namely biological tissue heating. The consequences of this temperature increase are unknown because it can vary depending on several factors, but it has to be studied and very well understood so that the scientific community can find new ways to apply this technique, improve its efficacy and, at the same time, avoid unnecessary aftereffects.

To achieve the desired goals this project was divided in several chapters:

Chapter 1 - Introduction: Includes a brief description of Glioblastoma Multiforme and the current standard of care. It is also described how TTFields work at the cellular level and how they can affect the mitotic process. Finally, a succinct discussion of the tissue heating studies in TTFields is made and an explanation is given on why they can not be considered to be representitive of what really happens.

Chapter 2 - Biological tissue heating: This section is dedicated to describing the main results presented in the literature regarding electric safety and tissue heating using the SAR and CEM 43^{o}C metrics, respectively. The thresholds that might be relevant for TTFields are presented.

Chapter 3 - COMSOL Multiphysics validation: All the simulations here performed are based on the calculations done using this specific software that allows to combine different physics. This chapter discusses how COMSOL works and its main advantages/disadvantages. To get acquainted with it and to have an idea of the deviation of the results it presents comparing with analytical solutions some tests were done that are also described.

Chapter 4 - Methods: This section explains the realistic head model used and how it was created. Additionally, the equations necessary to solve the problems proposed and which simulations were done alongside with their purpose is explained.

Chapter 5 - Results: Shows the main findings for each simulation namely the SAR, CEM 43^{o}C and the temperature of each biological tissue as a function of time. The efficacy in terms of the time that Optune® is on for each case is also discussed.

Chapter 6 - Discussion: Discusses the importance of shutting down the device when the electrode's temperature reaches 41^{o}C, the electric distribution in the brain and in the tumour, how it is possible to improve the efficacy of Optune® and evaluates the damage done by this technique to the healthy tissues. Lastly, some simplifications that were done and how they might have affected the results are discussed alongside with the limitations of this project and future work.

Chapter 7 - Conclusion: Presents a brief conclusion of the main points discussed.

Appendix: This section gathers all the additional information, the abstracts sent to different conferences and the report sent to Novocure™ with the main conclusions of this project.

Chapter 1

Introduction

1.1 Glioblastoma Multiforme

Glioblastoma multiforme (GBM), also known as fourth level astrocytoma according to the World Organization of Health (WHO), is the most common type of primary malignant tumour that appears in the brain in adults, with half of the patients older than 65 years at the time of diagnosis and a global incidence rate of 10 per 100 000 people worldwide [1]. The term astrocytoma is used when cancer has its origin in the astrocytes. These star-shaped glial cells have a very important role in the brain and in the spinal cord such as maintenance of an appropriate ion balance, support to the neurons and to the Blood-Brain Barrier (BBB) cells, communication between neurons and glial cells, among others [2]. A high drop in life quality is expected in people who have this disease, especially because it can appear in different brain regions and is characterized by a rapid progression and a short survival time. The median overall survival is only 3 months without treatment and 14.6 months with optimal treatment [3]. Even for those that glioblastoma was treated, in a vast majority of cases it recurs within 9 months of the initial treatment, with a two year survival rate of only 20% and a five year survival rate less than 5% [3, 4].

Although this disease's aetiology can be related to genetic factors, race and in some cases head injuries [5], there is not enough evidence to prove correlation, and the only known cause is exposure to high ionizing radiation doses. Depending on the size and location of the tumour the initial symptoms vary a lot, but most of them include headaches, personality changes, dizziness, nausea, among others [6]. Throughout time, several methods to treat GBM were studied, but during the last 40 years treatment options have not changed dramatically nor have the survival rates improved significantly [6]. The current standard of care for newly diagnosed patients is first surgery when possible, to remove the gross tumour volume, followed by radiation therapy and chemotherapy using temozolomide (TMZ). Regarding the latter, it can be used alone or combined with Tumour Treating Fields (TTFields). For recurrent cases, additional surgery may be necessary followed by radiation therapy, anti-angiogenic therapy and chemotherapy. If these options do not longer work then TTFields alone can be used [7].

1.2 Tumour Treating Fields

TTFields are a technique that was first reported in 2004 by Kirson et. al [8], where the results obtained after applying an electric field with certain features on cell cultures of mouse melanoma

and rat glioma showed an anti-mitotic effect. These low-intensity (1-3 V/cm) and intermediate-frequency (100-300 kHz) alternating electric fields proved, in the recent years, the capability to affect tumour cell's proliferation without increasing toxicity on non-dividing healthy cells.

One of the major effects of TTFields is the inhibition and/or prolongation of mitosis in dividing cells. Kirson et. al [8] reported a mitosis rate two times slower (124 min vs. 62 min) after applying an electric field with an intensity of 1.0 - 1.4 V/cm, 24 hours after seeding a cell-culture with syngeneic mice tumour cells and for up to 72 hours at 100 kHz. This phenomenon was hypothesized to occur during metaphase when tubulin polymerization controls the proliferation mechanism. It is known that tubulin polymerizes into microtubules which are responsible for pulling apart the two sister-chromatids, formed during interphase, towards opposite sides of the cell by the action of the centrosomes. The applied field will re-align tubulin subunits according to its direction, which can delay and/or prevent the normal polymerization process of the mitotic spindle and consequently compromise normal cell division [9, 10] (figure 1.1a and 1.2).

The second mechanism by means of which TTFields affect cell proliferation was observed in mouse melanoma cultures during cytokinesis, where 25% of the cells undergoing mitosis were destroyed due to the applied electric field as the formation of the cleavage furrow approached complete cell separation [8, 10, 11] (figure 1.1b and 1.2). At this stage due to the cells' hourglass morphology, formed during anaphase and telophase, the non-uniform induced electric field increases the dielectrophoretic forces that are responsible for pushing charged and polar particles towards the cleavage furrow and consequently disrupt the correct cell separation [9].

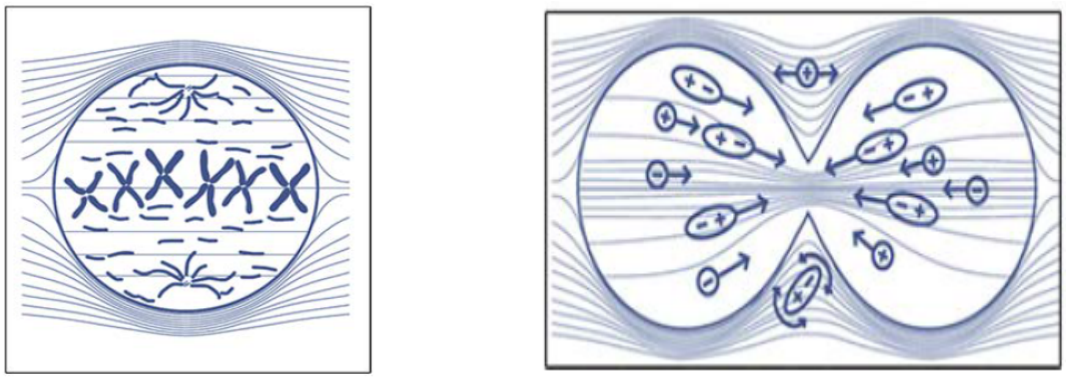

(a) (b)

Figure 1.1: TTFields mechanisms of action: (a) First mechanism: When an electric field is applied tubulin subunits within the cell line up with the field's direction thus compromising the formation of the microtubules; (b) Second mechanism: Cell's shape after anaphase induces a non-uniform and high field at the furrow region. The application of an electric field can pull these molecules to this region thus disrupting the cell's division. Images from [9].

These interferences with cell division can lead to aneuploid or polyploid nuclei and cause genomic instability, leading to cell death or senescence. Although this is the goal when applying this technique to tumour cells, for healthy cells these problems must be taken into consideration. The main role of the mitotic checkpoints is precisely to prevent these cells from keeping on proliferating and, if necessary, repair or destroy them. There are three main checkpoints: one during mitosis (the spindle checkpoint) and two during interphase (G1 at the G1/S transition and G2 at the G2/M transition) (figure 1.2). While the latter two check for cell size, nutrients,

growth factors, DNA damage and replication problems, the spindle checkpoint is responsible for verifying if the chromosomes are well attached to the spindle during metaphase in order to allow a correct separation of the sister-chromatids [12]. In particular, most of the brain cells do not divide themselves when reaching adult age [13] and remain in the G0 phase permanently. Because of this they are not affected by the action of these electric fields. However, brain tumour cells do keep proliferating, thus the advantage of this technique to treat this type of cancer [14].

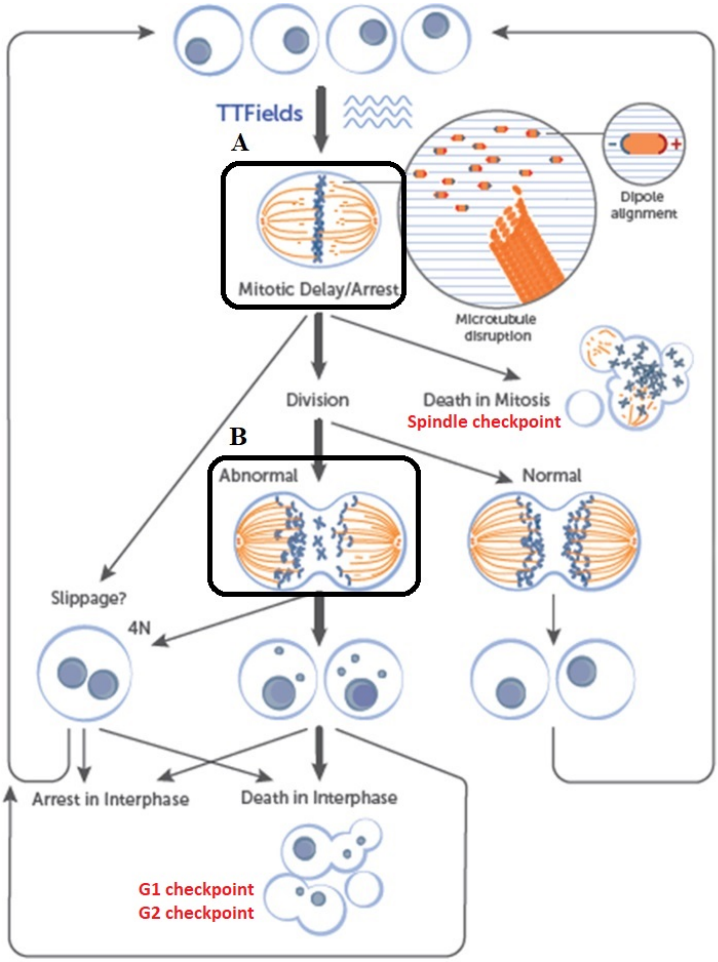

Figure 1.2: TTFields at a cellular level. There are two mechanisms of action of these fields: microtubule disruption and consequent mitotic delay or arrest (A) and cell disruption due to the accumulation of ions and dipoles at the cleavage furrow during cytokinesis (B). There are three checkpoints responsible for checking cell integrity during mitosis (spindle checkpoint) and during interphase (G1 and G2 checkpoints). Adapted from [10].

This technique was approved by the Food and Drug Administration (FDA) to be used in the treatment of GBM patients which had a recurrence (in 2011) and in the treatment of newly diagnosed GBM patients (in 2015) applied jointly with chemotherapy. These fields are applied using an appropriate apparatus named Optune®, formerly known as NovoTTF-100A, and developed by Novocure™ (`http://www.novocure.com`) (figure 1.3). Using a portable device that can be powered by batteries or by plugging into a socket, the current is injected via two sets of arrays placed on the shaved scalp of the patient in two different perpendicular directions alternately. Because a gel is used to make it easier to deliver the desired current, some people with known sensitivity to conductive hydrogels may not be able to use this technique in their treatment. Furthermore, other situations such as an active implanted medical device and pregnancy are

also exclusion criteria, due to the fact that there are not any studies regarding the influence of TTFields in these cases [7].

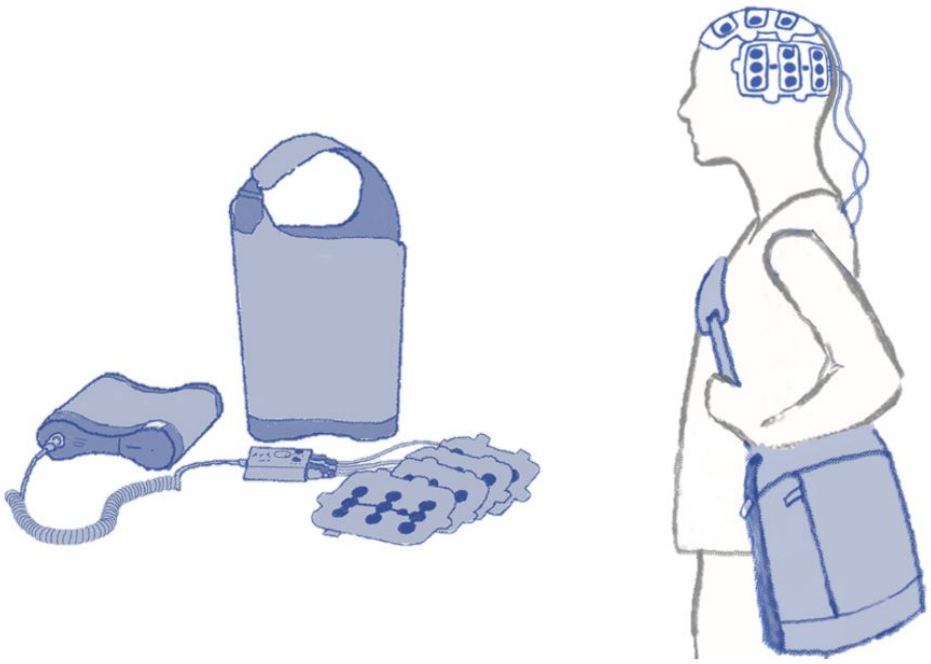

Figure 1.3: Optune® system, where the battery is kept inside the bag and the electric fields are applied through two perpendicular pairs of arrays connected to a generator, also kept inside the bag. Adapted from [7].

Given that TTFields effects are also dependent on the duration, intensity of the applied field and cell's doubling time, it is expected that an increase of the duration of exposure and field intensity, within a certain range, can enhance efficacy for slow dividing cells, as Giladi et. al [10] proved using in-vitro cell cultures. Some important results that helped to improve this technique efficacy were the study of Kirson et. al [15], where the authors concluded that alternately switching the direction of the applied field could enhance the results by 20% compared to the situation where only one direction was used, and the study of Kanner et. al [4] where it was observed that the fraction of dead tumor cells increased with application time of the fields. Currently, a daily usage of at least 18 hours is recommended because it showed significant improvements in clinical trials. Salzberg et. al [16] also reported that at least four weeks of treatment are necessary to see meaningful aftereffects. Up until now, the only side effects reported when using TTFields alone were malaise, muscle twitching and skin ulcers in few cases [7] and skin dermatitis underneath the region where the electrodes are positioned, which can be explained as a combination of factors such as chronic moisture, heat, occlusion of the skin, chemical irritation by constituents of the hydrogel and medical tape [8]. In all studies this problem was readily solved using topical corticosteroids and periodic electrodes changes [16–19]. As mentioned before, in-vitro studies showed significant cell damage when the magnitude of the applied field was at least 1 V/cm in the tumour cells and these results were enhanced for values up to 3 V/cm. However, constantly applying these fields leads to biological tissue temperature increase due to Joule heating. This problem is a known limitation of this technique and, in order to avoid severe burns, especially of the scalp, Optune® shuts down the applied current everytime the electrodes' temperature reaches 41^{o}C [20]. Thereby, the temperature decreases and excessive

heating problems are avoided. However, when these fields are not being applied GBM is also not being treated, which justifies the fact that such a high daily usage compliance is necessary to obtain better results.

1.3 Tissue heating in TTFields

To the author's knowledge, there are no studies that correctly model Optune®'s way of working taking into consideration these thermal limitations apart from the studies of Sun [21] and Castellvi et. al [22]. Regarding the first one, the author did several simplifications which could, most probably, significantly affected the conclusions. First, the model used was a semi-sphere and each tissue was also modelated as a semi-sphere with a specific radius. Secondly, the array configuration does not represent Optune® because it consisted in a set of 19 cooper electrodes (7 in the front, 7 in the middle and 5 in the back, while Optune® consists on four pads of 9 electrodes each as shown in figure 1.3). Also the injected current does not correspond to what is really done with Optune®. Concerning the thermal part, the author considered only conduction as a meaningful heat transfer process neglecting other modes such as convection, blood cooling, metabolic heat and evaporation. Not surprisingly, the results obtained indicate a maximum temperature increase in the scalp of 0.5 ^{o}C/s which Sun [21] considered too small to be harmful, without any proper explanation for such conclusions. On the other hand, the study of Castellvi et. al [22] considers a system that is far from representing Optune®, while all tissues were represented as cylinders. Although almost all the thermal exchanges modes were considered, there are some others assumptions that may have played an important role in the results obtained by the authors, which indicate that tissues temperature can increase up to 0.5^{o}C, but tumour's temperature increase is not high enough to attribute this technique efficacy to heat as it happens in hyperthermia. Despite the fact that these conclusions could be debatable regarding their reliability, this latter conclusion is an interesting topic to be tested and discussed.

Chapter 2

Biological tissue heating

Biological tissue heating has been a subject of study for a long time. In some cases, such as hyperthermia and ablation techniques, it is desirable to increase the temperature in the tumoural tissue while not increasing it by a large amount in healthy cells. This can be done in a handful of different ways that are dependent on the tumour location and extension, but that include increasing blood perfusion, using microwave, ultrasound, laser or radiofrequencies, among others [23, 24]. Although hyperthermia can be divided in local, regional or whole-body and the side effects can vary depending on the parameters mentioned before, in general, the main problems related to this technique include burns, nausea, vomiting and diarrhea. On the other hand, there are techniques like Magnetic Resonance Imaging (MRI), Transcranial Magnetic Stimulation (TMS) or transcranial Direct-Current Stimulation (tDCS) where excessive tissue heating is not desirable and should be controlled. For the latter two, several studies showed no significant tissue heating with a maximum increase reported to be less than 10^{-6} ºC [25–27]. As for MRI, tissue heating depends on the frequencies used, repetition time, type of coils, shape of the anatomical region exposed to the fields, along with other factors [28]. For this technique, it is not possible to directly measure the temperature increase due to the applied pulses and as so other quantities that indirectly give information about the energy absorbed by the body have been used in the literature and guidelines limiting the threshold for this quantity have been developed. There are some studies that showed that when performing the diagnosis, this technique can lead to a higher energy absorption in some tissues and to hotspots with values that surpass the thresholds defined by the international agencies. The consequences are still under investigation [29].

2.1 Metrics

The most used quantity in hyperthermia to evaluate thermal damage is the Cumulative number of Equivalent Minutes at 43ºC (CEM 43ºC). Defined by Sapareto and Dewey [30] for the purpose of having a way to convert exposure times at different temperatures to a unique time at 43ºC, the mathematical description of this expression is given by:

$$\text{CEM } 43 \text{ °C} = \sum_{i=1}^{n} t_i \cdot R(T)^{43-T_i} \tag{2.1}$$

Where t_i (min) is the $i-th$ time interval, n the total number of time intervals, T_i (ºC) the mean temperature in that period of time and R is a constant related to the thermotolerance

acquired by the cells when heated. This phenomenom was first investigated in in-vitro studies using human cells cultures and its value is temperature dependent:

$$R(T) = \begin{cases} 0.25 \Leftarrow T \leq 43°C \\ 0.50 \Leftarrow T > 43°C \end{cases} \tag{2.2}$$

The choice of 43ºC as the reference temperature has to do with the variation of cell death with the temperature seen in the Arrhenius plots where a slope change was observed at this value (figure 2.1).

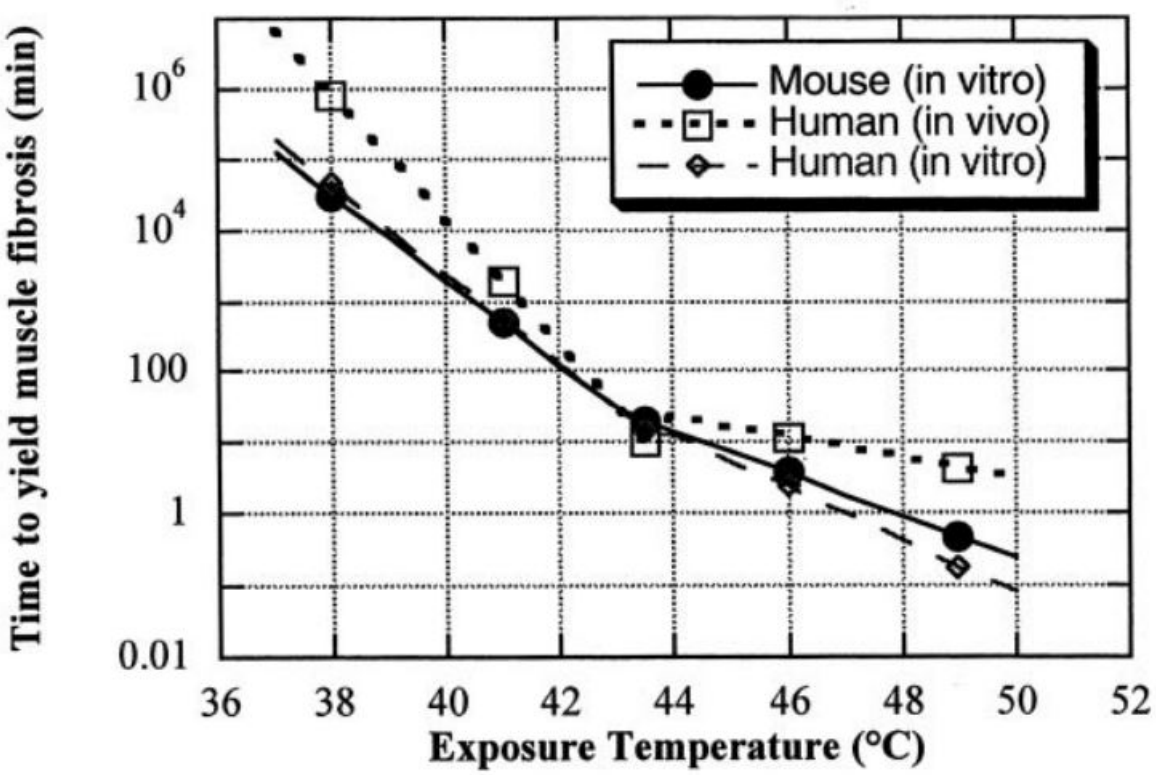

Figure 2.1: Necessary time to achieve muscle fibrosis for mouse (in-vitro) and human (in-vivo and in-vitro) cell cultures. A slope change is seen for an exposure temperature around 43ºC due to the thermotolerance acquired by the cells. Image from [31].

In techniques such as MRI other metrics were developed based on the values obtained through computational simulations. The Specific Absorption Ratio (SAR) is the most used quantity for this technique and is defined as:

$$SAR = \frac{\sigma |\boldsymbol{E}|^2}{\rho} \tag{2.3}$$

Where σ is the electrical conductivity (S/m), $\boldsymbol{E}$ is the electric field (V/m) and ρ (kg/m^3) is the density. The units of SAR are therefore W/kg. Usually, absorption within 1 g or 10 g of tissue are also reported because they can give information about the existence of hotspots. For

frequencies higher than 10 GHz, however, SAR is not considered to be a good measurement because the depth of penetration is much smaller and almost all the energy is absorbed at the skin level.

For TTFields there are not any reliable heating studies reported in the literature and consequently there is not any specific metric to measure the temperature increase. However, SAR can be used to quantify heating due to the applied electric fields and the obtained results can be compared to those defined by international agencies. On the other hand, CEM 43^{o}C might be a suitable metric to evaluate thermal damage as a net effect of all the contributions to the temperature variation which include the electric field itself, metabolism, blood heating/cooling, conduction and convection, despite the fact that there is not any entity that has defined guidelines regarding this matter. It is important to bear in mind that both these quantities have limitations and the thresholds discussed in this next section may not be applicable to other techniques besides those for which they were developed for as it will be discussed later. The use of these metrics may raise questions about the side effects of TTFields that are not discussed elsewhere.

2.2 Important results for TTFields

In a first stage, the important thresholds for TTFields regarding SAR and CEM 43^{o}C levels are only for the head. If these limits are largely surpassed an extensive analysis concerning the rest of the human body should be done to evaluate its consequences.

2.2.1 SAR limits

International agencies have created guidelines in regards to the SAR values for MRI treatments to prevent excessive heating due to the electromagnetic pulses used to flip proton spins. Regarding head limits, the FDA defines in their guidelines "Criteria for Significant Risk Investigations of Magnetic Resonance Diagnostic Devices" a maximum SAR value of 3.2 W/kg averaged over the head and for a time period of 10 minutes. Alternatively, a maximum average head temperature of 38^{o}C can also be used as a limit. On the other hand, the International Electrotechnical Commission (IEC) considers in the "2010 60601-2-33" guidelines two different thresholds, one for normal operating mode (10 W/kg) and one for the first level controlled mode (20 W/kg). The first should be used when no physiologic stress is expected by the patient and the second when patients might experience some stress due to age, over-weight, etc. Both these values are averaged over any 10 grams of head tissue and for a duration of 6 minutes. These quantities are summarised in table 2.1.

Table 2.1: Head SAR limits for local exposure defined by different agencies.

FDA	IEC
3.2 W/kg Averaged over the head Averaged over 10 minutes OR Temperature no greater than 38^{o}C	10 or 20 W/kg Averaged over any 10 grams Averaged over 6 minutes

2.2.2 CEM 43^{o}C thresholds

Dewhirst et. al [31] and Yarmolenko et. al [32] performed an extensive literature review regarding thermal damage thresholds in hyperthermia treatments using radiofrequencies (the first reviewed 109 papers while the second analysed 152). Information concerning organs that can be compromised due to TTFields were withdrawn from these papers and are presented in table 2.2. Because it is much easier to make this type of studies in animals rather than in humans, in almost all the papers analysed experiments were performed in rats, rabbits or dogs (original papers used by the authors are not here referenced, but can be easily found in [31, 32]). Consequently, it is important to bear in mind that these results may differ a lot for humans and they are also highly dependent on many other key aspects such as different heating regimes (longer exposure at lower temperatures compared to shorter exposure at higher temperatures), anaesthesia used and when the results were registered, for example. Not surprisingly, different authors do not report the same threshold values for CEM 43°C at which an isoeffect was observed. Additionally, the fact that most papers just report acute changes (tissue evaluated 0-30 days after exposure) rather than chronic effects (tissue evaluated >30 days after tissue exposure) also limits the validity of the results here presented.

In the case of TTFields the scalp is one of the tissues that can heat the most. For the skin, it was seen that for low values of CEM 43^{o}C only minor and acute changes occurred like superficial burns which could be easily treated. As this value increased burn damage also augmented reaching dangerous skin damage for values higher than 20 minutes. Other studies also showed significant erythema for CEM 43^{o}C values as high as 112 minutes and variations at a functional level. This latter included an increase of the thresholds for cold and warm detection, while heat and mechanical pain thresholds decreased returning to their basal state after four hours. Complete skin necrosis occurred for values higher than 288 minutes and up to 1.5×10^{4} minutes.

After passing the scalp, the injected current goes to the skull. Regarding bone, only one study reported changes. Resorption was observed at three different CEM 43^{o}C values: 16, 80 and 128 minutes. This is a natural process that occurs in the human body to control the calcium blood levels, but also to maintain and remodel bone structure and integrity. This phenomenon occurs due to the action of the osteoclasts and is compensated by the action of osteoblasts that create bone tissue. Studies with rabbits showed, however, that heat can induce irreversible bone resorption for CEM 43^{o}C values as low as 16 minutes with the percentage of damage being increased for higher exposure times.

There are several studies that investigated the impact of heat in the brain at a vascular and functional levels as well as in cell death. Although the thresholds vary between studies all of them showed an increase of the BBB permeability for CEM 43^{o}C values as low as 0.03 minutes. The main function of the BBB is to control the components that pass from the systemic circulation to the brain and thereby prevent the entrance of any molecule or bacteria that can be harmful. An increase of its permeability occurs under certain conditions like inflammation, injuries or stroke and can be very dangerous if not controlled right away. However, sometimes it is also desirable to increase it to facilitate drug delivery in certain treatments.

Not so consistent results were found for the cerebral blood flow. Two studies showed an increase for 0.03 and 16 CEM 43^{o}C while two other papers reported a decrease for 1 and 34 CEM 43^{o}C. Despite the fact that there are not compatible results it is important to note that

cerebral blood flow does change during heating. This should be carefully supervised because a very low flux can lead to ischemia while a very high flux can lead to a dangerous intracranial pressure [33]. Concerning cell death a maximum value was observed for values around 2 CEM 43ºC in brain cells, nerves and glial cells. It is noteworthy that similar situations in humans can be very harmful because most brain cells do not divide themselves at adult age.

Heating also changed metabolic effects in the brain: the levels of Gamma-AminoButyric Acid (GABA), glutamate and glycine increased for 0.115 CEM 43ºC, but decreased for values above 1.29 CEM 43ºC. GABA is the major inhibitory neurotransmitter in the Central Nervous System (CNS) and has the capability of reducing neuronal excitability by binding to specific transmembrane receptors which lead to cell hyperpolarization. A deficiency of GABA can lead to insomnia, depression, hypertension, panic disorders, low growth of hormone levels, convulsions, amid other problems, while high levels of GABA are related to tiredness and affect cognitive thinking. Glutamate is the major excitatory neurotransmitter in the brain and is related to cognitive function, memory, learning, as well as other functions. While low levels of this neurotransmitter have been associated with some diseases such as autism, high levels of glutamate are related to other brain diseases, cognitive impairments and brain motor malfunction. Furthermore, traumatic brain injuries where an increase of the BBB permeability was seen led to more glutamate entering the brain, thus increasing brain damage [34]. Glycine is an inhibitory transmitter of the spinal cord and it participates in the processing of motor and sensory information. Changes related with an increase of glycine concentration can lead to anxiousness, low mood, stress and immune issues.

Finally, changes in metabolism were also observed is some studies. Some of them include an increased activity of Lactate DeHydrogenase (LDH) and Succinate DeHydrogenase (SDH) as well as in RiboNucleic Acid (RNA) content in three different clusters of cells in the hypothalamus: supraoptic nucleus (that produces some of the most important neuropeptide hormones), paraventricular nucleus (that has an important role in the regulation of some autonomic functions) and median preoptic nucleus (involved in thermoregulation). It was seen that, for 1.07 CEM 43ºC, metabolism had increased at least 20 times compared to the basal values, with lactate being the one whose levels most augmented, reaching levels 35 times higher in average. Regarding the levels of lactate, pyruvate, glutamate and glycerol, another study showed an increase of these levels in the brain for increasing CEM 43ºC. The choice to evaluate these specific metabolites was not random as knowing their concentration in the extracellular compartment of the brain might be important in oncology. In the study of Roslin et. al [35] higher glutamate levels were observed in necrotic tumours than in non-necrotic ones, although there is still no satisfying justification for this fact. Glycerol levels were also higher in patients with necrotic tumours which can be explained due to the degradation of cell-membrane glycerophospholipids. Because some tumours do not have enough oxygen to suppress their needs, they use glycolysis rather than respiration to obtain energy which explains why pyruvate and lactate also had a higher concentration. The fact that an increase of these components was observed with increasing CEM 43ºC suggests that for long time exposures to hyperthermia tumour cells oxygenation is compromised, as expected.

Still in regards to the brain, Matsumi et. al [36] performed a histological evaluation of the monkeys' brain after exposing it to heat at different temperatures for a time period of 60 minutes. Their results showed the existence of an oedema in the white matter and atrophied neurons as well as coagulative necrosis of brain cells for a temperature of 44ºC or higher (>30 CEM 43ºC). This brain oedema can be related with a BBB disregulation and can lead to an

increase intracranial pressure as the authors concluded.

Between the skull and the brain there is CSF. There are not many studies regarding thermal damage to this structure, but the paper of Frosini [37] showed that if the rabbit body is subjected to heat stress at 0.78 CEM 43^{o}C CSF levels of GABA and taurine increase significantly compared to the basal levels to protect neurons and to decrease body temperature. As described by the author, some studies found that taurine and GABA can induce hypothermia through different mechanisms like vasodilation which can be a possible explanation for these observations. On the other hand, there are other neurotransmitters such as aspartate and glutamate, whose action can lead to heat production, that did not increase their concentration in this study. In the case of ions it was seen that sodium, magnesium and potassium concentrations did not change significantly but calcium's did. This can be explained by the fact that calcium also plays a role in down-regulating the human body temperature.

Lastly, regarding the eyes, CEM 43^{o}C levels of 0.026 minutes caused no damage to the cornea of rabbits, while at 21.3 minutes some relevant effects such as epithelial cell oedema and collagen disorganisation were seen. Necrosis of the cornea cells was observed at 2.2×10^4 minutes seven days after treatment. However, some beneficial outcomes were seen for 0.313 CEM 43^{o}C namely near vision improvement. Concerning the retina, no thermal damage to the rabbit eye was reported for values between 0.02 and 1.5 minutes while for values as high as 926.2 minutes only acute lesions were seen.

Table 2.2: Thermal thresholds defined in terms of CEM 43^{o}C. Data withdrawn from [31, 32, 36, 37].

Tissue	Change	CEM 43^{o}C (min)	Species
Skin	Acute and minor changes	0 - 20	Mouse
	Erythema and functional changes	112	Human
	Necrosis	288 - 15 000	Human
Bone	Resorption	16 - 128	Rabbit
Brain	BBB permeability	0.03 - 1.3	Rats
	Cerebral blood flow	0.03 and 16 (increase)	Humans Rats
		1 and 34 (decrease)	Rabbits Rats
	GABA, glycine and glutamate levels	0.115 and 1.29	Rats
	Metabolism	1.07	Rats
	CNS damage	2	Rats
	Coagulative necrosis, oedema and atrophied neurons	30	Monkey
CSF	Taurine, GABA and ion levels	0.78	Rabbit
Eye	No damage to the eye	0.02 - 1.5	Rabbit
	Near vision improvement	0.313	Rabbit
	Cornea epithelial cells oedema and collagen disorganisation	21.3	Rabbit
	Retina acute lesions	926.2	Rabbit
	Cornea cell's necrosis	22 000	Rabbit

Chapter 3

COMSOL Multiphysics validation

As seen in the last chapter most of the heat studies were performed in non human subjects not only due to safety matters but also because of all the ethical problems related with these experiments. In order to obtain more reliable results for the human case, computational models have been widely used in several fields because they allow to simulate in an easy way different systems which we cannot test experimentally such as diseases spreading or a certain treatment outcome. The advances of the last years in computation hardware allowed to use more realistic models and at the same time decrease solution's errors and simulation time and computational simulations are now considered to be the third pillar of science methodology along with theory and experiment [38].

The use of computational models has to guarantee that certain key aspects are accomplished before using the results to compare with what is seen experimentally, in-vitro or in-vivo. The verification and validation of the model can be done in three different stages [39] and they have to ensure that: 1) the mathematical equations used to implement the model and the processes of study are correctly implemented; 2) the model represents accurately the problem in hands and 3) it is necessary to know the errors and uncertainties of the results obtained. These errors can be classified as numerical or modelling errors [39]. The first group is a consequence of using computational techniques (e.g.: Newton-Raphson, Euler, Runge-Kutta, etc) to solve mathematical equations which implies discretization, incomplete grid convergence and rounding errors. The second group is related to assumptions and approximations in the mathematical representation of the physical problem, which are a consequence of the geometry of the model, boundary conditions used, unknown material properties, among others.

COMSOL Multiphysics (`http://www.comsol.com`) is a computational tool that through Finite-Element Analysis (FEA) solves Partial Differential Equations (PDE) and allows to combine different physics problems (e.g.: heating due to the Joule effect) and study their main aspects. The main idea of FEA is instead of trying to solve the problem by applying the physical equations to all the geometry in hands, a mesh is created. This mesh is constituted by a variable amount of small elements with different shapes. These elements are connected by nodes, in which the boundary conditions are applied, the problem solved and the final solution obtained. Additionally, it is also possible to obtain the solution in intermediate points through interpolation. All of these features allow to change a continuous domain to a discrete one. Regarding the elements, there are three important parameters used to characterize them: shape, size and quantity [40]. At the nodes the variables of interested, the Degrees of Freedom (DoF), are calculated and the

amount of DoF is directly related with the time that it is necessary to run the simulation.

COMSOL is the software used throughout this project. In order to get acquainted with it and to understand how it works, its main features, advantages and disadvantages several different studies were made. Additionally, these tests were also used to evaluate numerical and modelling errors. In order to accomplish these tasks, COMSOL v.4.3b and Matlab 2017b (`https://www.mathworks.com`) were used.

3.1 Validation tests

When it comes to comparing analytical and COMSOL results, there are some factors that are important to bear in mind: it is easier to compare the results when the geometry tested is simple (like a sphere or a parallelepiped) rather than complex (e.g.: a realistic head model) because there are analytical expressions only for the first one. Very often, steady-state solutions are also easier to work with and to compute instead of time-transient solutions due to computation time and memory that are necessary to run and store these solutions. One of the best ways to do this comparison for this project is using the electric and heat transfer equations. Regarding the first, there are some papers in the literature that already validated the solutions (e.g.: [41]), while for the latter the equations for conduction, convection and radiation processes can be used to achieve the desired goal.

Conduction can be defined as the energy transfer that occurs from a more energetic body to a less energetic one due to the diffusion of energy caused by the random molecular motion. Its equation can be described as:

$$\boldsymbol{F} = -kA\nabla T(\boldsymbol{r}, t) \tag{3.1}$$

Where $\boldsymbol{F}$ (SI units: W) is a uniform flux perpendicular to an area A (m^2), T (K) is the temperature and k is the thermal conductivity (W/(m·K)).

Convection, on the other hand, occurs when a fluid in motion and a bounding surface are close to each other and at two different temperatures thus exchanging heat. The equation that describes this process is given by:

$$\boldsymbol{F} = hA(T_s(\boldsymbol{r}, t) - T_\infty) \tag{3.2}$$

Where F and A are defined as in equation (3.1), h (W/(m^2· K)) is the convection heat transfer coefficient, T_s (K) and T_∞ (K) are the surface and fluid temperatures respectively.

Lastly, radiation is defined as the energy emitted by a body that is at a nonzero temperature and is represented by:

$$\boldsymbol{F} = \epsilon\sigma A(T_s^4(\boldsymbol{r}, t) - T_{sur}^4) \tag{3.3}$$

F and A are defined as before, ϵ is the emissivity (unitless), σ is the Stefan-Boltzmann constant (5.67×10^{-8} W · m^{-2} · K^{-4}) and T_s (K) and T_{sur} (K) are the body and surrounding temperatures accordingly.

As a starting point and due to the simplicity of these expressions, a comparison was made

between the analytical and computational solutions (using matlab and COMSOL respectively) when implementing these equations in order to get an idea of the deviation of the results given by COMSOL for simple heat processes. The geometries that were used are presented in figure 3.1. Whether it was a sphere or a parallelepiped, the material thermal parameters were chosen to match those of the scalp:

$$\begin{aligned} \text{Density } (\rho) &= 1000 \quad \text{kg/m}^3 \\ \text{Thermal conductivity (k)} &= 0.34 \quad \text{W/(m} \cdot \text{K)} \\ \text{Heat capacity at constant pressure } (c_p) &= 3150 \quad \text{J/(kg} \cdot \text{K)} \end{aligned}$$

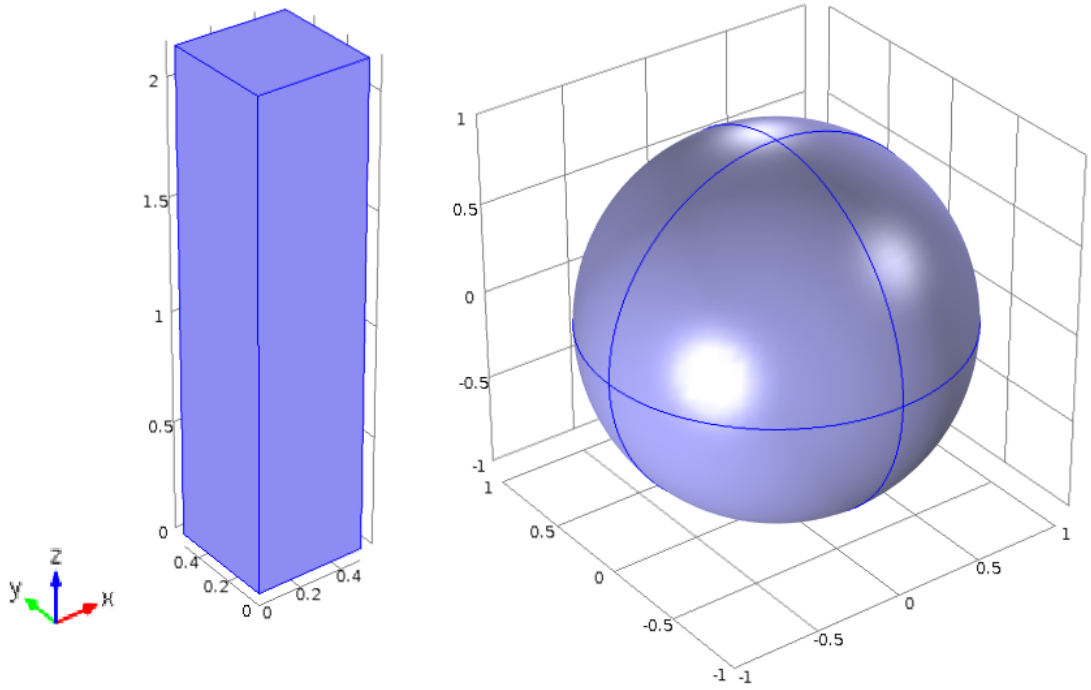

Figure 3.1: Simple geometries used. Left: Quadrangular parallelepiped with dimensions (0.5 × 0.5 × 2.15) m. Right: Sphere with 1 m radius.

For a steady-state situation and if a uniform flux is applied at one side of the quadrangular parallelepiped in the z-direction, equation (3.1) can be simplified with the temperature changing linearly in this direction. Thus for a given thermal conductivity and heat flux and knowing the temperature at one end of the parallelepiped it is possible to calculate the temperature for each value of z and compare the results obtained analytically and using computational methods (Test 1) (figure 3.2).

For this problem the solution to equation (3.1) is:

$$T(z) = T_1 + \frac{F \cdot z}{k \cdot A} \tag{3.4}$$

The following arbitrary values were chosen:

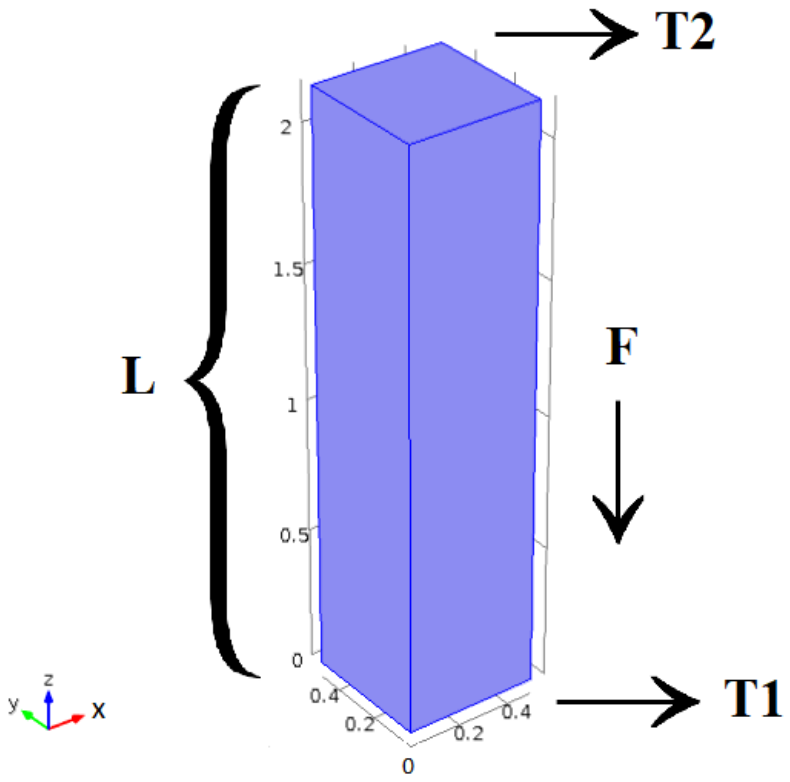

Figure 3.2: Initial conditions for Test 1. F represents the flux which is directed from one face of the parallelepiped, that is at a temperature T_2, towards the opposite side at a temperature T_1. Both sides are separated by a distance L.

$$\text{Flux } (F) = 500 \quad \text{W}$$
$$\text{Temperature at the cooldest side } (T_1) = 400 \quad \text{K}$$

Surface temperature obtained using COMSOL is presented at figure 3.3. Deviations from the analytical solution were measured using the Root Mean Square (RMS) quantity, defined as:

$$RMS = \sqrt{\frac{1}{N}\sum_{i=1}^{N}(T^i_{analytical} - T^i_{computational})^2} \tag{3.5}$$

Where the index i represents a spatial point and N the total number of points, which was the same for COMSOL and matlab. The RMS for three different mesh sizes (coarse, normal, fine) is summarised in table 3.1 (Test 1, page 23).

As mentioned before, the former problem was for a steady-state condition. For time-dependent problems, time must also be taken into consideration. For the same geometry but now considering that the parallelepiped is at a temperature T_1 and only one face is at temperature T_2 and no heat flux is applied, it is possible to study the temperature variation across space and time until it reaches a steady-state solution, which will be the same as the former problem if the temperatures T_1 and T_2 are set to be 400 K and 3543.3 K, respectively. To have an equation

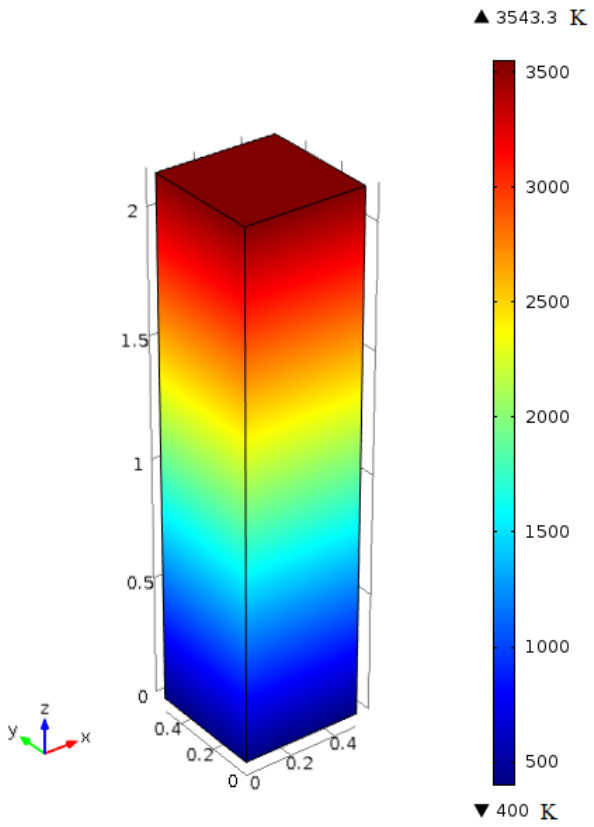

Figure 3.3: Results obtained using COMSOL for the steady-state conduction process validation test (Test 1) for a normal mesh size. A flux is directed from the hotter face towards the colder. The temperature varies linearly with z, as expected.

for this problem it is necessary to start with the wave equation for heat:

$$\frac{\partial T(\boldsymbol{r},t)}{\partial t} - \alpha \nabla^2 T(\boldsymbol{r},t) = 0 \tag{3.6}$$

Where T is the temperature, t is the time (s) and α (m^2/s) is the thermal diffusivity defined as:

$$\alpha = \frac{k}{\rho \cdot c_p} \tag{3.7}$$

In this expression, k represents the thermal conductivity, ρ the density and c_p the specific heat transfer. For the aforementioned problem, equation (3.6) can be solved using the variable separation technique and applying the initial conditions, which leads to:

$$T(z,t) = T_1 + \frac{(T_2 - T_1)}{L} z + \sum_{n=1}^{\infty} B_n \sin\Big(\frac{n\pi z}{L}\Big) exp\Big[-\frac{1}{\tau}\Big(\frac{n\pi}{L}\Big)^2 t\Big] \tag{3.8}$$

Where:

$$\tau = \frac{1}{\alpha} = \frac{\rho \cdot c_p}{k} \tag{3.9}$$

$$B_n = \frac{2}{L}\int_0^L (T_i(z,0) - T_{st}(z)) \sin\Big(\frac{n\pi z}{L}\Big) dz \tag{3.10}$$

T_{st} and T_i are the steady-state and initial temperature fields, given by:

$$T_{st}(z) = \frac{T_2 - T_1}{L} z + T_1 \tag{3.11}$$

$$T_i(z,0) = \begin{cases} T_2 \Leftarrow z = L \\ T_1 \Leftarrow 0 \leq z < L \end{cases} \tag{3.12}$$

These equations were first implemented in matlab and then in COMSOL (Test 2). Because there is an infinite summation in expression (3.8) it was necessary to know at which value this series should be truncated. In order to do that, a loop cycle with an increasing truncation value was implemented. The impact of this term on the final solution was evaluated by doing a mean relative difference between temperature fields of two consecutive solutions. The other chosen parameters were:

$$\text{Spatial discretization (dx)} = L/50 \quad m$$
$$\text{Time discretization (dt)} = 5 \times 10^4 \quad s$$

The integral in the expression (3.10) was evaluated using the *integral* function of matlab which uses the global adaptive quadrature method to calculate it. The absolute and relative tolerances were chosen to be 10^{-10} and 10^{-6} respectively. For the summation, it was assumed that n=∞ could be approximated by the value from which the difference between two consecutive solutions was not higher than 1%, which corresponded to n = 6. Due to the discontinuity in T_i at x=L for t=0, matlab has an oscillatory behaviour for the first five times (figure 3.4) and because of that these lines were not considered in the comparison with the COMSOL results.

A comparison of the COMSOL results was performed for the same initial conditions and time and spatial steps, as well as for the the same mesh qualities as before, using the RMS quantity (table 3.1, Test 2, page 23).

For convection processes, heat flux can be described by equation (3.2). If this heating mechanism is the only one present in the system, the temperature will be uniform throughout the volume (see next paragraph) and the increase in the energy of the body during a time dt can be written as:

$$-hA(T(t) - T_\infty)dt = mc_p dT \tag{3.13}$$

Where the variables nomenclature is the same as used before. This equation can be solved to:

$$\frac{T(t) - T_\infty}{T_i - T_\infty} = e^{-\tau t} \tag{3.14}$$

With:

$$\tau = \frac{hA}{\rho V c_p} \tag{3.15}$$

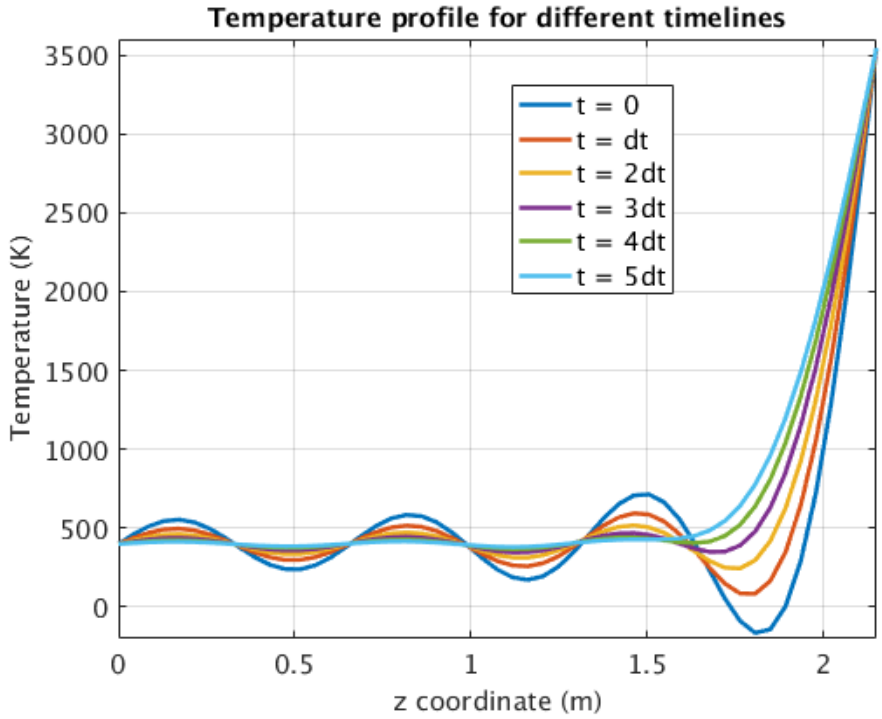

Figure 3.4: The oscillatory behaviour of the temperature profile for the first five times due to to the step function of $T_i(z)$ using matlab. From t=0 to t = 4dt (where dt = 4×10^4 s) the function has a harmonical behaviour and so only times starting at 5dt were considered for comparison with COMSOL results.

A is the surface area (m^2) and V the solid's volume (m^3). These equations are only valid when it is assumed that the temperature distribution across the solid is uniform at all times and therefore the energy transfered through conduction does not play a major role. In real situations, the solid might not be at a uniform temperature and consequently, equation (3.14) should only be used if the Biot number, a factor that takes into consideration the ratio of conduction resistance within the body with the convection resistance at the surface of the body, is less or equal to 0.1:

$$B_i = \frac{V/(kA)}{1/h} \leq 0.1 \tag{3.16}$$

These equations were implemented in matlab and in COMSOL (Test 3) using the sphere shown in figure 3.1 and a heat transfer coefficient of h = 0.05 W/(m^2· K), T_∞ = 400 K and T_i = 300 K. For this set of values $\tau \approx 4.4 \cdot 10^{-8}$ s^{-1} and B_i= 0.05. The results obtained for dt = 10^5 s and t_{final}=7×10^7 s are presented in figure 3.5 and the RMS for different mesh sizes is summarised in table 3.1 (Test 3, page 23).

All the problems analysed so far involved very simple equations. However, there are some papers that present more complex analytical solutions. For example, Werley and Gilligan [42] deduced an equation for the temperature of a sphere when it is subjected to a uniform flux on one side (figure 3.6). It is assumed that this sphere does not exchange heat with the environment, thus increasing its temperature indefinitely. After some time, a constant rate of temperature change is reached. Equation (3.17) represents this problem mathematically.

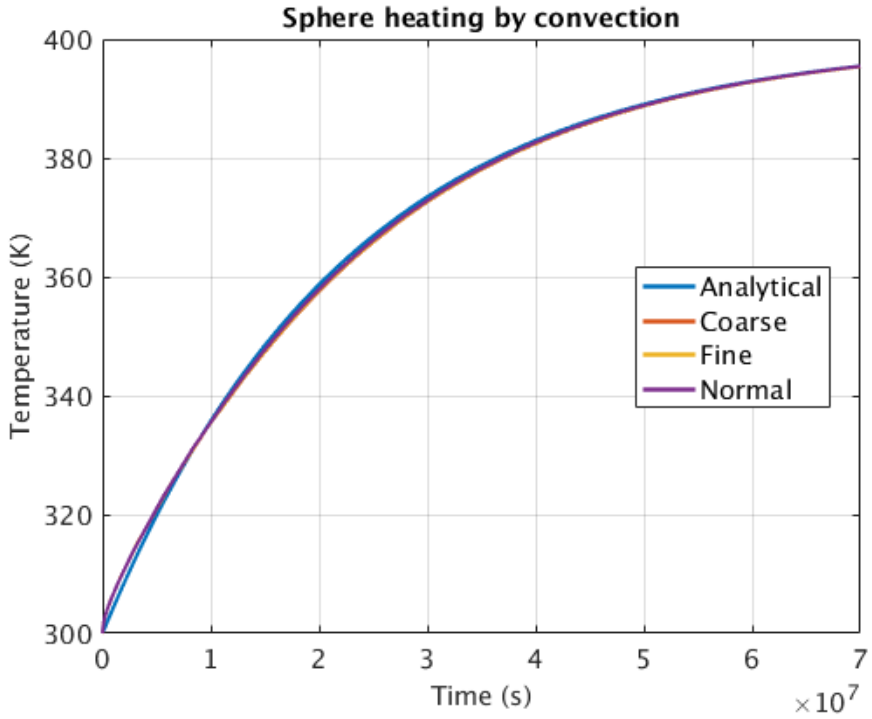

Figure 3.5: Sphere surface temperature variation through convection for three different mesh sizes and for matlab. Some colours may not be seen in some regions due to the overlap of the temperature profile of a different mesh. Time step used was 10^5s.

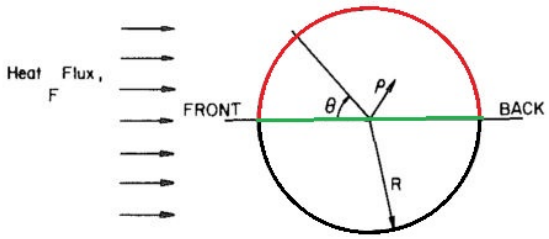

Figure 3.6: Sphere with a radius R subjected to a uniform heat flux, F, at the front side. ρ and θ can be any value between 0 and R and 0 and π, respectively. The red and green lines will be used to perform a temperature analysis. Adapted from [42].

$$\frac{kT(r,\theta,t)}{RF} = \frac{kT_0}{FR} + \frac{3t}{4} + \frac{5r^2-3}{40} - \frac{1}{2r}\sum_{m=1}^{\infty}\frac{\sin(\beta_m r)\exp(-\beta_m^2 t))}{\beta_m^2\sin(\beta_m)} + \cos(\theta)\left\{\frac{r}{2} - r^{-0.5}\sum_{m=1}^{\infty}\frac{J_{3/2}(\mu_m r)\exp(-\mu^2 t)}{J_{3/2}(\mu_m)[\mu_m^2-2]}\right\} - \sum_{n=1}^{\infty}\frac{2n+0.5}{2n^2+n-1}P_{2n}(0)P_{2n}(\cos(\theta))\left\{\frac{r^{2n}}{4n} - r^{-0.5}\sum_{m=1}^{\infty}\frac{J_{2n+0.5}(\gamma r)\exp(-\gamma^2 t)}{J_{2n+0.5}(\gamma_m)[\gamma_m^2-2n(2n+1)]}\right\} \quad (3.17)$$

Where the variables and constants presented are: thermal conductivity (k), temperature (T), initial temperature (T_0), radius of the sphere (R), incident flux (F), radial position in the sphere (ρ), angle (θ), specific heat (c_p), thermal diffusivity (α), time (τ), summation indices (m,n),

Bessel function of n-th order (J_n) and Legendre polynomial of m-th order (P_m). Additionally, the following expressions were defined:

$$\text{Thermal diffusivity: } \alpha = \frac{k}{\rho c_p} \tag{3.18}$$

$$\text{Dimensionless time: } t = \frac{\alpha \tau}{R^2} \tag{3.19}$$

$$\text{Dimensionless position: } r = \frac{\rho}{R} \tag{3.20}$$

β_m, γ_m and μ_m are the roots of:

$$\tan(\beta_m) - \beta_m = 0 \tag{3.21}$$

$$\frac{d}{d\gamma}\gamma_m^{-1/2} J_{2n+1/2}(\gamma_m) = 0 \tag{3.22}$$

$$\frac{d}{d\mu}\mu_m^{-1/2} J_{3/2}(\mu_m) = 0 \tag{3.23}$$

The results obtained by the authors are presented in figure 7 where the plotted quantity is the temperature profile minus an average temperature (T_{AVG}) (equation (3.24)) along the green (figure 3.7a) and red (figure 3.7b) lines of figure 3.5.

$$T_{AVG} = T_0 + \frac{FR}{k}\frac{3t}{4} \tag{3.24}$$

To implement equation (3.17) in matlab it was first necessary to find the roots of equations (3.21) to (3.23). This was done using the bisection method with a maximum error of 0.025. Regarding the infinite summations, they were truncated at 50 for both m and n indexes using the same way of thinking as in the time-transient conduction test to find the truncation value of n.

It was not possible to compare the analytical results obtained through matlab with those of the paper other than qualitatively because the authors did not specify any temperature value for the different times. Nonetheless, the graphs obtained are very similar and thus it can be concluded that this implementation was well performed.

In order to compare these results with COMSOL's (Test 4) the quantity plotted was slightly changed. Instead of plotting the temperature deviation relative to an average temperature, just the temperature profile was plotted, because it allows an easier comparison (figure 3.8).

The RMS was calculated for the green and red lines separately for different mesh qualities. The final deviation was assumed to be the mean of these two RMS (table 3.1, Test 4, page 23). Additional information about each test is presented in table A1 in the "Appendix" section.

3.2 Main conclusions

All the results obtained in this section indicate that COMSOL's results can deviate from the real solutions, whether it was a steady-state (Test 1) or a transient problem (Tests 2, 3 and 4). As one might expect the steady-state conduction test (Test 1) that was done was a very simple situation to work with and the solution was very straight-forward. As a result, RMS values were

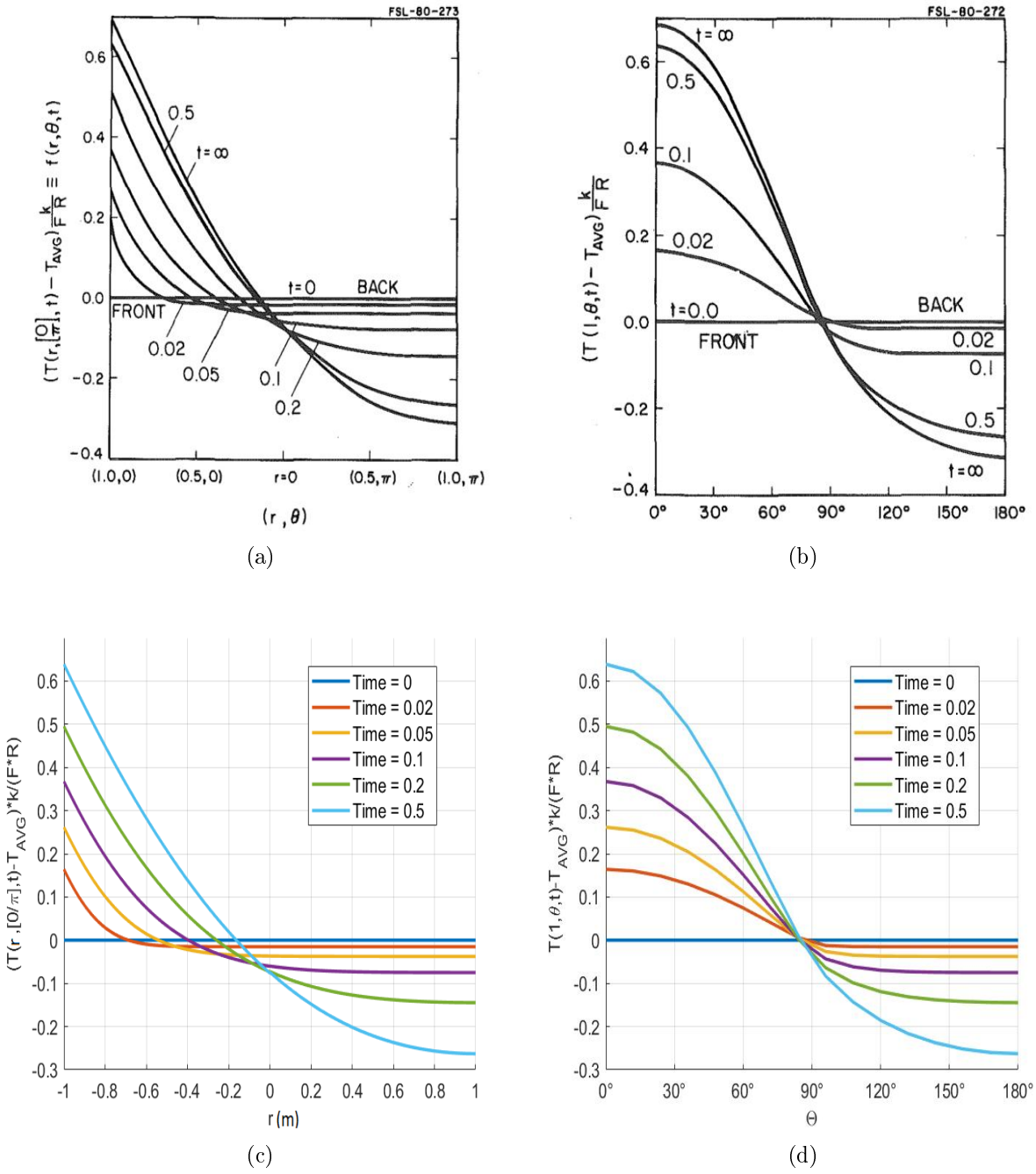

Figure 3.7: Comparison between Werley and Gilligan's results ((a) and (b)) and those obtained implementing their equations in matlab ((c) and (d)). Plots (a) and (c) correspond to a temperature profile analysis along the green line of figure 3.6 and plots (b) and (d) correspond to the red line analysis of the same figure. Timelines presented here are dimensionless. Images (a) and (b) were withdrawn from [42].

practically zero. For the convection study (Test 3), RMS indicate that the deviations are not higher than 1 K in 390 K, which corresponds to a maximum deviation of 0.2% for the three mesh qualities tested, with this value decreasing for more refined meshes. Theoretically, lower RMS values are expected for finer meshes because the estimated solution is closer to the real one as the problem is solved in more nodes. For the time-transient conduction problem (Test 2), this value was around 3 K in 3500 K (around 0.1%), which could have been influenced by the assumptions made when solving for the analytical solution using matlab such as the integral

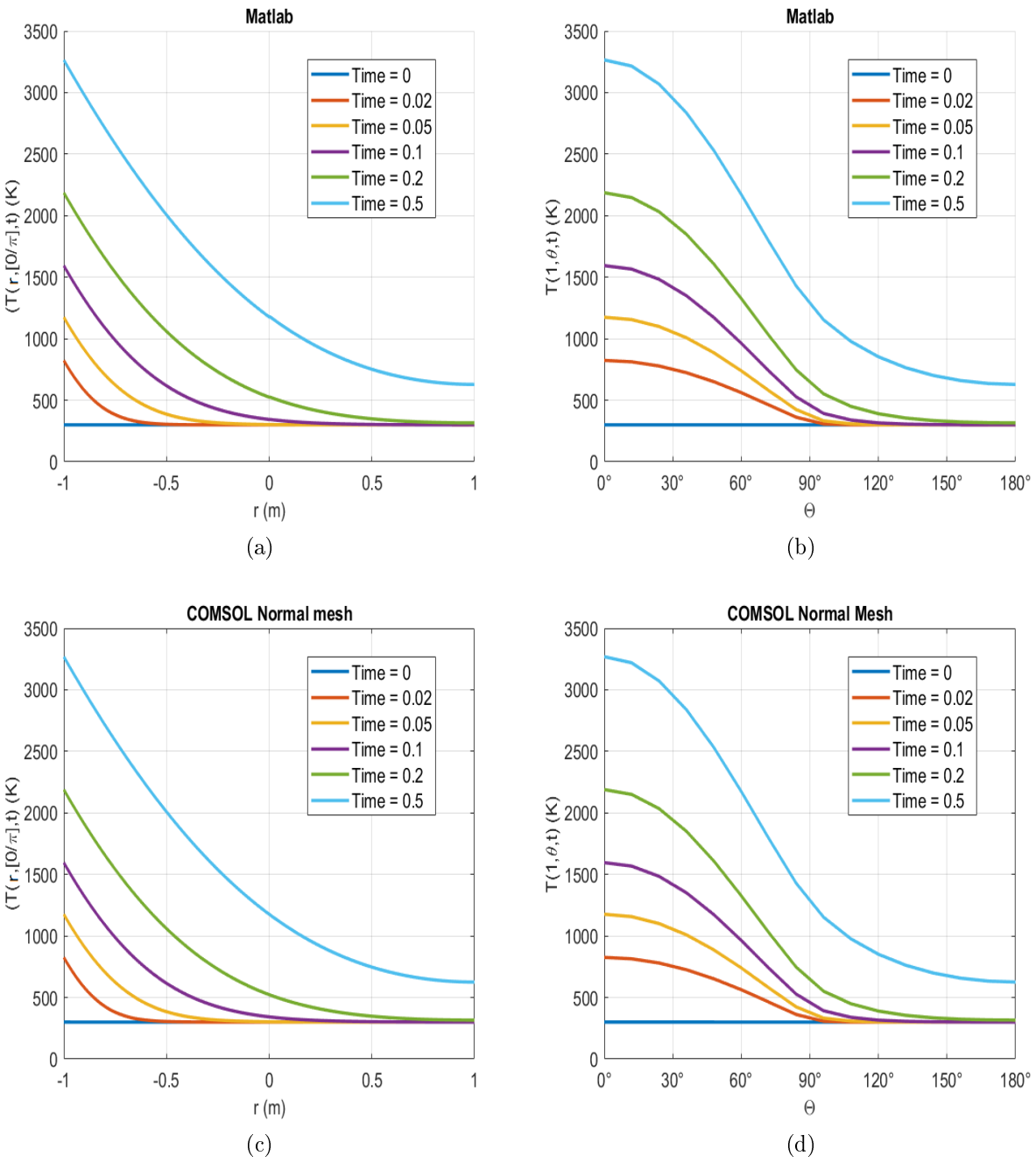

Figure 3.8: Comparison between matlab ((a) and (b)) and COMSOL with a normal mesh ((c) and (d)) results. Plots (a) and (c) correspond to a temperature profile analysis along the green line of figure 3.6 and figures (b) and (d) correspond to the red line analysis of the same figure. Timelines presented here are dimensionless times. Both spatial and time discretizations were the same for all graphs.

calculation or the truncation value of n in the infinite summation. Lastly, when implementing a more complex formula (Test 4) considering a uniform heat flux the mean RMS was lower than 1.5 K in 3250 K (0.05%) for all mesh sizes. Although the mean RMS for a finer mesh is slightly higher than for the coarser ones in this situation, these values are very close to each other.

The study of Gerlich et. al [43] regarding COMSOL validation as a simulation tool for heat transfer in buildings indicate that to get precise results via COMSOL it is necessary to reduce

Table 3.1: RMS for all the tests performed and for there different mesh qualities.

Test \ Mesh	Coarse	Normal	Fine
1	<1E(-10) K ($\approx$ 0%)	<1E(-10) K ($\approx$ 0%)	<1E(-10) K ($\approx$ 0%)
2	3.31 K (0.09%)	3.27 K (0.09%)	3.15 K (0.09%)
3	0.83 K (0.2%)	0.78 K (0.2%)	0.69 K (0.2%)
4	1.37 K (0.04%)	1.37 K (0.04%)	1.46 K (0.05%)

solver's relative and absolute errors at least 10 times relative to the solver's default settings. Furthermore, the authors also reported that it is important to use a very fine mesh in all problems. Throughout all this section, the tolerance values used for errors was the default's (0.05) and only three mesh types were tested among of seven total different options available. This has to do with the fact that for real problems with complex geometries, it is not feasible to work with very small elements because computational time would increase a lot. In the same way, decreasing solver's tolerance might lead to lack of convergence for more complex problems, although in these cases a smaller value could have been used. Nonetheless, the RMS values obtained indicate that COMSOL's solutions pratically do not deviate regarding the real solutions and, according to these results, it is expected a maximum deviation lower than 1%.

Regarding COMSOL as a simulation tool, it is clear that it has a lot of advantages such as the possibility of coupling different physics (in this project the thermal and electric modes will be coupled), the ability to change the governing equations and the friendly user interface. One of the big disadvantages has to do with the default choice of the solver. COMSOL's chooses the solver that requires less memory and is more robust and does not optimize this choice for each problem, which may lead to a lack of convergence. Although the user can change this solver manually, it is not straight-forward for those who do not have enough knowledge of FEA to chose which one is the most suitable for each problem.

Chapter 4

Methods

4.1 The realistic head model

The realistic head model was not built specifically for this project. It was originally created to study the electric field in the cortex during a transcranial Current Stimulation (tCS) treatment [44] using MRI images available for the single-subject template Colin27 and made available by BrainWeb (`http://brainweb.bic.mni.mcgill.ca/brainweb`). Two datasets were used: T1 and proton density (PD), both of them already aligned to the Montreal Neurological Institute (MNI) stereotaxic space with FSL FLIRT (`https://fsl.fmrib.ox.ac.uk/fsl/fslwiki/FLIRT`). Voxel dimensions are 1x1x1 mm^3. The segmentation using Brainsuite (`http://neuroimage.usc.edu/neuro/BrainSuite`) resulted in surface meshes that delimited five different biological tissues: scalp and skull (through the PD images), CSF, white matter (WM) and grey matter (GM) (using the T1 images). These surfaces were then imported into Mimics (`http://biomedical.materialise.com/mimics`) where small irregularities were smoothed out. Additionally, in order to represent the best way possible a realistic head some modifications were made to include the superior orbital fissures and the optic foramina (these plugs are small holes that were drawn in the cranium to represent the place where some structures such as the optical nerve pass to the brain). At this stage, the lateral ventricles were also defined, the electrodes added to the model and a volume mesh generated. Finally the model was imported to COMSOL Multiphysics to run simulations. Additional information about the creation of this head model can be found in [44].

The modifications regarding electrodes position to use this model to study TTFields are described in detail in [14]. In this paper, two pairs of multi-transducer arrays were capacitively coupled on the surface of the scalp. In order to accurately represent the Optune® device, one of the pairs was placed over the left (L) and right (R) temporal and parietal regions and the other pair was placed over the supraorbital region (A) and the back of the head (P). From now on, the first pair is going to be refered as the LR configuration and the second one as the AP configuration. Each set consists on nine interconnected electrodes (3x3) with centres separated by 22 mm by column and 33 mm by row. Each electrode is represented as a ceramic disk with 1 mm height and 9 mm radius. Between each electrode and the scalp a thin layer of gel with 10 mm radius and variable thickness (between 0.5 and 2 mm) was added to improve current delivery. A virtual lesion intended to represent a GBM was placed within the right hemisphere, near a lateral ventricle and totally embedded in the WM (figure 4.1). This tumour was represented by two concentric spheres, one that represents a necrotic core with 14 mm diameter and the other

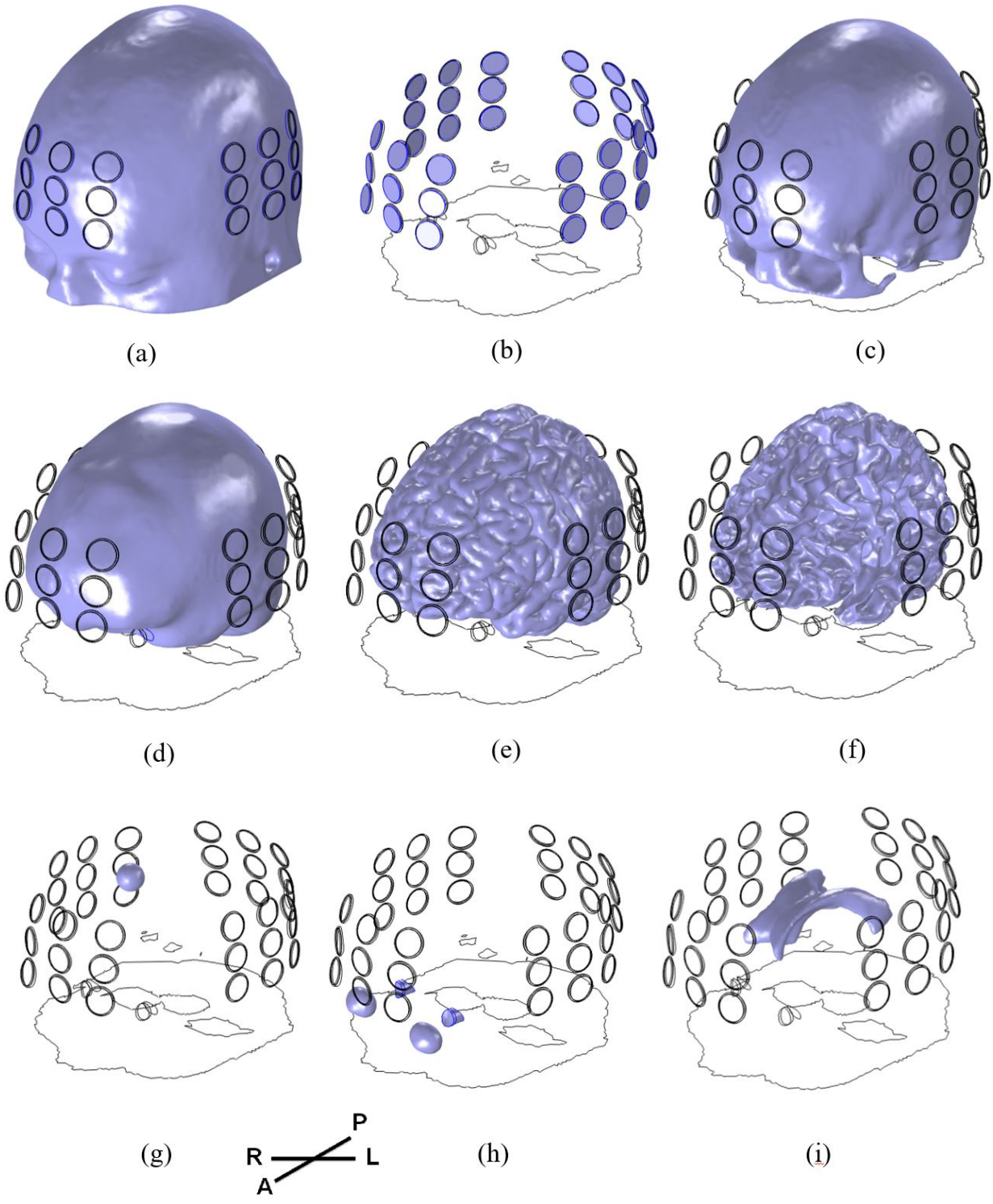

Figure 4.1: Tissues delimited: (a) scalp with electrodes; (b) electrodes; (c) skull; (d) CSF; (e) grey matter; (f) white matter; (g) shell of the virtual lesion; (h) eyeballs (in a more anterior position) and plugs (in a more posterior position); (i) ventricles. The axis system applies to all subfigures. A: Anterior, P: Posterior, L: Left; R: Right;

that represents an active shell with 20 mm diameter. The mesh for this model is represented in figure 4.2 and it consists on 2.2×10^6 tetrahedral elements, 5.6×10^5 triangular elements, 8 952 edge elements and 272 vertex elements, 6.2×10^6 DoF, and an average mesh quality of 0.447.

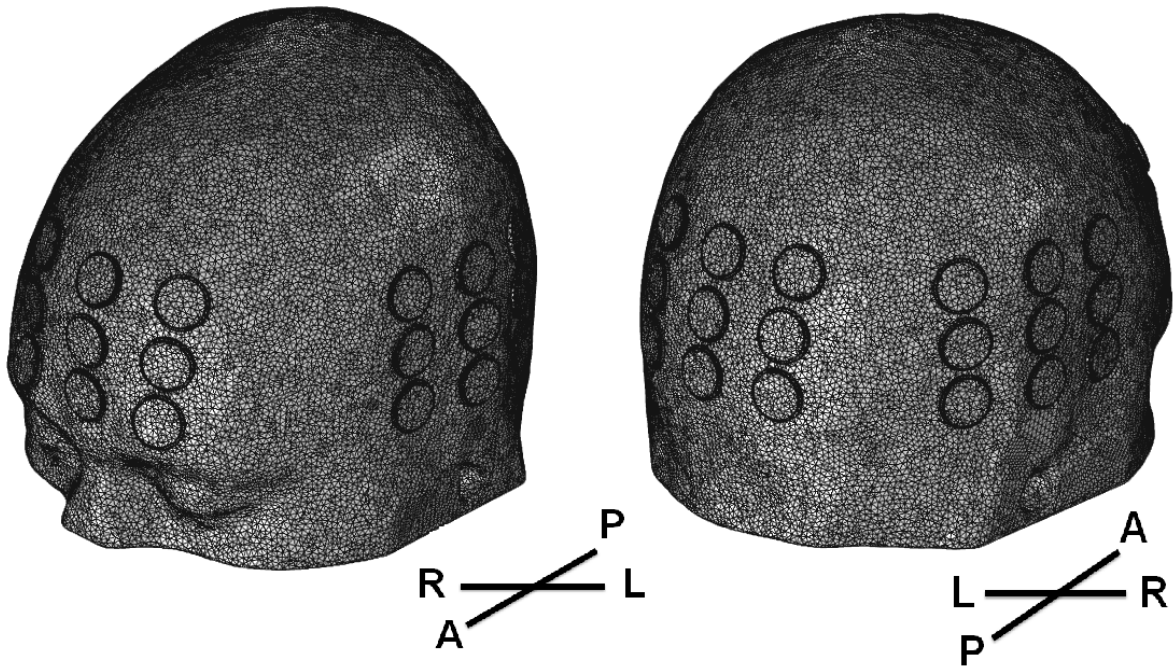

Figure 4.2: Mesh of the human head model (2.2×10^6 tetrahedral elements, 5.6×10^5 triangular elements, 8952 edge elements and 272 vertex elements, 6.2×10^6 DoF and an average mesh quality of 0.447) from two different perspectives.

4.2 Solving the model

For this project, two different COMSOL Multiphysics interfaces were used: the electric currents (frequency-domain study) and the heat transfer in solids (Joule heating, frequency-domain time-transient study), both with a frequency set to 200 kHz. The solver relative tolerance was 10^{-6} for both interfaces. Because the electromagnetic wavelength in the different tissues is significantly larger than the size of the head the electroquasistatic approximation of Maxwell's equations can be used. The boundary conditions for the electric module were the same as the ones described in the paper of Miranda et. al [14]: continuity of the normal component of the current density ($\boldsymbol{J}$) at all interior boundaries (equation 4.1) and electric insulation at the external boundaries where current is not being applied (equation 4.2) (Neumann boundary conditions) and fixed potential where current is being injected (equation 4.3) (Dirichlet boundary condition):

$$\boldsymbol{n_2} \cdot (\boldsymbol{J_1} - \boldsymbol{J_2}) = 0 \tag{4.1}$$

$$\boldsymbol{n} \cdot \boldsymbol{J} = 0 \tag{4.2}$$

$$V = V_0 \tag{4.3}$$

In the former equations, $\boldsymbol{n}$ represents the normal to the surface. As it can be easily concluded, equation 4.1 applies to all tissues, gel and electrodes, while equation 4.2 applies only to the scalp, gel and electrodes. The last equation applies to all transducers. In regards to the thermal part, a Neumann boundary condition was also applied to the scalp, electrodes and gel that are in contact with the environment that reflects the energy transferred by convection (equation 4.4).

$$-\boldsymbol{n_i} \cdot (-k_i \nabla T(\boldsymbol{r}, t)) = h(T_{room} - T(\boldsymbol{r}, t)) \tag{4.4}$$

In the above expression, k_i represents the thermal conductivity of the $i-th$ tissue or material in contact with the air (scalp, electrodes or gel), h is the convection coefficient and T_{room} is the room temperature. The initial temperature of each tissue or material is defined by equation (4.5) and to obtain the temperature field as a function of space and time, Pennes' equation [45] was used (equation (4.6))

$$T = T_0 \tag{4.5}$$

$$\rho_j c_j \frac{\partial T(\boldsymbol{r}, t)}{\partial t} = \nabla \cdot (k_j \nabla T(\boldsymbol{r}, t)) + Q_{b_t}(\boldsymbol{r}, t) + Q_{m_t} + Q_{r_j}(\boldsymbol{r}, t) \tag{4.6}$$

Where ρ_j, c_j and k_j are, respectively, the density, specific heat at constant pressure and thermal conductivity of the $j-th$ tissue or material (gel or transducer). Q_m ($\mathrm{W/m^3}$) is the metabolic heat generation of each tissue and Q_{b_t} ($\mathrm{W/m^3}$) is the energy transfered to the blood, per unit time, defined as follows:

$$Q_{b_t}(\boldsymbol{r}, t) = \omega_{b_t} \rho_b c_b (T_{blood} - T(\boldsymbol{r}, t)) \tag{4.7}$$

Where ρ_b and c_b are the density and specific heat of blood and ω_{b_t} ($\mathrm{s^{-1}}$) is the blood perfusion. T_{blood} is the blood temperature assumed to be constant. Finally, $Q_r(\vec{r}, t)$ is the heat source due to spatial heating which corresponds to the Joule effect in this case and is expressed as:

$$Q_{r_j}(\boldsymbol{r}) = \boldsymbol{J} \cdot \boldsymbol{E} \tag{4.8}$$

With $\boldsymbol{E}$ (V/m) representing the electric field and $\boldsymbol{J}$ ($\mathrm{A/m^2}$) the current density. To apply the fields alternately this equation has to be slightly changed to:

$$Q_{r_j}(\boldsymbol{r}) = Q_{r_{j\,AP}}(\boldsymbol{r}) + Q_{r_{j\,LR}}(\boldsymbol{r}) = \boldsymbol{J_{AP}} \cdot \boldsymbol{E_{AP}} \cdot Pulse(t) + \boldsymbol{J_{LR}} \cdot \boldsymbol{E_{LR}} \cdot Pulse(t+1) \tag{4.9}$$

Where $Pulse(t)$ is a rectangular function that evaluates to one when the integer part of time is odd and to zero when it is even.

In practice, everytime one electrode reaches 41ºC Optune® shuts down and this term is zero:

$$Q_{r_j}(\boldsymbol{r}) = 0 \Leftarrow \exists\, \text{electrode} : T_{\text{electrode}} \geq 41°C \tag{4.10}$$

All the parameters used for the simulations are described in table 4.1 except the values of the convection constant (h) which was assumed to be 4 $\mathrm{W/(m^2 \cdot ºC)}$ [27, 46] and room and blood temperatures that were assumed to be 24ºC and 36.7ºC, respectively. Optune® injects 900 mA per array (900 mA amplitude, 1.8 A peak-to-peak) and to satisfy this requeriment, trial and error simulations were done to obtain the potential difference between the left and right arrays (V_{LR}) and the anterior and posterior arrays (V_{AP}) that respected this condition. The results showed that a potential difference of 68.9 V (amplitude) in the LR direction and of 92.6 V (amplitude) in the AP direction was necessary. These two values were fixed throughout the

simulations (equation (4.3)). The electric parameters in table 4.1 are the same as in [14] and the thermal ones were obtained after an extensive research of the most used values in the literature [27, 46–61]. For simplification, the ventricles were assumed to be filled with CSF and the plugs were assumed as being scalp. The properties of the eyeballs were assumed to be those of the vitreous humour because it is the bigger structure of the eye.

4.3 Simulations performed

Having presented the realistic head model and the equations used to solve for the variables of interest it is necessary to specify the simulations performed.

4.3.1 Simulation 1 - Importance of the shutdown

This simulation intends to study what would happen if there were no temperature sensors, or, in other words, if Optune® did not shut down when the transducers' temperature reached 41ºC. Undoubtedly, this does not correspond to a real situation because even if the temperature sensors stop working for any reason the heat felt by the patient would be so high that this problem would be rapidly noticed and the device turned off. In terms of modeling, this corresponds to not applying the load defined by equation (4.10).

4.3.2 Simulation 2 - Model how Optune® works

This is the main goal of the project. The results obtained allow to study the duty cycle of the device, conclude about tissue heating and investigate the hypothesis that this technique does not increase tumour temperature to such an extent to attribute its efficacy to hyperthermia. To perform this simulation the Optune® system was modeled as realistically as possible. Additionally, instead of shuting down the device when any electrode average temperature reached 41ºC, a threshold of 40.4ºC was defined. This corresponds more or less to have 5% of the electrode at 41ºC. The rationale for this has to do with the fact the temperature sensor being rather small compared with the electrode size. Although there is no information made available by Novocure™ regarding sensor's size or volume this 5% corresponds to have one sensor with more or less 12.7 mm^2 area and 1 mm thickness which is inside the range found in the market (see for example IFM (`http://www.ifm.com`) or TME (`http://www.tme.eu`)). This new threshold was used in all the simulations performed.

4.3.3 Simulations 3 and 4 - Study Optune®'s efficacy in different environments

One way to dissipate heat is through air cooling and the rate of energy transfer depends on the external temperature. Theoretically, if the room temperature is sufficiently low Optune® is applying the field during more time and consequently its efficacy is increased. In the same way of thinking, in extremely hot places heat transfer with the environment can heat the head even more and this technique may not be the most suitable to treat GBM. As one might conclude, the external temperature is not constant and varies throughout the day and place. As so, this study aims to understand how can Optune®'s efficacy (in terms of time applying the fields) change depending on the external temperature. Although being approved by the FDA, there

Table 4.1: Values of the physical properties and initial values used for each tissue or material. These values were chosen after an extensive literature review of the values used in several papers [14, 27, 46–61].

	Parameter	Scalp	Skull	CSF	GM	WM	Eyeballs	Tumor core	Tumor shell	Electrodes	Gel	Blood
Electric	Electric conductivity σ (S/m)	0.25	0.013	1.79	0.25	0.12	1.50	1.0	0.24	0	0.10	—
	Relative permittivity ϵ (1)	10 000	200	110	3 000	2 000	966	110	2 000	10 000	100	—
	Initial electric potential V_0 (V)	0	0	0	0	0	0	0	0	V_{LR} V_{AP}	0	—
Thermal	Density ρ (kg/m^3)	1 000	1 500	1 000	1 035.5	1 027	1 005	1 025	1 025	6 060	1 000	1 050
	Specific heat c (J/(kg $\cdot$ ºC))	3 150	1 700	4 200	3 680	3 600	4047	3 600	3 600	527	4 186	3 600
	Thermal conductivity k (W/(m$\cdot$ºC))	0.34	1.16	0.6	0.565	0.503	0.59	0.6	0.6	6	0.6	0.505
	Blood perfusion rate ω (s^{-1})	0.00143	0.000143	0	0.01329	0.0037	0	0	0.004	0	0	—
	Metabolic heat Q_m (W/m^3)	363	70	0	16 229	4 517.9	0	0	4 517.9	0	0	—
	Initial temperature T_0 (ºC)	T_{blood}	T_{blood}	T_{blood}	T_{blood}	T_{blood}	T_{blood}	T_{blood}	T_{blood}	T_{room}	T_{room}	T_{blood}

Values: $V_{LR} = 68.9$ V; $V_{AP} = 92.6$ V; $T_{blood} = 36.7$ ºC; $T_{room} = 24$ ºC;

are only a small number of countries that use TTFields as a standard of care to treat GBM due to all the requirements needed to ensure a correct use of it, being the United States of America (USA) one of them. Considering only states with more than 20 million people, the average winter temperature of the coldest state is 7.9ºC and occurs in California (mean temperature according to the data obtained during the years of 1971 to 2000 and available by "Current Results" [62]). On the other hand, the hottest average temperature during summer is 27.3ºC and occurs in Texas [62]. The information made available by Novocure^{TM} in [7] also shows that there are several "Optune® doctors" in these two states, so it is likely that a reasonable amount of patients being treated with TTFields live in these areas. These two temperatures are going to be used to quantify the duty cycle increase/decrease due to external factors. These simulations imply changing the room temperature (T_{room}) of equation (4.4) to the values mentioned:

$$\text{Simulation 3: } T_{room} = 27.3°C$$
$$\text{Simulation 4: } T_{room} = 7.9°C$$

4.3.4 Simulation 5 - Half intensity, always on

The optimal frequency to treat GBM is 200 kHz which implies that, in one second, the applied field has changed 200 000 times in just one direction. In the following second the same occurs but in a perpendicular direction. In the limit, such a rapid change can be thought to cause no major effect and may be seen as countinously applying the electric fields in both directions, but with half the injected current. This simulation aims to verify how the results change if Optune® worked this way. To perform this simulation equations (4.3) and (4.9) have to be changed to:

$$V'_{\text{AP}} = \frac{V_{\text{AP}}}{2}$$
$$V'_{\text{LR}} = \frac{V_{\text{LR}}}{2}$$
$$Q_{r_j}(\boldsymbol{r}) = \boldsymbol{J'_{AP}} \cdot \boldsymbol{E'_{AP}} + \boldsymbol{J'_{LR}} \cdot \boldsymbol{E'_{LR}}$$

4.3.5 Simulation 6 - Independent temperature sensors

The temperature sensors incorporated in Optune® control if any transducer reaches 41ºC and shuts down the applied current for all the electrodes if that condition is verified. However, it might happen that a more rapid increase is seen for just one configuration while the other remains at a relatively low temperature. Thus with this simulation the aim is to see the major differences when independent temperature sensors for the AP and LR configurations are used. This allows one configuration to remain active when the other shuts down. Thus equation (4.10) has to be changed to:

$$Q_{r_{j\,AP}}(\boldsymbol{r}) = 0 \Leftarrow \exists\,\text{electrode}_{\text{AP}} : T_{\text{electrode}_{\text{AP}}} \geq 41°C$$
$$Q_{r_{j\,LR}}(\boldsymbol{r}) = 0 \Leftarrow \exists\,\text{electrode}_{\text{LR}} : T_{\text{electrode}_{\text{LR}}} \geq 41°C$$

4.3.6 Simulation 7 - Current controller

Optune® injects 900 mA per array which results in an unequal current distribution to the nine electrodes. This can be seen as having one current controller per array. Because the prices of these controllers (see for example Moglix (`https://www.moglix.com/`)) are not high compared to the price of Optune®, Novocure™ may consider using one controller per transducer and injecting 100 mA per electrode if the results are significantly better. This simulation intends to express the major differences of these two ways of working in numbers. In practice this is the same as changing equation (4.3) at each transducer to:

$$I = I_0 = 100\,\mathrm{mA}$$

Chapter 5

Results

Due to computational time and memory limitations, the duration of all the simulations performed here was limited to 400 seconds. This value was chosen because the preliminary calculations showed that the electrodes should reach the shut down temperature more or less 100 seconds after the treatment had started. This leads to the remaining 300 seconds that should be representative of the treatment itself. Some notes regarding how this truncation could have affected the results are presented in the "Discussion" section. All the tests were performed in COMSOL v.4.3b and each simulation took around 60 hours in a workstation with 2x 4-core CPU's (Intel Xeon W5580 @ 3.2 GHz) and 48 Gb RAM and took up a total space of approximately 40 Gb (temporary files not included). The volume average SAR values and the volume average CEM 43ºC for one treatment day and for all simulations are showed in tables 5.3 (page 50) and 5.4 (page 51), respectively. It is assumed that for the remaining time to reach the 18 daily hours the temperature values do not change significantly compared to what was obtained at the last time step simulated, thus this is the value assumed for the necessary calculations. There are two CEM 43ºC values reported: one for the average of the whole head volume and one for the average inside a cylinder defined by the hottest electrode that gives information about the local heating. Lastly, with the purpose of approximating these simulations as much as possible to a real situation a steady-state study for every test was first done without applying any electric field so that the head and the environment become in thermal equilibrium. The values of this simulation were then used as the initial condition for the tests performed. The Generalized Alpha Method was chosen as the solver because it is the most accurate for time-transient problems among the available options [63].

5.1 Simulation 1 - Importance of the shutdown

In order to model how Optune® works, it is necessary to inject 900 mA per array which are distributed unequally to all the nine electrodes of each array, depending on the contact impedance at each electrode. The current distribution across all the 36 transducers can be seen in figure 5.1.

This heterogenous distribution is also partly responsible for the non-uniform electric field that is seen in the brain (white matter plus grey matter). In figure 5.2 the electric field distribution in a sagittal, coronal and transversal slices of the brain through the tumour is shown. It is also important to verify that the electric field within the tumour has at least an intensity of 1 V/cm

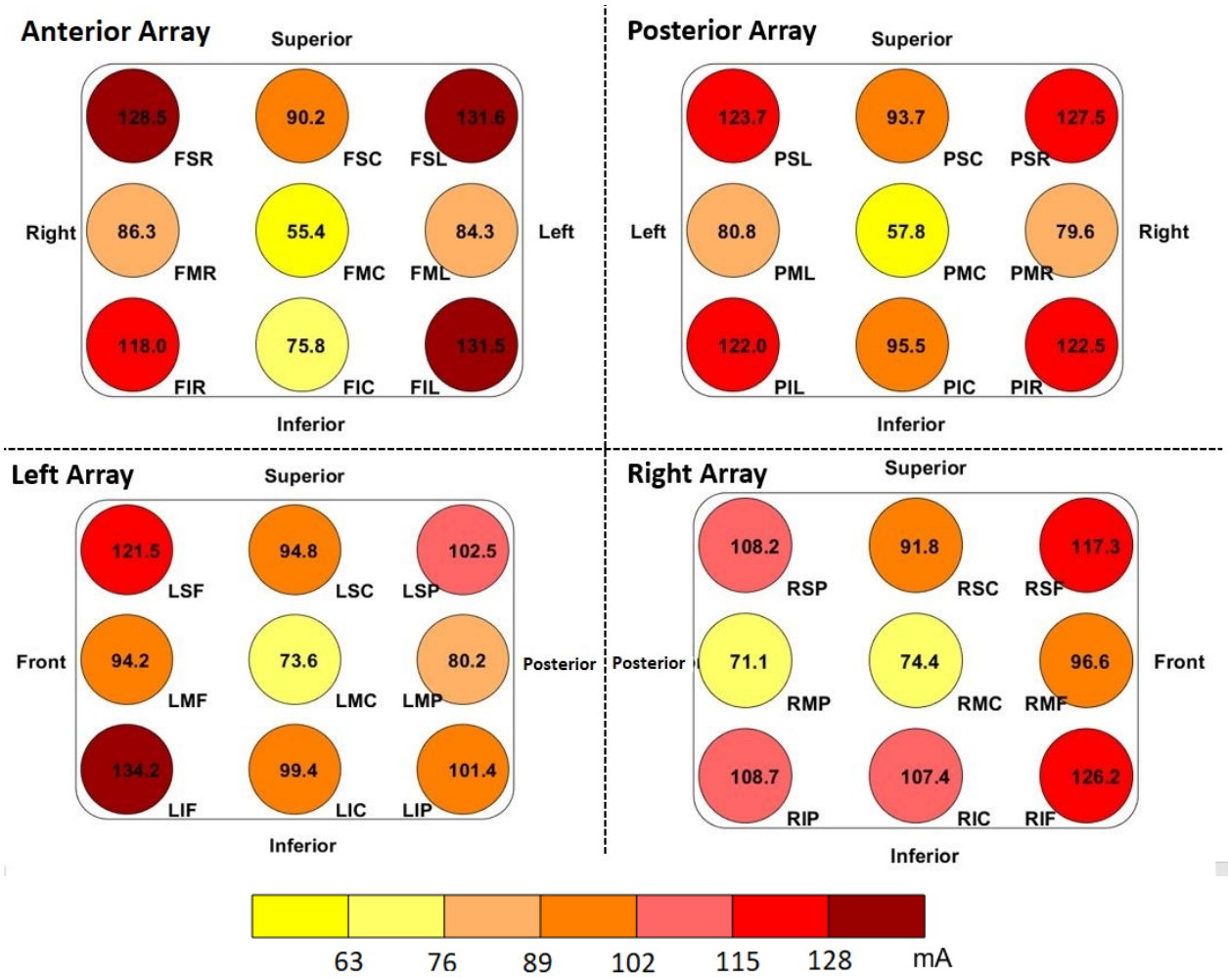

Figure 5.1: Current that passes through each electrode. Electrodes are identified by a three letter combination. The first letter indicates the array (F: Front; P: Posterior; L: Left; R: Right), the second represents the row within the array (S: Superior; M: Middle; I: Inferior) and the third represents the position within the row (F; P; L; R; C: Central). The same axis orientation was used as in figure 4.1.

which ensures TTFields efficacy. In table 5.1 (page 50) data concerning the Above-Threshold Volumes (ATV) of each tissue for three different limits is given. In this context, ATVx means the percentage of the tissue volume that it is above x V/cm. Having the electric field distribution it is now possible to calculate the average SAR values for each tissue and for both configurations (table 5.2, page 50). Also, to make an easier comparison with the FDA and the IEC limits it was calculated the average SAR for the whole head and for a 10g cube containing the region where the electric field magnitude is maximum. This corresponds to two different volumes, one for each configuration, in the skull. For the LR configuration the cube defined has a side length of 21.2 mm and for the AP configuration it has 20.6 mm. Both of these cubes contain scalp, skull, CSF, WM and GM.

Regarding the importance of controlling the temperature, the graphics shown in figures 5.3 and 5.4 represent the average temperature variation of each transducer as a function of time considering that Optune® never shuts down. Its is noteworthy to see that the temperature of several electrodes would exceed 41°C. Figure 5.5 illustrates the average temperature of each biological tissue in the same conditions. It is also important to note that the electrodes do not

heat due to Joule effect because their electric conductivity is zero. Instead, their temperature increase is explained by heat transfer from the gel.

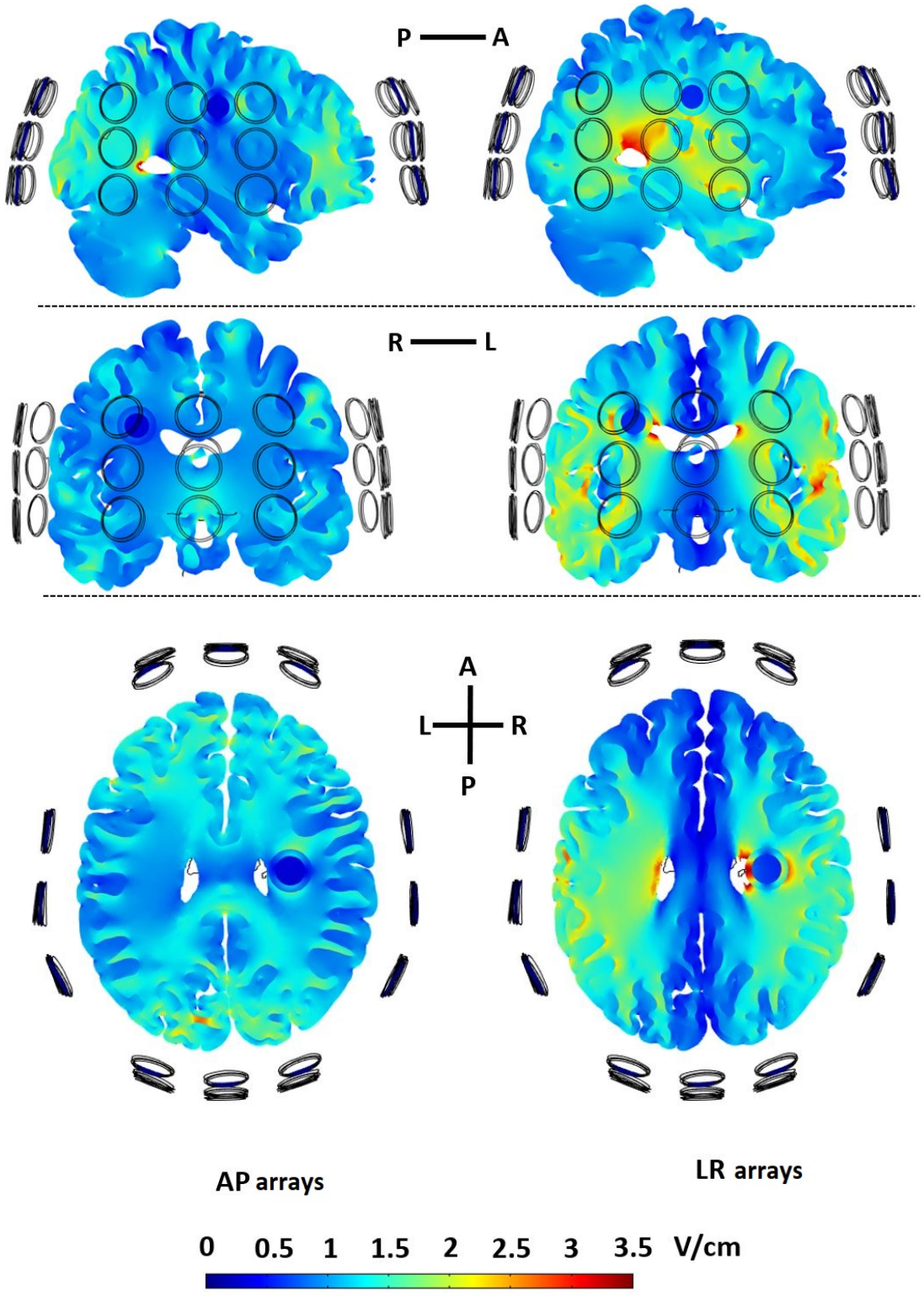

Figure 5.2: Electric field magnitude in the brain and in the tumour in a sagittal (first row), coronal (second row) and transversal (third row) planes for both AP (first column) and LR (second column) configurations. As it can be easily seen the threshold of 1 V/cm in the tumour is surpassed for both configurations although it is larger for the LR due to the higher field compared to the AP's at this location. Values greater than 3.5 V/cm are coloured as dark red. The axis orientation that is shown is for both configurations of the same row.

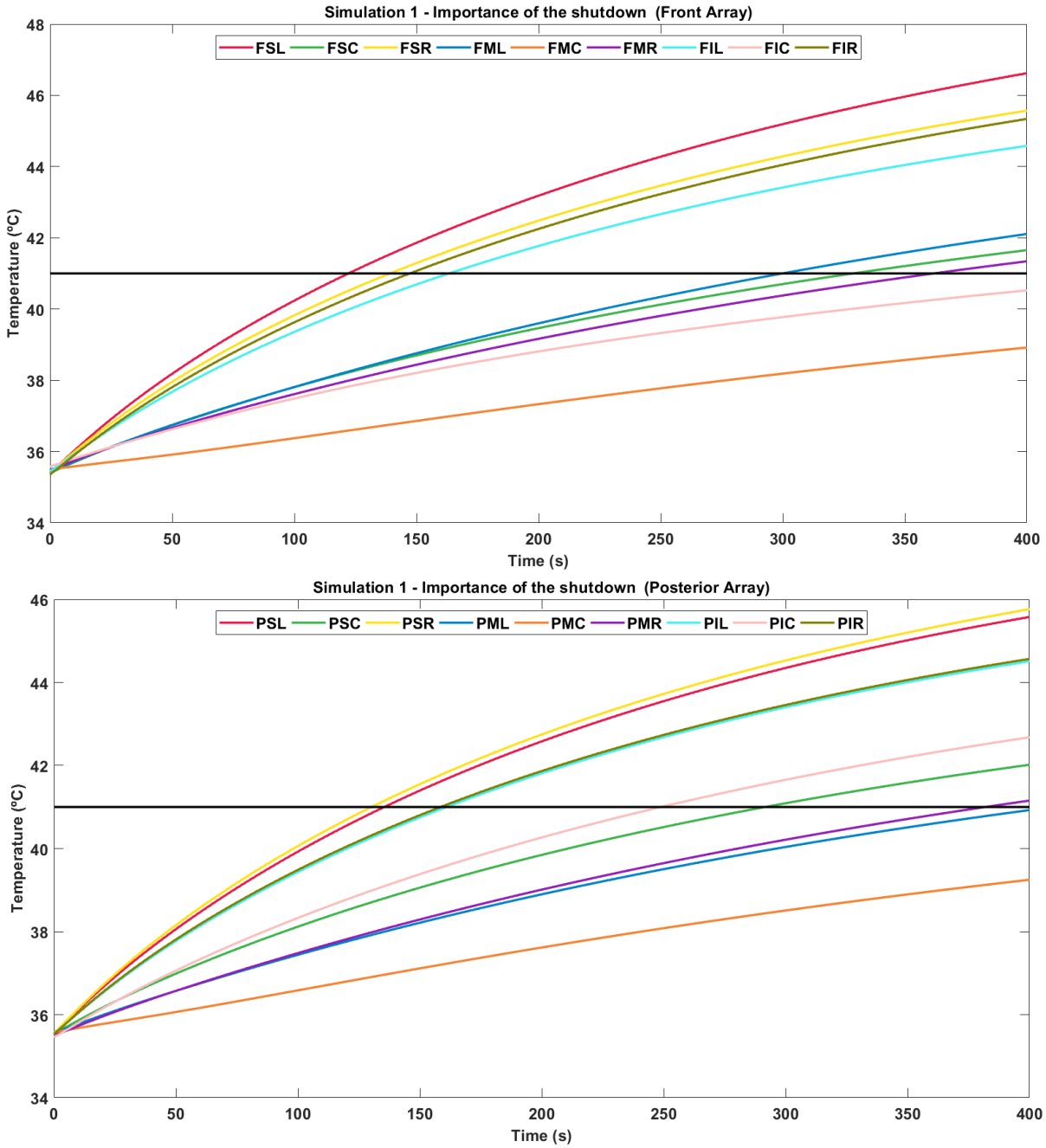

Figure 5.3: Average temperature variation as a function of time for the front (up) and posterior (down) arrays if the fields were always on (Simulation 1). Current is being injected in the AP and LR directions alternately. It is easily seen that several electrodes surpass the threshold of 41ºC (black line) in just 400 seconds. Transducers naming is the same as used before.

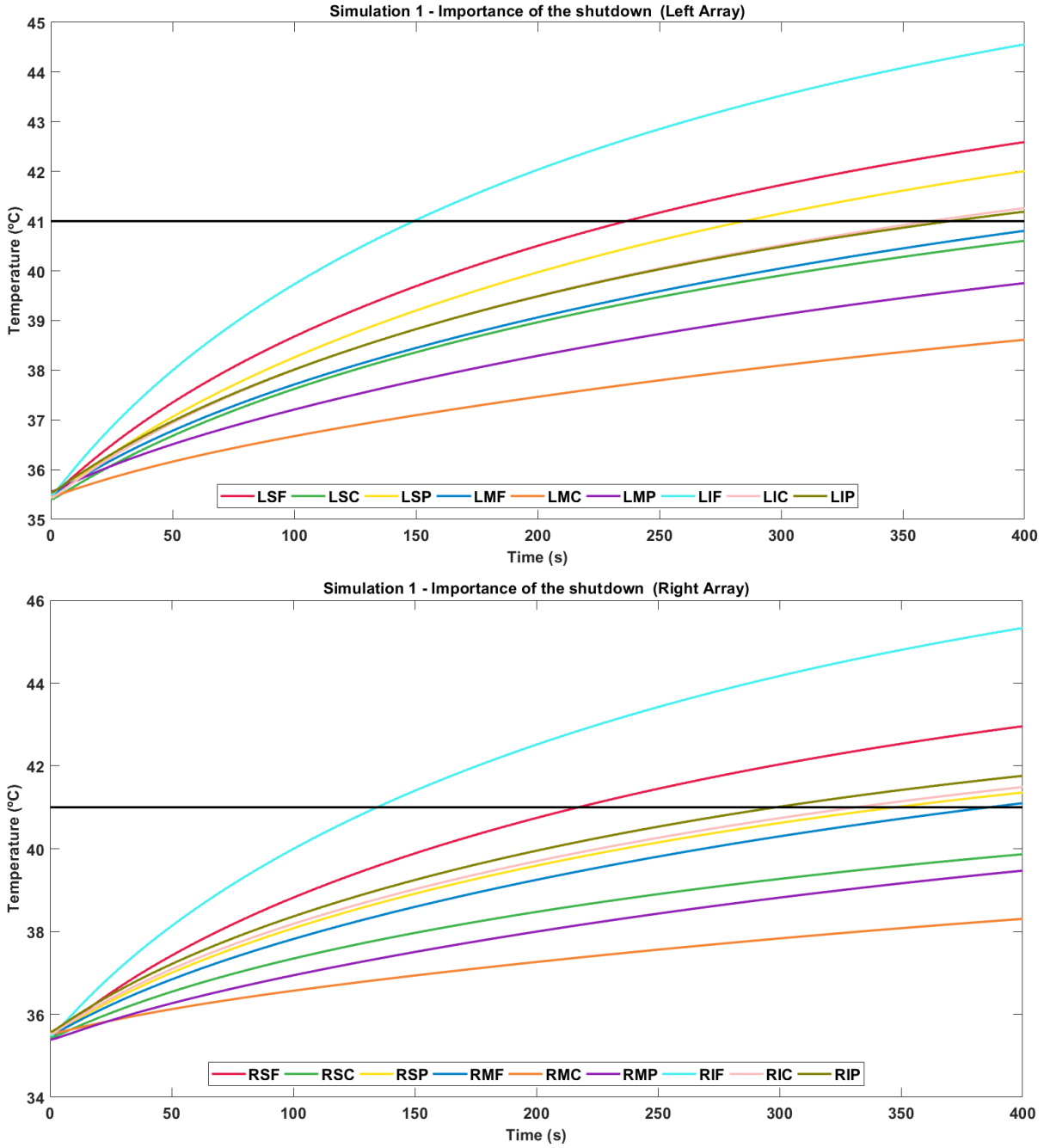

Figure 5.4: Average temperature variation as a function of time for the left (up) and right (down) arrays if the fields were always on (Simulation 1). Current is being injected in the AP and LR directions alternately. It is easily seen that several electrodes surpass the threshold of 41ºC (black line) in just 400 seconds. Transducers naming is the same as used before.

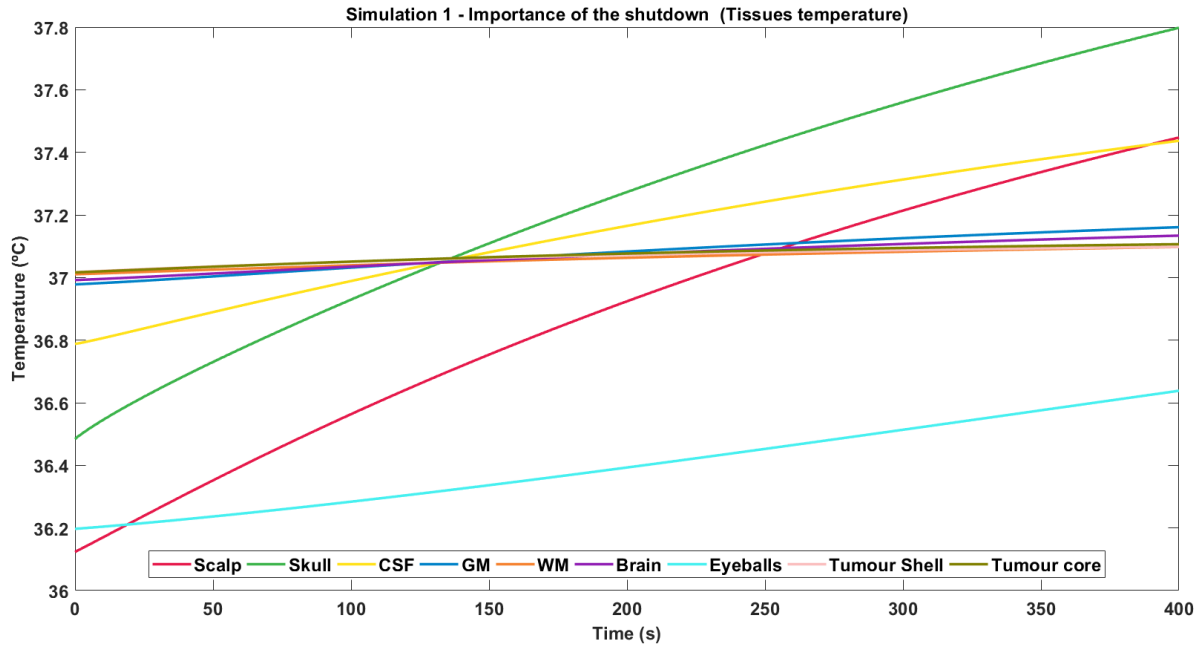

Figure 5.5: Average tissues temperature as a function of time. Scalp's temperature starts as the lowest because it is the only tissue in contact with the environment that is at 24ºC (Simulation 1). As the depth from the surface increases the temperature gradually augments reaching a value close to the blood's.

5.2 Simulation 2 - Model how Optune® works

Figures 5.6 and 5.7 show the temperature of each electrode as a function of time as Optune® alternates between the AP and LR arrays. It is clear that just one electrode controls the turning on and off of the device. From now on it will be referred as the Most Significant Electrode (MSE). For this situation in particular it is one transducer that is in the front array (F), superior row (S) and left position (L) (FSL).

As it might be expected it is the electrode where the injected current is the highest according to figure 5.1. In fact if the correlation between the injected current and the temperature that each electrode reaches at the end of the simulation is made one obtains a value of 0.63 and a p-value around 10^{-5} which indicates that these two values are significantly correlated. This is more noticeable comparing figures 5.1 and 5.8. This latter shows the temperature of each transducer at the end of the simulation.

Having these results it is now possible to study the duty cycle. After the first shut down that occurs at the time 105s and until the end of the simulation (295 seconds), the AP field was applied for 55s and the LR for 29s. These values indicate that the current is being injected in the front and posterior pads 37% of the time it could be on while this value decreases to 20% for the left and right pads. Overall, these values point out to Optune® is being used to treat GBM 31% of the time.

With this data, it is now possible to study if the thresholds presented in table 2.1 (page 8) are surpassed. The comparison with the limits defined by the FDA and by the IEC is not direct because both of these agencies define a time average of 10 and 6 minutes respectively. The simulation done was for 6 minutes and 40 seconds, but not all this range can be used because for nearly 100 seconds the fields were always being applied which correspond to the start of the

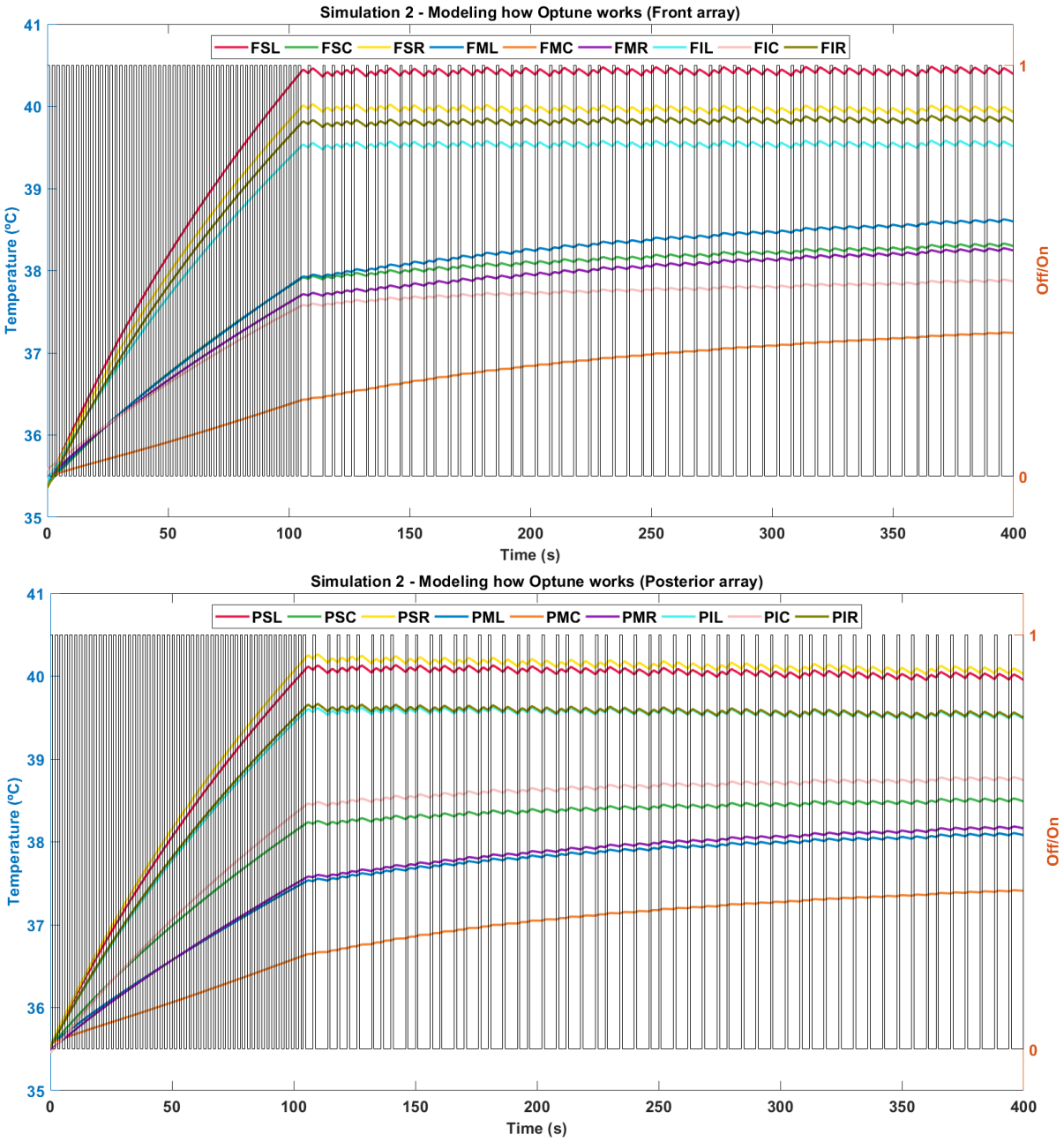

Figure 5.6: Temperature variation as a function of time for the front (up) and posterior (down) arrays (Simulation 2). As it can be seen the temperature (left y-axis) never increases above 40.4ºC. It is clear that just one electrode (FSL) controls the turning on (1 in the right y-axis) and off (0 in the right y-axis) of Optune®. In these plots when the device is on it means that the current is being injected in the AP direction. Transducers naming is the same as used before.

treatment and not to a representation of the treatment itself. Nonetheless, assuming that the remaining 295 seconds are a realistic representation of what actually happens, it is possible to extrapolate the results for higher times. Thus, equation (5.1) can be used to calculate the effective SAR (SAR_{eff}). In this formula On_{conf} refers to the fraction of time that each configuration is being applied, the SAR values are the ones presented in table 5.2 (page 50) and Δt_{conf}^{max} is the maximum time that each configuration can be applied (which corresponds to half the time of evaluation, $\Delta t_{evaluation}$).

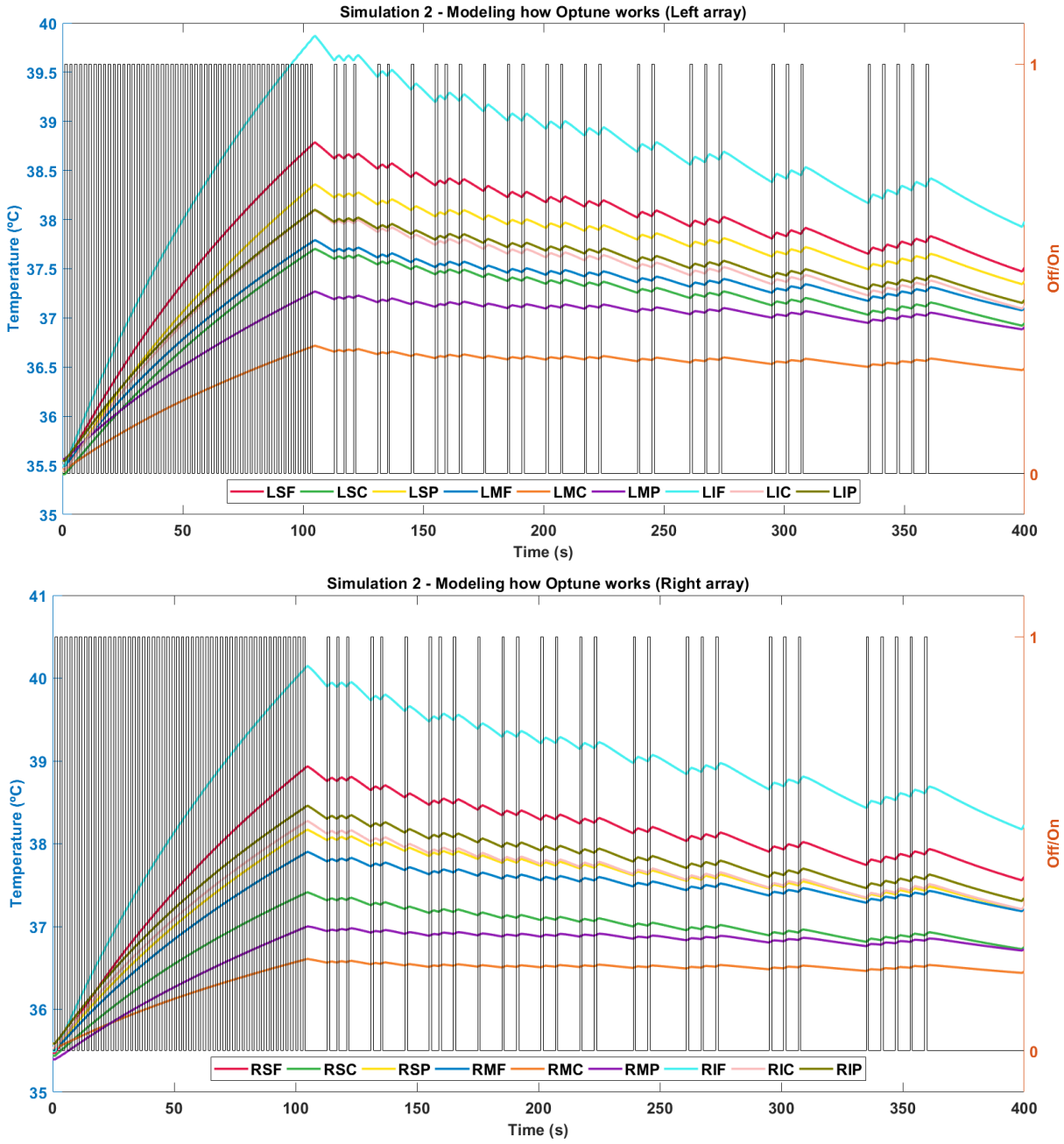

Figure 5.7: Temperature variation for the left and right arrays (Simulation 2). In these plots when the device is on (1 in the right y-axis) it means that the current is being injected in the LR direction. Transducers naming is the same as used before.

$$SAR_{\text{eff}} = \sum_{\text{conf}} \frac{On_{\text{conf}} \times SAR_{\text{conf}} \times \Delta t_{\text{conf}}^{\max}}{\Delta t_{\text{evaluation}}} = \sum_{\text{conf}} On_{\text{conf}} \times SAR_{\text{conf}} \times 0.5 \tag{5.1}$$

So in this case:

$$SAR_{\text{eff}}^{\text{FDA}} = \frac{0.37 \times 16.6 \times 5 + 0.20 \times 12.2 \times 5}{10} = 4.3 \text{ W/kg}$$
$$SAR_{\text{eff}}^{\text{IEC}} = \frac{0.37 \times 77.6 \times 3 + 0.20 \times 127.8 \times 3}{6} = 27.1 \text{ W/kg}$$

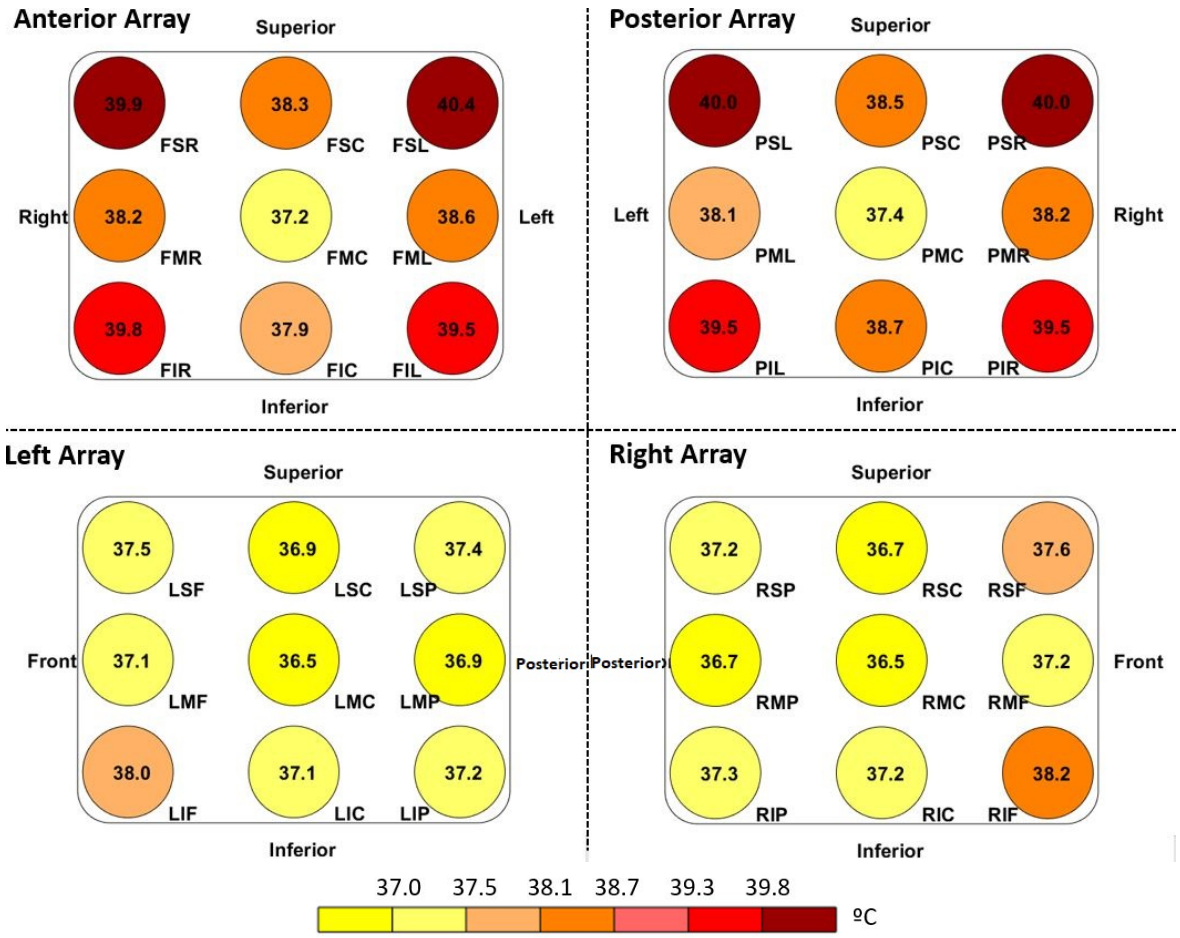

Figure 5.8: Final temperature of each electrode at the end of simulation 2. Transducers naming is the same as before.

The results for the effective SAR for this and for the remaining simulations is displayed in table 5.3 (page 50). The average temperature of each tissue as a function of time is plotted in figure 5.9. With this information, it was possible to calculate the CEM 43ºC for each tissue (table 5.4, page 51)

5.3 Simulation 3 and 4 - Study Optune®'s efficacy in different environments

The effects of changing in room temperature are here presented. For a temperature of 27.3ºC it was seen that the MSE remains the same and that Optune® first shuts down 94 seconds after the treatment had started. In terms of the duration of the applied current the AP field was on for 52 seconds of the 153 seconds it could have been (34%), while the LR was on for 29 seconds (19%) leading to an overall of 27%. The temperature variation for the front pad and for the tissues are shown in figures 5.10 and 5.11, respectively. When the environment temperature is 7.9ºC Optune® first shuts down after 164 seconds. The AP field was applied for 55 seconds (47%) and the LR for 51 seconds (43%). Overall, the device is on 45% of the time. The temperature for the front pad and for the tissues is presented in figures 5.12 and 5.13. For the remaining pads of both simulations the graphics are shown in figures A1 to A6 in the "Appendix" section.

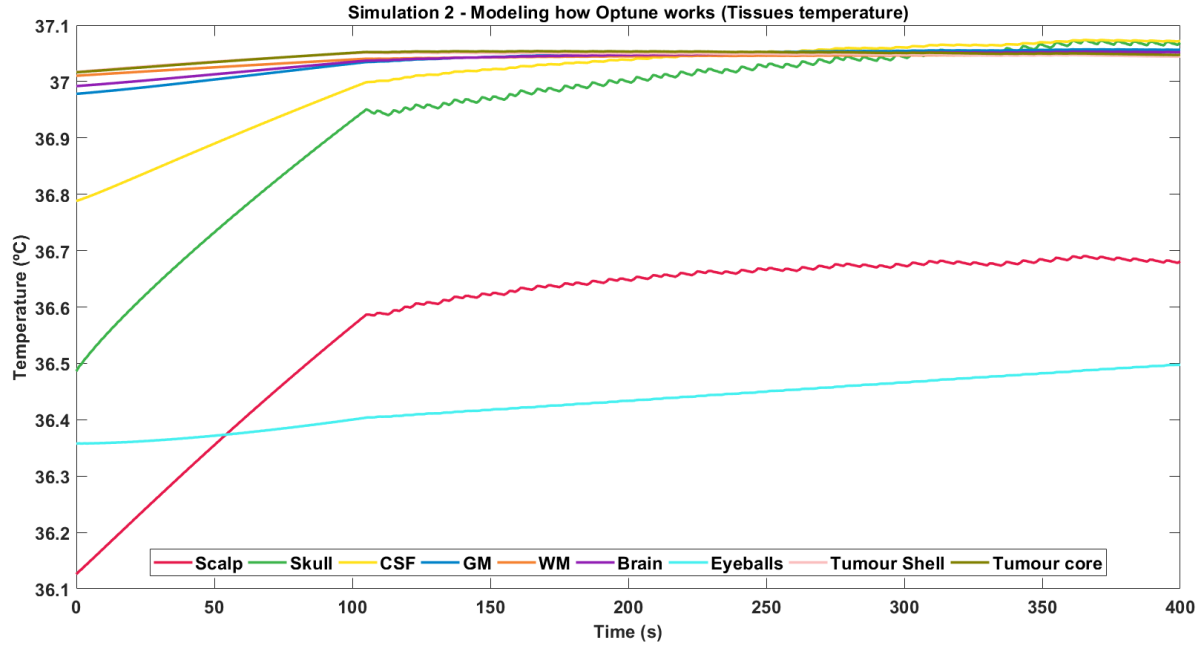

Figure 5.9: Average tissues temperature as a function of time. Scalp's temperature starts as the lowest because it is the only tissue in contact with the environment that is at 24ºC (Simulation 2). As the depth from the surface increases the temperature gradually augments reaching a value close to the blood's.

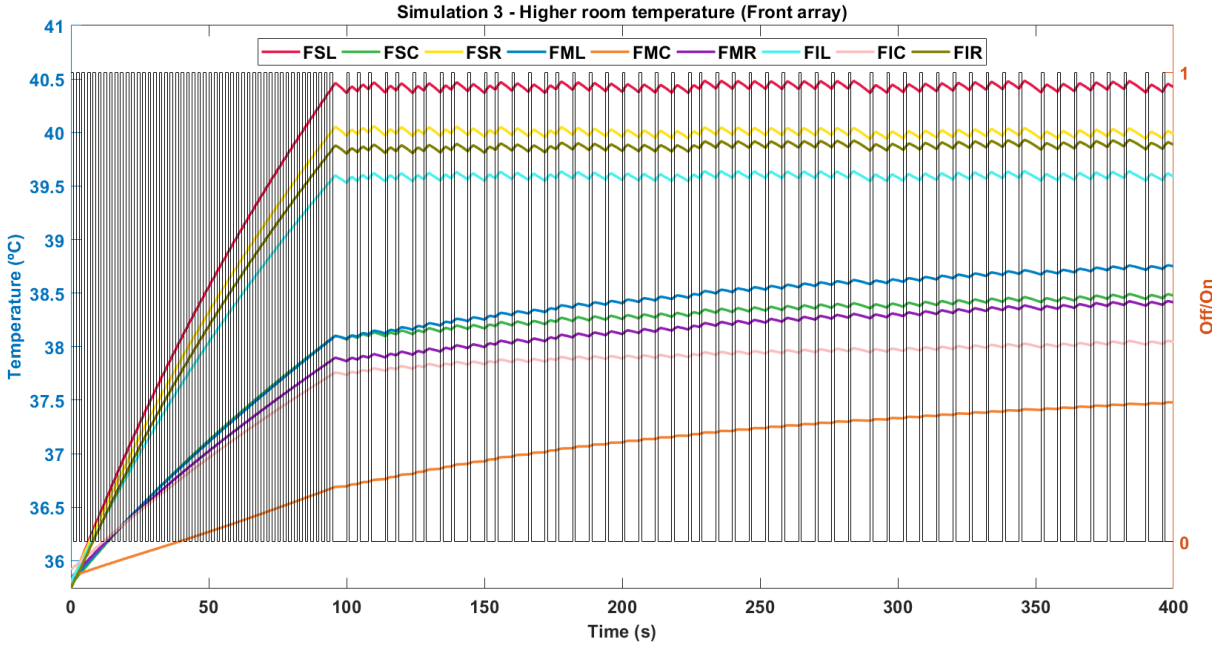

Figure 5.10: Temperature variation as a function of time for the front array when the room temperature is 27.3ºC (Simulation 3). As it can be seen the temperature (left y-axis) never increases above 40.4ºC (as it can be seen the MSE is the FSL). In this plot when the device is on (1 in the right y-axis) it means that the current is being injected in the AP direction. Transducers naming is the same as used before.

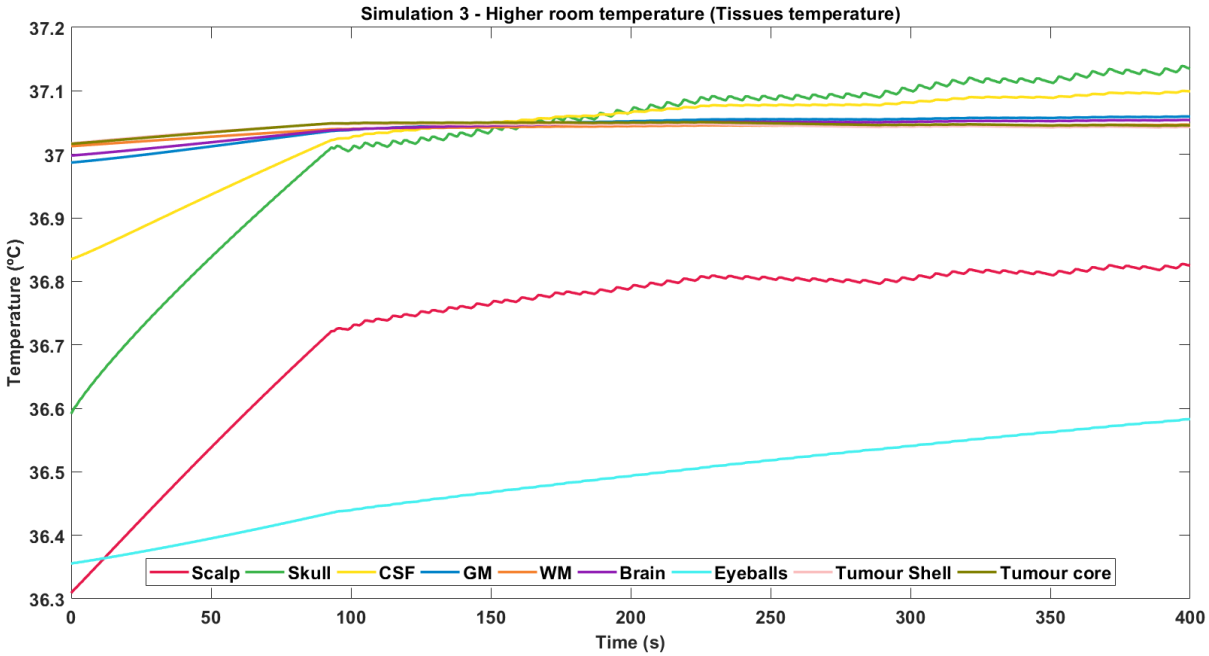

Figure 5.11: Average tissues temperature as a function of time. Scalp's temperature starts as the lowest because it is the only tissue in contact with the environment that is at 27.3ºC (Simulation 3). As the depth from the surface increases the temperature gradually augments reaching a value close to the blood's.

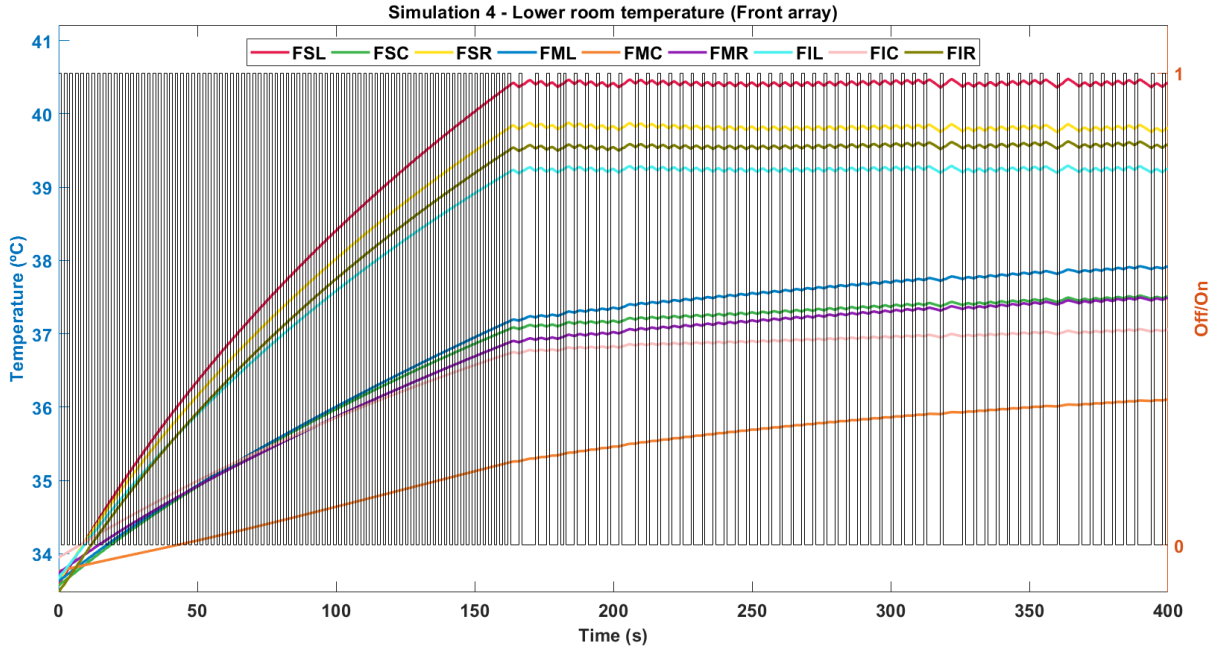

Figure 5.12: Temperature variation as a function of time for the front array when the room temperature is 7.9ºC (Simulation 4). As it can be seen the temperature (left y-axis) never increases above 40.4ºC (as it can be seen the MSE is the FSL). In this plot when the device is on (1 in the right y-axis) it means that the current is being injected in the AP direction. Transducers naming is the same as used before.

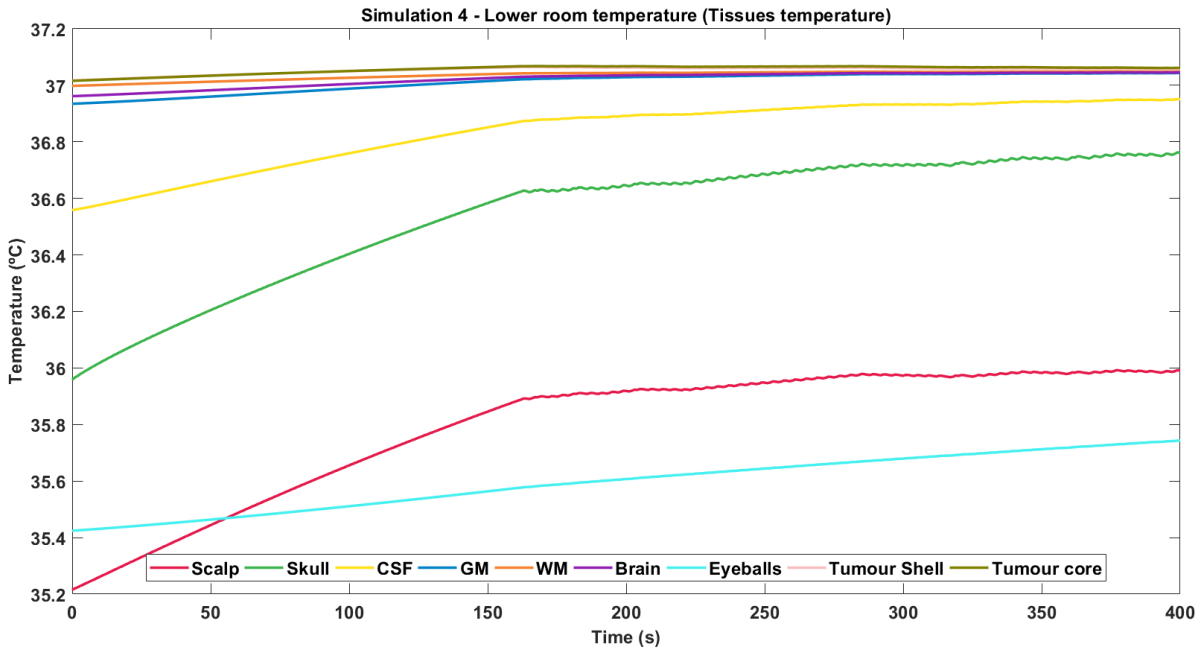

Figure 5.13: Average tissues temperature as a function of time. Scalp's temperature starts as the lowest because it is the only tissue in contact with the environment that is at 7.9ºC (Simulation 4). As the depth from the surface increases the temperature gradually augments reaching a value close to the blood's.

5.4 Simulation 5 - Half intensity, always on

When the potential difference between the arrays is halved, the current injected in each electrode is also halved, as expected. This corresponds to injecting 50% the current shown in figure 5.1 for each transducer. The electric field in the brain and in the tumour for this situation is shown in figure 5.14 for the same cut planes as in figure 5.2. The ATV and SAR values for each tissue are different compared to the previous simulations and so they were also calculated and are presented in tables 5.1 and 5.2, respectively (Simulation 5, page 50).

To calculate the effective SAR equation (5.1) was used, but now the sum had only one term because only one configuration (AP+LR) exists. Regarding Optune®'s duty cycle it was seen that it first shuts down 313 seconds after the treatment started and that the fields were applied for 62s out of the 86s possible (72%). As before, the results regarding the temperature variation of the pad that has the MSE (FSL) and of the tisses are shown in figures 5.15 and 5.16, while the temperature profile for the remaining pads are shown in the "Appendix" section (figures A7, A8 and A9).

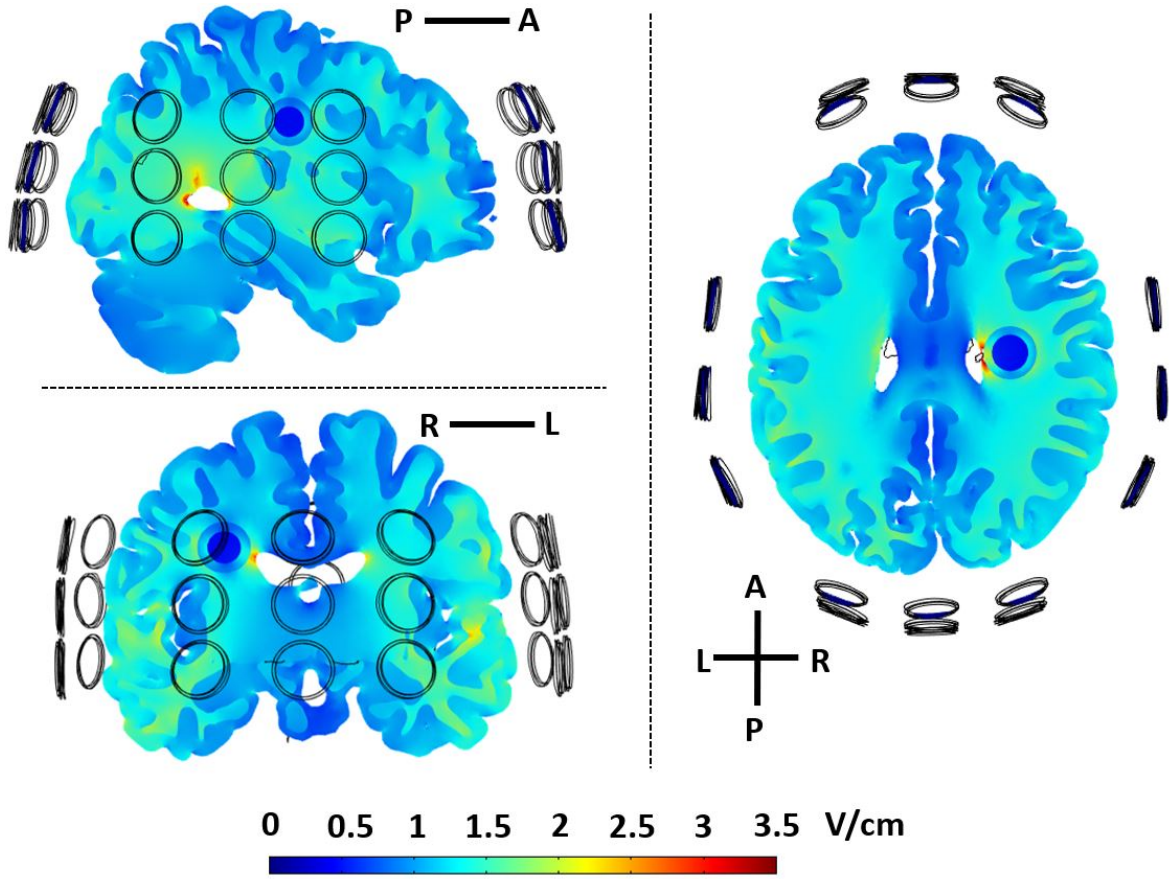

Figure 5.14: Electric field magnitude in the brain and in the tumour in a sagittal (left column, first row), coronal (left column, second row) and transversal (right column) planes when both AP and LR configurations are applied at the same time but with half the intensity comparing to the former simulations. Values greater than 3.5 V/cm are coloured as dark red.

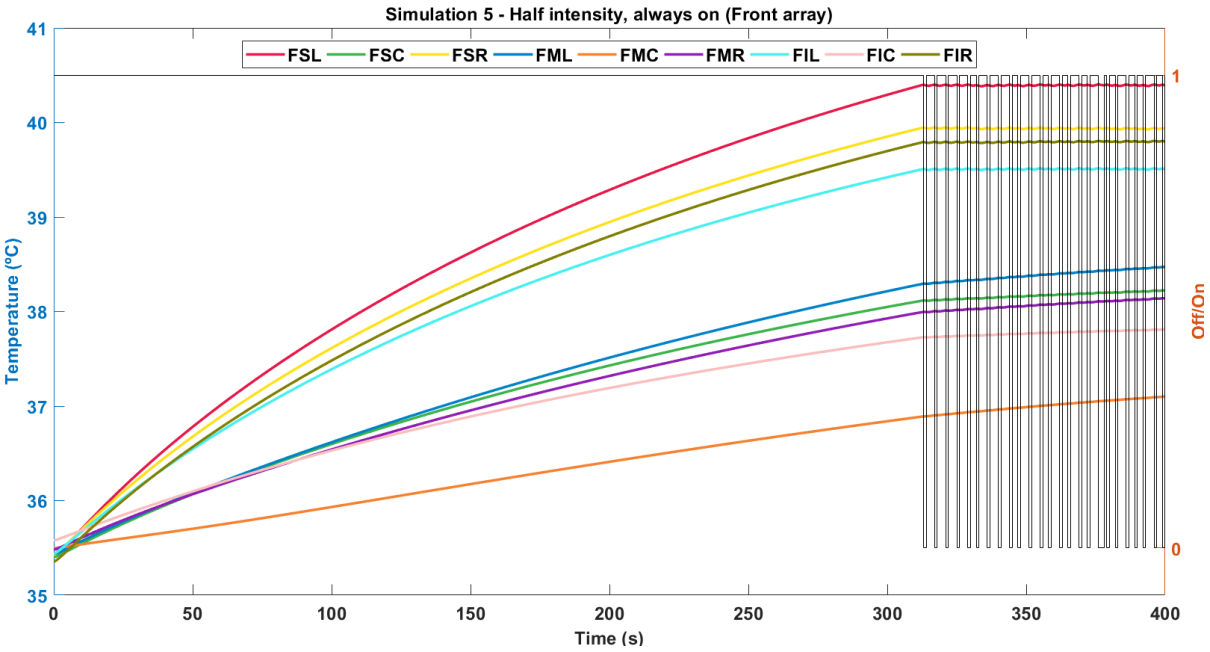

Figure 5.15: Temperature variation as a function of time for the front array when both configurations are applied at the same time, but with half the current injected (Simulation 5). As it can be seen the temperature (left y-axis) never increases above 40.4^{o}C (as it can be seen the MSE is the FSL). In this plot when the device is on (1 in the right y-axis) it means that the current is being injected in the both AP and LR directions. Transducers naming is the same as used before.

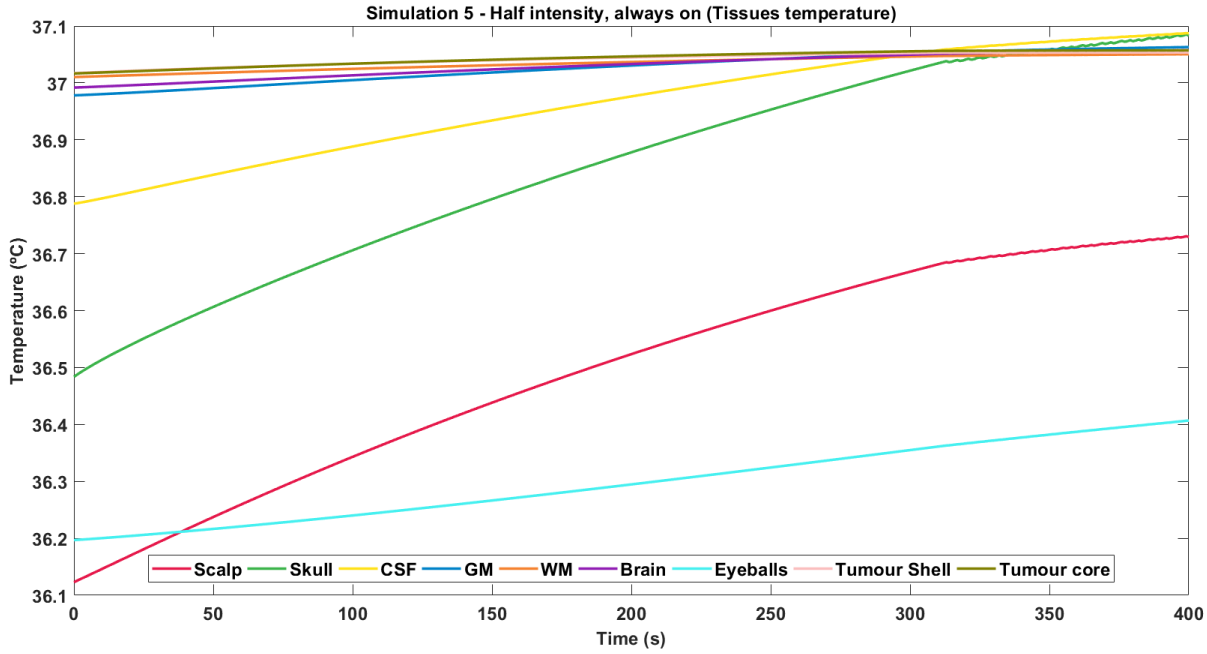

Figure 5.16: Average tissues temperature as a function oft time (Simulation 5). Scalp's temperature starts as the lowest because it is the only tissue in contact with the environment that is at 24ºC. As the depth from the surface increases the temperature gradually augments reaching a value close to the blood's.

5.5 Simulation 6 - Independent temperature sensors

Using independent temperature sensors showed very interesting results. As it was expected, the AP sensor was the first to reach the shutdown temperature (MSE: FSL), around 104 seconds after treatment had started. The LR sensor had its first shutdown 9 seconds later and the MSE for this situation was the RIF. This latter is one of the transducers where the higher current is injected considering only the LR configuration, according to figure 5.1. Regarding their efficacy in terms of time, the AP fields were applied for 55 seconds and the LR for 62. This corresponds to a 37% of time deliverying the current for the first and 43% for the second. The variation of the temperature for the arrays containing the MSE for each situation is shown in figures 5.17 and 5.18, respectively and tissues' temperature change over time in figure 5.19. Information about the other arrays is presented in figures A10 and A11.

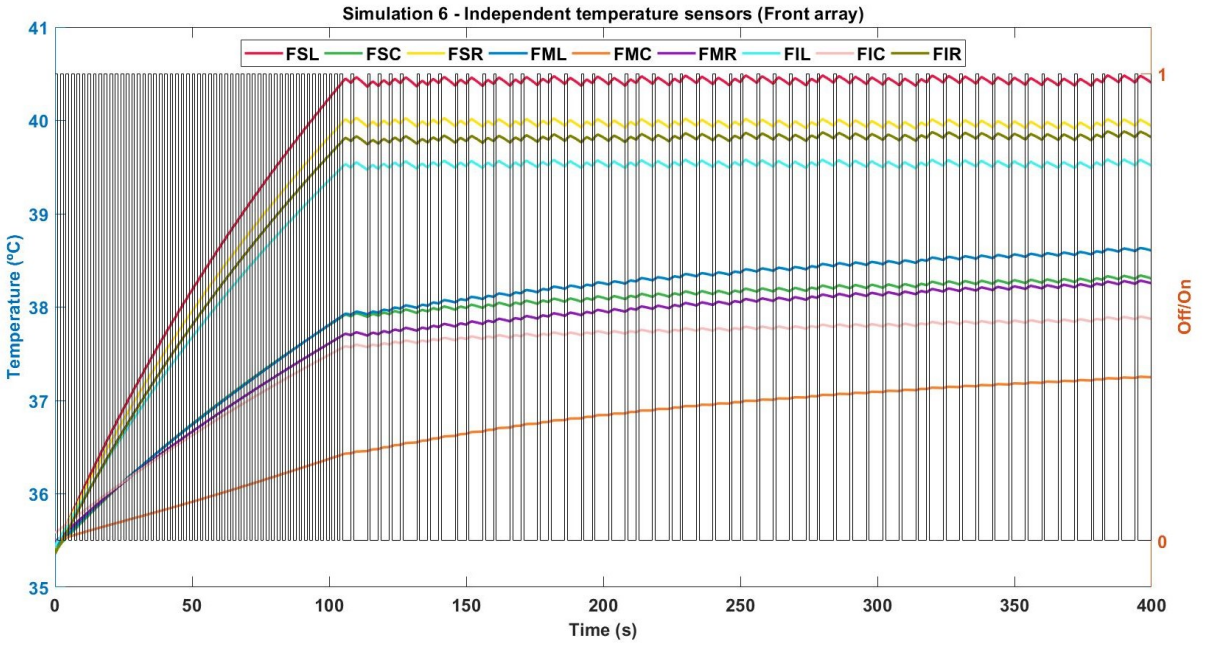

Figure 5.17: Temperature variation as a function of time for the front array when independent temperature sensors are used (Simulation 6). As it can be seen the temperature (left y-axis) never increases above 40.4ºC (as it can be seen the MSE for this configuration is the FSL). In this plot when the device is on (1 in the right y-axis) it means that the current is being injected in the AP direction. Transducers naming is the same as used before.

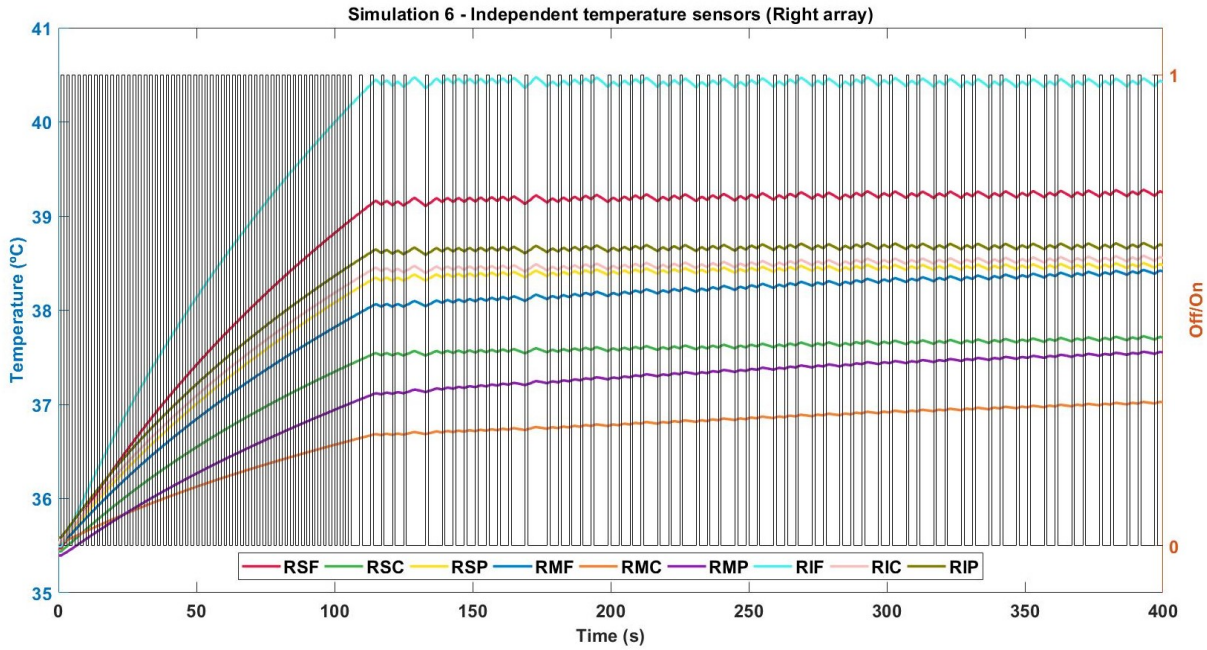

Figure 5.18: Temperature variation as a function of time for the right array when independent temperature sensors are used (Simulation 6). As it can be seen the temperature (left y-axis) never increases above 40.4ºC (as it can be seen the MSE for this configuration is the RIF). In this plot when the device is on (1 in the right y-axis) it means that the current is being injected in the LR direction. Transducers naming is the same as used before.

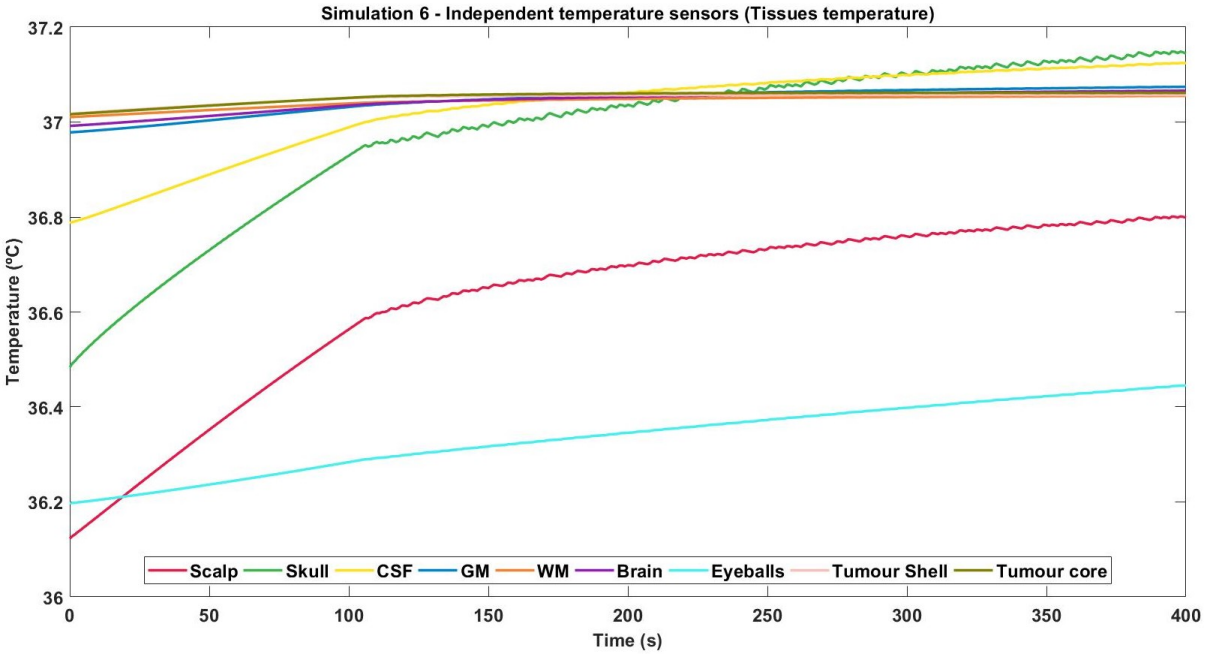

Figure 5.19: Average tissues temperature as a function of time (Simulation 6). Scalp's temperature starts as the lowest because it is the only tissue in contact with the environment that is at 24ºC. As the depth from the surface increases the temperature gradually augments reaching a value close to the blood's.

5.6 Simulation 7 - Current controller

Controlling the injected current at a transducer level rather than at the array level produced a very similar electric field in the brain compared to the one presented in figure 5.2 and thus it is not shown. However, through the ATV values (5.1, page 50) it is possible to demonstrate that there are some differences produced in each biological tissue. Figure 5.20 shows the potential that each electrode has to be at to inject 100 mA. The results allowed to conclude that the first shutdown occurs 162 seconds after the treatment started. The AP field was applied for 61 seconds (51% time efficacy), while the LR was on for 28 seconds (24%). Overall this gives a value of 37%. It is noteworthy that in this case, the MSE starts as the PIC, but a few seconds later changes to the PML (figures 5.21). Tissues temperature is shown in figure 5.22 and the temperature for remaining pads in figures A12 to A14.

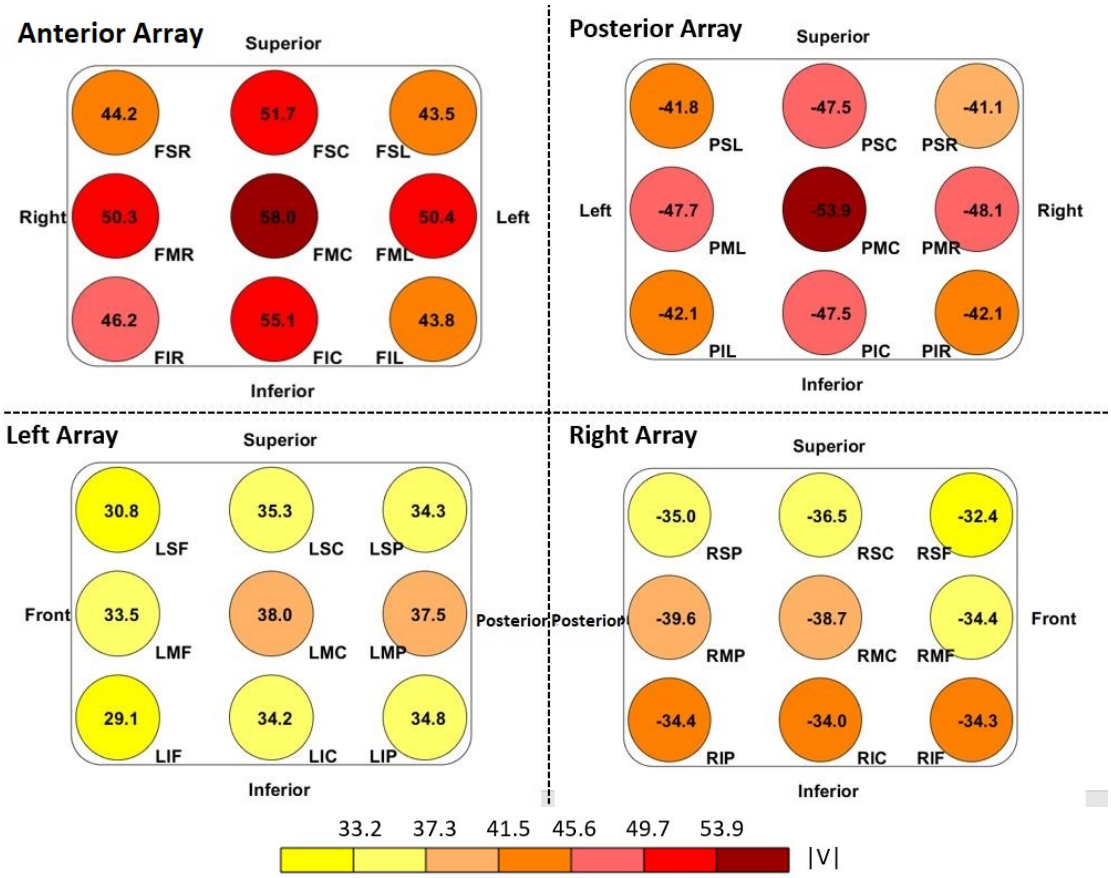

Figure 5.20: Potential of each electrode to ensure 100 mA per transducer.

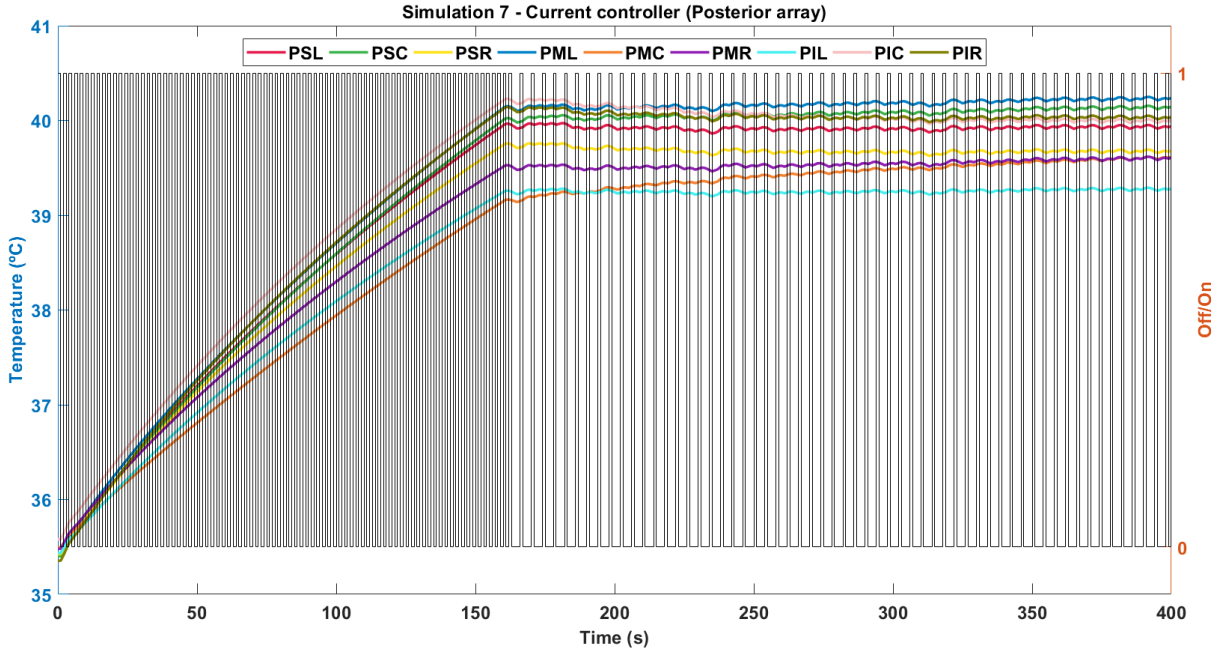

Figure 5.21: Temperature variation as a function of time for the posterior array when current is controlled at a array level (Simulation 7). As it can be seen the temperature (left y-axis) never increases above 40.4^{o}C (as it can be seen the MSE starts as the PIC but a few seconds later changes to the PML). In this plot when the device is on (1 in the right y-axis) it means that the current is being injected in the AP direction. Transducers naming is the same as used before.

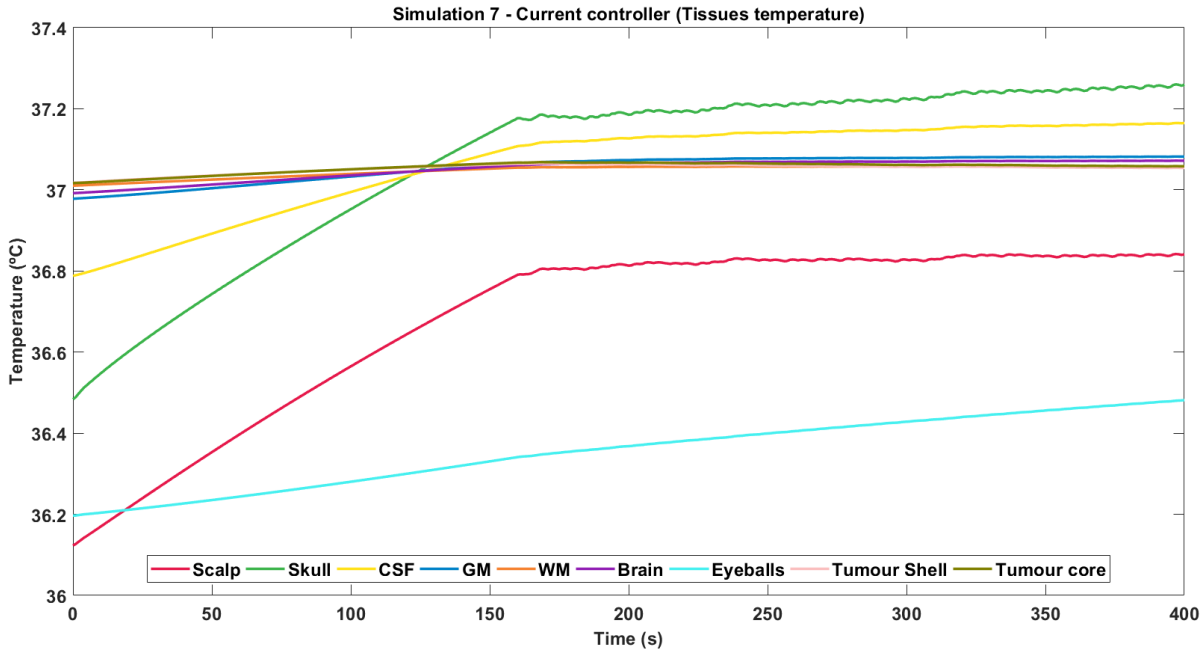

Figure 5.22: Average tissues temperature as a function of time (Simulation 7). Scalp's temperature starts as the lowest because it is the only tissue in contact with the environment that is at 24ºC. As the depth from the surface increases the temperature gradually augments reaching a value close to the blood's.

5.7 Additional data

In this subsection information that concerns all the simulations is presented, namely the tables regarding the ATV's, SAR in each tissue, effective SAR and CEM 43ºC values. Additionally, figure 5.23 plots the efficacy of every simulation normalized by the results of the standard one (simulation 2). For this latter, the efficacy is in terms of time that the fields are applied.

Table 5.1: ATV's for each tissue and each configuration considering three different thresholds: 1 V/cm (ATV1), 2 V/cm (ATV2) and 3 V/cm (ATV3).

Sim.	ATVx	Configuration	Scalp	Skull	CSF	Brain		Tumour		Eyeballs
						GM	WM	Shell	Core	
1 2 3 4 6	ATV1 (%)	AP	83.2	98.5	17.2	50.5	80.8	13.0	0	10.0
		LR	73.9	93.4	13.7	45.9	83.2	72.3	0	0
	ATV2 (%)	AP	33.1	76.3	0	0.1	2.3	0	0	0
		LR	33.2	66.0	0.2	1.1	7.7	8.1	0	0
	ATV3 (%)	AP	21.4	64.1	0	0	0.1	0	0	0
		LR	21.9	52.5	0	0	0.1	1.0	0	0
5	ATV1 (%)	AP+LR	88.2	99.8	11.7	51.1	94.8	50.7	0	0
	ATV2 (%)		44.8	87.9	0	0	0.5	0	0	0
	ATV3 (%)		25.5	73.1	0	0	0	0	0	0
7	ATV1 (%)	AP	82.8	98.4	18.8	52.3	81.7	13.6	0	8.6
		LR	72.4	92.7	13.6	45.6	82.2	71.6	0	0
	ATV2 (%)	AP	32.9	76.3	0	0.2	2.7	0	0	0
		LR	32.7	64.8	0.2	1.3	7.8	8	0	0
	ATV3 (%)	AP	21.7	63.8	0	0	0.2	0	0	0
		LR	22.1	51.4	0	0	0.2	0.9	0	0

Table 5.2: Average SAR values for each tissue, for the whole head and for the 10g cube that contains the point where the electric field magnitude is the highest for each configuration. All values are in W/kg.

Sim.	Conf.	Scalp	Skull	CSF	Brain		Tumour		Eyeballs	Head	Head 10g
					GM	WM	Shell	Core			
1, 2, 3 4, 6	AP	32.5	30.6	12.2	2.7	2.0	1.4	1.2	8.8	16.6	77.6
	LR	22.8	20.9	10.5	2.8	2.4	4.6	3.7	0.8	12.2	127.8
4	AP+LR	19.8	15.3	10.7	2.6	2.1	2.6	2.3	3.6	10.5	43.2
7	AP	33.1	32.6	12.6	2.8	2.0	1.4	1.2	8.5	17.9	127.2
	LR	22.7	21.1	10.4	2.8	2.4	4.7	3.7	0.7	12.6	135.3

Table 5.3: Effective SAR and average head temperature for each simulation according to the definitions made by the FDA and the IEC.

Simulation	FDA		IEC
	SAR (W/kg)	T (ºC)	SAR (W/kg)
1	14.4	37.4	102.7
2	4.3	37.0	27.1
3	4.0	37.0	25.3
4	7.0	36.7	48.0
5	7.6	37.0	31.1
6	5.7	37.0	41.8
7	6.1	37.0	48.7

Table 5.4: CEM 43^{o}C values for every tissue for one treatment day and for each simulation. When no value is presented it means that the cylinder defined by the MSE does not pass by that tissue. All values are in minutes.

Simulation	Scalp	Skull	CSF	Brain		Tumour		Eyeballs
				GM	WM	Shell	Core	
1 (Volume)	0.49	0.79	0.48	0.33	0.30	0.30	0.31	0.16
1 (Cylinder)	6715.90	145.65	0.86	0.43	0.30	–	–	–
2 (Volume)	0.17	0.29	0.29	0.29	0.28	0.28	0.28	0.13
2 (Cylinder)	12.60	3.47	0.45	0.33	0.29	–	–	–
3 (Volume)	0.21	0.32	0.30	0.29	0.28	0.28	0.28	0.15
3 (Cylinder)	12.13	3.32	0.44	0.33	0.28	–	–	–
4 (Volume)	0.07	0.19	0.25	0.28	0.28	0.29	0.29	0.05
4 (Cylinder)	17.82	4.95	0.48	0.34	0.29	–	–	–
5 (Volume)	0.18	0.30	0.30	0.29	0.28	0.28	0.29	0.12
5 (Cylinder)	11.61	3.00	0.43	0.32	0.29	–	–	–
6 (Volume)	0.20	0.32	0.31	0.29	0.28	0.29	0.29	0.12
6 (AP cylinder)	12.76	3.53	0.45	0.34	0.29	–	–	–
6 (LR cylinder)	4.58	1.27	0.47	0.30	0.28	–	–	–
7 (Volume)	0.21	0.38	0.33	0.30	0.29	0.29	0.29	0.13
7 (Cylinder)	8.99	5.79	0.39	0.32	0.30	–	–	–

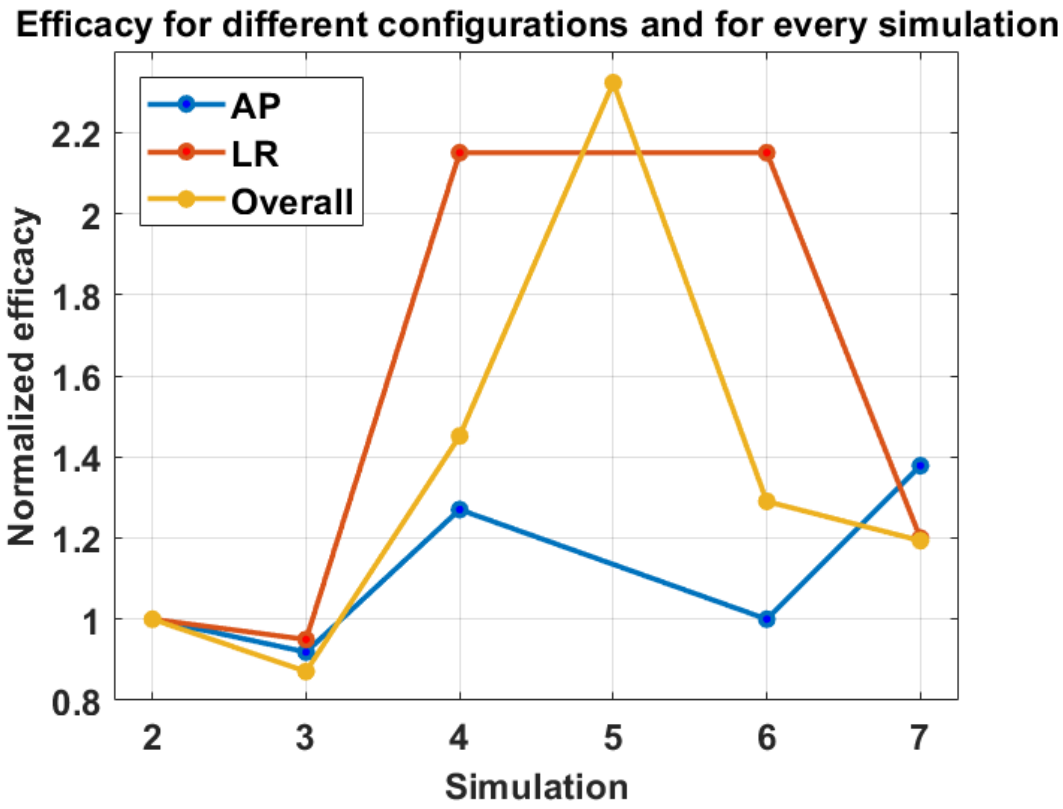

Figure 5.23: Efficacy of every simulation normalized by the results of simulation 2. Simulation 2: Modeling how Optune® works; Simulation 3: Room temperature at 27.3^{o}C; Simulation 4: Room temperature at 7.9^{o}C; Simulation 5: Half intensity, both fields applied; Simulation 6: Independent temperature sensors; Simulation 7: Current controller at the transducer level. The efficacy values are in terms of the time that the fields are being applied in each case.

Chapter 6

Discussion

The conclusions obtained in Chapter 3 showed a good agreement between the values given by COMSOL and those obtained solving the analytical solutions. Thus a significant deviation regarding the real values is also not expected for the simulations performed with the realistic head model.

6.1 Importance of the shutdown

It is clear that the temperature increase is an important limitation of the efficacy of TTFields. In fact, 400 seconds after the treatment started there are some transducers that would have reached values higher than 44^{o}C and by the behaviour showed in figures 5.3 and 5.4 it can reach values even higher than this. A more in-depth study about this matter showed that the maximum temperature for the AP transducers can be as high as 55^{o}C and for the LR around 47^{o}C when a steady-state is reached (results not shown here). This implies that tissues temperature can also increase by an excessive amount and thus the Joule heating effect can be very harmful. Figure 5.5 shows that less than six and a half minutes (400 seconds) are enough to increase the scalp's and skull's average temperatures by more than 1^{o}C. However, looking at the average temperature can hide the existence of hotspots since a higher increase is expected near the electrodes where the electric field is high. An evaluation using the cylinder defined by the MSE showed average values higher than 44^{o}C for the scalp, around 41.6^{o}C for the skull and approximately 38^{o}C for the CSF (data not shown). This corresponds to CEM 43^{o}C values that in somes cases largely surpass the thresholds presented in table 2.2, which clearly illustrates the need of controlling the temperature and shutting down the fields when the temperature reaches a specific threshold value, although why it is 41^{o}C is unclear and not reported by Novocure^{TM}. Curiously, the thermal damage, measured using CEM 43^{o}C, in the brain when the fields are always being applied is just a little above the values obtained when the temperature is controlled. This will be discussed in more detail further ahead.

6.2 The electric field

Figure 5.1 can be seen as a representation of how the current is distributed across the transducers for the standard way of working of Optune®. It is noteworthy to verify that each array behaves as an isopotential surface and consequently there are edge effects. These are more pronounced

the higher the potential, which is verified if one makes a comparison between the LR (lower absolute potential) and the AP (higher absolute potential) pads. This leads to the varied current distribution seen for each transducer. Additionally, the fact that tissues' thickness underneath each electrode can be very different (thus different impedance) also contributes to this diversification. When the electric field produced by these currents is analysed a highly non-uniform distribution is obtained (figure 5.2), which is explained by the heterogeneous current distribution, the complex shape of the head and the different dielectric properties of the tissues that are part of it as explained in [14, 44]. A higher electric field magnitude is expected near the active transducers (i.e., near those where the current is being injected) which was observed but not shown here. In tissues with low electric conductivity such as the skull these fields reach their maximum value at the regions where the applied current is perpendicular to a tissue interface. This effect can be very well observed in figure 5.2 for the LR configuration where the magnitude was enhanced in the regions close to the ventricles where a high conductivity change is seen due to passage of current from the ventricles (considered to be filled with CSF with $\sigma = 1.79$ S/m) to the WM ($\sigma = 0.12$ S/m) [14]. The physical phenomenon behind this effect is a secondary field generated by an accumulation of electric charges at tissue interfaces that depends only on the ratio of the conductivities of the two adjacent tissues and it is proportional to the strength of the normal component of the applied field for purely resistive tissues. This is the case because for the parameters used the following expression is true $\sigma \gg \omega\epsilon_r\epsilon_0$ (σ is the tissue conductivity, ω the angular frequency, ϵ_r the relative permittivity and ϵ_0 the vacuum permittivity) [14, 44]. The effects of the directionality of the fields in the tumour can also be seen in this figure. This effect is more clear for the LR configuration due to the electric field it produces at the tumour site.

A more detailed analysis of this data (table 5.1, Simulations 1, 2, 3, 4 and 6) showed that around 13% of the tumour shell is above 1 V/cm when the AP field is applied while this value increases to 72% for the LR configuration. Although the magnitude does not reach values higher than 2 V/cm for the first configuration, for the latter around 8% of the volume is found above this threshold and 1% above 3 V/cm. Despite the fact that the AP configuration only leads to a relatively small electric field magnitude in the tumour for this particular head model its importance is explained by the in-vitro experiments made by Kirson et. al [15] where the application of the fields in two perpendicular directions showed to affect more tumour cells, that are randomly aligned, enhancing the results by 20% compared to when only one direction is applied. Finally, it is also noteworthy the fact that the electric field magnitude in the necrotic core being quite low due to its high conductivity. Still concerning table 5.1 one can conclude that both configurations induce fields significantly higher than 1 V/cm in practically all biological tissues. For the brain, in particular, this value is high compared with what is seen in stimulation techniques such as in tCS and tDCS where magnitudes around 0.2 V/m and 0.5 V/m, respectively, are enough to affect neural modulation [64, 65], but it is comparable to those used in TMS where values in the order of 1 V/cm in the brain can affect neuromodulation and also act as a neurostimulator [66, 67]. However, the frequencies used are very different. In TMS, for example, frequencies as low as 3 kHz are employed while for TTFields, and in particular, for GBM, a 200 kHz frequency is used. For this latter value, the membrane is not able to depolarize and thus there is not stimulation [44, 68]. Regarding non-mitotic effects of the electric fields in the scalp, skull, CSF and eyeballs there is not much described in the literature. The study of Stupp et. al [18] reported that 3% of the 116 patients treated with just TTFields suffered from severe (grade 2)

haematological consequences which may be an indicator of the existence of some problems at the bone marrow level although there is a lot more investigation that should be done to corroborate these findings. However, it is important to bear in mind that these fields are blind in regards to which tissues they affect. This means that they will affect the mitotic process in healthy tissues and in blood vessels more or less in the same manner they do it in the tumour, although the optimal frequency to treat GBM may not be the one that is more efficient to affect the proliferation of the cells of the scalp or of the skull, for example. This can be problematic in several ways because if the doubling times of healthy and tumour tissues are similar (for example the glioma cell lines have a doubling time of 24 hours [8], while for the skin some studies report 62.5 hours [69] although it can be lower) their protective role can be compromised and even affect the electric field distribution if an agglomerate of dead cells happens to occur.

Thus it is important to try to minimize the electric fields in the healthy cells while increasing it on the tumour. When the electric field in the head tissues was changed in simulation 5, all the ATV values (table 5.1) for the scalp and the skull were enhanced compared to the previous case which can be explained by the field produced by the two configurations being additive and these being the two tissues closer to the transducers. As the distance from the head surface increases, these fields can still produce an intensity of at least 1 V/cm in the different tissues, but because the currents were halved they are not strong enough to reach 2 V/cm in the more internal tissues. Regarding the necessary threshold in the tumour site, around 51% reached the therapeutical limit of 1 V/cm which indicates the potential of the combined configuration if the electric field in the healthy tissues can be considered to be harmless. In the case of simulation 7, the ATV values were very similar to the ones obtained when the current was controlled at the array level and so the same conclusions drawn before apply to this case.

As mentioned before, there are not any problems reported in the literature about the impact of these fields in healthy cells mitosis, maybe because it is not relevant or maybe because a time longer than the median survival rate is necessary for its consequences to become perceptible. Either way, one interesting point that might help to enhance the electric field in the tumour and decrease it in other tissues is using the same approach that is currently used in TMS that involves indirectly applying these electric fields through a magnetic field based on Maxwell's equations. Of course that there are several technical problems that should be solved first like the coil size, how to apply it in a continuous way and for such long periods of time, how should the device be so it can be carried by the patient, the fact that it is much more difficult to stimulate deep targets, among many others.

6.3 Optune®'s duty cycle

The analysis of Optune®'s duty cycle showed very surprising results. First of all, it is important to note that the efficacy obtained for each simulation could change if more time was simulated. Simulation 5 for example had a high effectiveness because it took longer to reach the first shutdown and so there was not much time to evaluate the on and off process. Nonetheless, the results obtained should give an idea of how the efficacy in terms of time applying the fields changes compared to the standard simulation (Simulation 2), to have an insight of what are the main features that can be improved to obtain a higher response rate to this therapy. The importance of maximizing the time during which TTFields are used to treat GBM was demonstrated

in the very first few papers about this technique by Kirson et. al [15] that proved that cells that were subjected to these electric fields could recover their doubling time few hours after they were shut down and confirmed in clinical trials by Kanner et. al [4] that showed that a high daily usage (at least 18 hours) significantly improved the results.

It is noteworthy that in almost all the simulations performed it is just one electrode that controls if Optune® is applying the fields or not. For this specific head model, this transducer is located at the front array (FSL) and so it is one of the responsible to produce the AP field. It is also the electrode where the injected current is the highest. However, this configuration is not the one that contributes the most to arrest cell proliferation, because as it was discussed the LR configuration is capable of producing an electric field in the tumour that can reach values as high as 3 V/cm. The problem is that it does not seem to be a pattern that can explain when the LR fields are applied which increases the uncertainty of the outcome. This unpredictability is even higher in practice if it is noted in figure 5.23 that a higher room temperature decreases the time that Optune® is on and a lower temperature augments it which indicates that treating the tumour is highly dependent on where the patient is throughout the day. In fact, the data obtained suggests that people that are being treat with TTFields should be in environments where the temperature is low. Of course that it has to be a trade-off between the efficacy improvement and the discomfort caused by the cold temperatures. One solution that might be helpful is to develop a special device, perhaps a helmet that facilitate the control of the temperature of the head. Additionally, and if this is not already implemented in Optune®, incorporating a time counter for each configuration might also be useful to get a clear idea of how long the fields are applied as a function of the daytime.

Another way to improve this technique is using independent temperature sensors (simulation 6) that has showed to not decrease the time that the AP fields are on and, at the same time, increase the LR's which might be a good addition to Optune® if the improvements seen in clinical trials are good enough to compensate an increased time applying the electric fields. Additionally, using current controllers (simulation 7) at the transducers levels also demonstrated improvements in the results while not changing significantly the electric field produced in the healthy tissues nor in the tumour (see table 5.1). Ultimately one can think that in the same way that adding more current controllers would lead to better results, maybe having the same number of independent temperature sensors as electrodes would also have the same effect. Of course that adding so many controllers and sensors is an idea that might have some drawbacks and be very cumbersome because it implies more regular verification tests, extra costs, among others. Lastly, simulation 5 intended to approximate how Optune® works to an hypothetical situation. Although the overall results showed a very high efficacy in terms of time that this configuration is on the fact that the elecric field does not reach 2 V/cm in the tumour might be a problem and further investigation should be carried to evaluate this and the impact of the high electric field in the superficial tissues along with the benefits of the lower fields in the deepest ones. The sum of the fields by itself does not increase the number of directions in which the electric field is applied. In fact, because this quantity is vectorial there is only one effective direction, given by the sum of the AP's and the LR's directions. One interesting point to analyse is applying this configuration but intentionally change the relative phase of the AP and LR fields to specific values so that more directions are included.

In conclusion, compared to the standard way of work the results obtained can be considered a principle of proof that a version of Optune® that controls the current at the transducer level, that has independent temperature sensors, one for each configuration, working independently and that works at low temperatures may be beneficial. Despite these conclusions, all these changes should also consider the impact caused in the other techniques that are used to treat the tumour like chemotherapy.

6.4 Tissue safety and damage

All the results obtained regarding electric safety and thermal damage were evaluated using SAR and CEM 43^{o}C. However, it is important not to forget that these were the quantities chosen because a better metric is lacking to evaluate TTFields damage. In fact, SAR was developed to be used in MRI for indirectly studying tissues heating due to the applied pulses for a typical diagnostic session that has a time duration in the order of the minutes for brain imaging [70] and not for a treatment that has a time extent of more or less 18 hours per day and is applied practically every day. In fact, in TTFields the electric field is the base of the treatment and thus it is not possible nor desirable to decrease the SAR values just to respect the thresholds because that might imply not to treat the tumour at all. Thus, whether the conclusions derived from the values obtained using this quantity should be applied to TTFields or even to other techniques besides MRI must be investigated. This measure is valid for pulses with a frequency between 10 and 400 MHz, while TTFields work range is between 100-300 kHz. Although it is known that for frequencies higher than 100 kHz thermal problems due to the absorption of the photons by biological tissue start to become relevant [71], there is not any study that concluded that this metric or the thresholds defined by the different agencies are valid throughout all the radiofrequency range. In fact, if SAR can be used for TTFields, new thresholds should be defined to account for the need to maximize the application of these electric fields.

On the other hand, CEM 43^{o}C is a parameter developed especially for hyperthermia treatments where a typical session may last around one hour. As previously mentioned, this empirical metric was developed based on in-vitro studies [30] and thus it is important to know its limitations. First of all, its applicability was only tested for a temperature range between 39^{o}C and 57^{o}C and consequently its validity outside this interval is unclear. Furthermore, the value of R can and should be tissue and species dependent which can largely influence the results. Also, it is not easy to perform the summation of equation (2.1) because the temperature can vary within the tissue and using an average value can hide some hotspots and can even depend on the measuring device. Over the past few years, there has been some discussion concerning the utility of CEM 43^{o}C to measure thermal damage in hyperthermia. There are some authors that recognize the lack of other thermal metrics, but still consider that this is not the most suitable to be used. The fact that this formula does not consider the reversible reaction of the total damage nor the difference of the thermal sensitivity depending on the pH and the high variability of the results depending on how the experiment is performed are some reasons pointed out by van Rhoon [72]. To make it worse, the thresholds for thermal damage vary widely depending on how the damage is evaluated, as seen in [31, 32].

All of these constraints imply that the results here presented should be take into consideration all these limitations and the conclusions here drawn have to be corroborated with data

from clinical trials. If indeed these metrics can be used and the thresholds are surpassed then another set of questions have to be discussed. For example, are the treatment outcomes worthy compared to the damage that is being done? Considering the low survival-rate that characterizes glioblastoma do the short term consequences severely deteriorate the life of the patient? For those who can survive longer, will the long-term consequences affect drastically their quality of life? On the other hand if these quantities are not satisfactory to evaluate TTFields therapy then an appropriate way to measure the combined effects of the electric fields and the temperature increase should be developed to compare different treatment methodologies including those done here (using independent sensors, current controlled at the array level or at the transducer level, etc.).

6.4.1 Electric safety

The SAR values for each tissue are summarised in table 5.2. As expected, the values vary depending on how and how much current is injected in each transducer. Because the primary electric field is higher close to the active electrodes the SAR values are also expected to be higher at the more superficial tissues, despite the existence of a secondary electric field that has a limited impact and thus does not significantly affect the results.

When the average values obtained for each simulation (table 5.3) are compared with those defined by the international agencies there is one point that it is transversal to all the tests done: the thresholds are always surpassed. In the case of simulation 1 higher SAR values were expected because the fields are always on, which leads to a higher rate of temperature increase in the head compared to the other situations. If the simulation lasted longer this value could increase even more and eventually exceed the limit of 38^{o}C defined by the FDA. Of course that this is just one more example of the importance of shutting down the fields. On the other hand, for different ambient temperatures (simulations 3 and 4) higher SAR values are expected when the room temperature is lower because the fields are applied during more time which is exactly what was seen. In simulation 3 it was observed that the SAR was around 4 W/kg that is somewhat close to what is permitted by the FDA (3.2 W/kg). This indicates that the limits imposed by this agency might be respected if the environment temperature is higher than 27.3^{o}C and the other parameters are fixed or, in other words, if the fields are applied less time than what was seen for this simulation. Clearly, this is one more example that if SAR is used as a metric then the thresholds should be redefined.

When the electrodes' potential is halved (simulation 5) the SAR values increased compared to the standard situation (simulation 2) because both fields are applied at the same time and thus the electric field produced by each configuration is additive, but also because this simulation had a very high time efficacy. It is interesting to compare the results of this simulation with those of when the room temperature is lowered because the FDA values are higher for the first, but the IEC's are higher for the second. This is a consequence of two factors: 1) although the intensity of the current is lower, Optune® is on during more time which leads to a higher SAR value according to the FDA for simulation 5; 2) the SAR defined by the IEC considers a more local measurement and the way it was calculated in this project was by defining a cube containing the point where the electric field was the highest. Because this field is proportional to the square of the applied voltage this leads to a higher value for simulation 4 and consequently to a higher local SAR. With regards to the situation when independent temperature sensors are used (simulation

6) the results showed increased SAR values compared to the standard simulation for the same environmental conditions (simulation 2) which is justified by the fact that the LR field is applied during more time while the AP efficacy did not change. Lastly, changing the way that the injected current is administrated (simulation 7) also led to higher SAR values because the time the fields were applied is higher.

One point that should be noted is that although the SAR values vary across simulations the head average temperature is practically always the same and near the initial temperature of 36.7ºC. This is a result of applying locally the fields which can hide the existence of some hotspots as it is discussed in the next section. In the case of TTFields, having the two fields applied simultaneously showed to be the configuration that increased the SAR the most according to the FDA, while controlling the current at the transducer level led to the highest SAR values in line with what is defined by the IEC. It is important to note that it may be beneficial and even desirable to increase the SAR values as much as possible to treat GBM.

6.4.2 Thermal damage

The thermal damage was evaluated using two different CEM 43ºC: the average in the whole volume for each tissue and the average value within a cylinder defined by the MSE, both for one treatment day. This last approach was done to evaluate possible hotspots that might occur underneath the transducers. Before analysing these results it is important to note that there might be an underestimation of the actual damage because when the simulations ended, some tissues had not reached a steady-state temperature yet and would probably increase more, mainly the most superficial ones.

Analysing table 5.4 there are two points that can be concluded right away: 1) underneath the transducers some hotspots occur that lead to CEM 43ºC values around 50 times higher than those seen in the volume average and 2) despite these hotspots the thermal damage in the brain underneath the electrodes does not change drastically compared to the average values. One possible explanation for the first point is the fact that the application of the current is also localized and there are regions such as the top of the head where the electric field is not very high and thus the heat exchanges with the blood and the environment can compensate the temperature increase due to Joule heating. Regarding the second point, it can be seen as a way the human body has to protect the brain from thermal damage and the role of all the other tissues that surround it that can act as a barrier [46]. For example, the area of interaction between the CSF and the brain is extremely large [73] and CSF's specific heat is one of the highest of the human head. This means that this tissue can store energy during more time and thus prevent abrupt changes of temperature that could compromise the brain homeostasis.

Comparing the data with was is shown in table 2.2 one can conclude that for the scalp the only effects expected to occur, both locally and for the whole volume, are acute and minor changes. In fact, in clinical trials it was observed that people treated with TTFields usually suffer from skin dermatitis in the regions underneath the electrodes [16–19] which is in agreement with these findings. Dangereous erythema, functional changes and tissue necrosis are not expected for TTFields according to the results obtained, although they can occur if it is proven that the CEM 43ºC values are additive throughout the days. However, assuming that they are not it is also not anticipated any major effects at the skull, CSF and eyes levels. This can be confirmed measuring the levels of calcium in the blood and in the CSF, for example. As mentioned before,

if there is irreversible bone resorption it is expected an increase of these ions in the blood, while if the CSF is subjected to a significant heat stress calcium will also increase its concentration in this fluid.

Nonetheless, there might be some changes at the brain level. The average CEM 43^{o}C in the brain is around 0.29 minutes. According to the reviewed data discussed before this can change the BBB permeability, cerebral blood flow and GABA, glycine and glutamate levels. Although the main effects of these changes were already discussed it in the "Biological tissue heating" chapter, it is important to make some notes about the impact they can have in TTFields. First of all the fact that GBM is an astrocytoma and the astrocytes give structural and functional support to the BBB cells, along with pericytes and extracellular matrix components [35], can also change the BBB permeability. It is of extreme importance to maintain a correct level to ensure neuronal circuits to function properly [74]. The consequences of an increased permeability can vary but include imbalance of ions and transmitters, entry of toxins and pathogens, the release of cytokines and chemokines, leakage of plasma proteins which can ultimately lead to neuronal dysfunction, neuroinflammation and neurodegeneration of cells, as Obermeier et. al [74] concluded. However, in some situations it is also desirable to increase this permeability to facilitate the administration of drugs [75]. In the case of TTFields this can be useful if there is a more appropriate drug than temozolomide (that is administrated as the chemotherapeutic agent) that could be used, but under normal conditions, it would not enter the brain.

Whether the cerebral blood increases or decreases is still to be investigated, but the results reported in the literature indicate that there are variations from its basal level. The consequences of this change were already discussed, but in terms of heating due to TTFields it can represent a change in how the brain cools down through heat exchanges with the blood. If this change is not so extreme that it can cause ischemia or lead to a higher intracranial pressure, then an increase flow would help to reduce brain's temperature and thus to reduce CEM 43^{o}C values. The opposite conclusions are attained if this change is in the reversed direction. It is important to note that because the brain metabolic activity is very high the heat dissipation through blood cooling plays a crucial role in reducing its temperature. It is through this complex mechanism of energy trading that this structure is capable of maintaining its temperature more or less constant and independent of the ambient temperature 2-3 centimeters below the cortical surface [73]. A closer look at figure 5.9 shows that the temperature of the brain barely changes, increasing less than 0.1^{o}C for the time simulated. This is of special importance taking into consideration that some studies reported that an increase of 0.5^{o}C in the brain can change cell excitability and a variation of 1^{o}C interferes in neuronal network functioning [60], while small changes can have an impact on the rate of chemical reactions and on the affinity of haemoglobin for oxygen [48] and for 40^{o}C cell damage and tissue ablation are very likely to occur [51].

Just as important according to the results obtained, an increase in the concentrations of GABA, glutamate and glycine might also take place. It is well known that GABA and glycine have an important role in reducing neuronal excitability to specific receptors thus being a potential way to reduce epileptic seizures for example [34]. Whether these neurotransmissors pass through the BBB or not is up for discussion, but if its permeability is increased then there is a higher chance that they can be found in the brain [34]. The actions of GABA and glycine are somewhat compensated by the increased concentration of glutamate. In fact, this relation should be seen in the perspective that an increase of glutamate can lead to an increase of GABA because

it is known that the first is the metabolic precursor of the second [76]. The increase of these neurotransmitters for the same values of CEM 43^{o}C can thus be seen as a relation cause-effect, although the consequences of these changes for TTFields are unclear. One can think that some kind of change in the thresholds of neuronal excitability might occur, however in terms of treatment efficacy this does not seem to be a problem mainly because the basis of this technique is not stimulating the cells but affecting the mitotic process. Without any doubt, there is a lot of work to be done to evaluate the consequences of these increases if these results are corroborated by experimental data. At first glance these neurotransmitters do not seem to affect TTFields, but they can have dangerous effects if the consequences are evaluated for the whole-body especially if their concentrations do not return to the basal values after the fields are shut down.

In the figures that represent tissues temperature (figures 5.9, 5.11, 5.13, 5.16, 5.19 and 5.22) it is important to make a few comments about the initial temperature of each tissue. The scalp is in direct contact with the environment and so it is the most sensible to room temperature changes. As so, when the room temperature is higher, the scalp's average temperature is also augmented compared to the case when the ambient temperature is 24^{o}C or 7.9^{o}C. As tissue depth is increased the average temperature of every structure tends to the blood's temperature. At the brain level, values around 37^{o}C are obtained independently of the outside temperature which was expected considering what was discussed before. It is interesting to note that despite the CEM 43^{o}C values for the whole head being higher when the outside room temperature is higher, the local values (those defined by the cylinder) are lower because the fields are being applied during less time. On the other hand, when the applied voltage is halved the temperature increase is also lower because the fields do not have an intensity high enough to cause a high Joule effect as in the standard situation. Regarding simulation 7 there are two local CEM 43^{o}C measures, one for each configuration. In the case of the AP cylinder, the values are a bit higher than those of simulation 2 because there is a little increase due to the LR configuration being more time on. The local CEM 43^{o}C values for this latter may seem low, but they can be explained by the volume of each tissue underneath each electrode: the average volume for the scalp underneath the LR electrode is 2920 mm^3 and the skull's is 623 mm^3, while in the case of the AP's these values are 1763 mm^3 and 1473 mm^3, respectively. Considering what was discussed about the regions where the electric field is higher, the potential of each configuration, tissues properties and the behaviour of the temperature profile as the distance from the head surface increases these observations are justified. Lastly, when the way the current is distributed is changed the local CEM 43^{o}C values became smaller due to a mix of different factors such as the injected current, the electric field, the volume of each tissue underneath the most significant electrode, etc.

Concerning the tumour itself, it is clear that its average temperature barely increases from its basal state (around 37^{o}C). To answer the question: "Can TTFields efficacy be attributed to tumour heating as it happens in hyperthermia?" we have to know the temperature that the tumour should reach so the treatment outcome could also be credited to the exposure to heat. For hyperthermia, the tumour's temperature is dependent on the method used to heat it. In regional hyperthermia, the temperature can reach values close 43^{o}C for a duration of 2h (120 CEM 43^{o}C) in a certain body region containing the tumour, while in whole-body hyperthermia the increase is limited to 42^{o}C [77]. This implies that the tumour has to reach a temperature higher than the 37.1^{o}C that was predicted for TTFields. Thus it can be inferred that this treatment efficacy

is not due to hyperthermia. Nonetheless, this might be confirmed with immunological data. It is expected that Heat Shock Proteins (HSPs) are not present on the surface of the tumour cells because they are only synthesised in response to a non-lethal, but significant heat shock [78].

As mentioned before, it is important to know how the thermal damage can be quantified throughout the treatment. If it is additive then some conclusions here made have to rethinked such as the brain concentrations of GABA, glycine and glutamate that can decrease for CEM 43ºC values higher than 1.29 minutes. The lowest CEM 43ºC values obtained for the whole head were for when the room temperature is lowered (Simulation 4), while the lowest values for local heating depends on the tissue evaluated. More study is needed to know which configuration is the one that has the best ratio between treatment outcomes and thermal damage because the conclusions vary depending on how the evaluations are performed.

6.5 Simplifications made and limitations of the results presented

In all computational studies, there has to be some degree of compromise between having the satisfactory results and the time spent in improving the simulation and working on its limitations. This project is no exception and therefore there are some important points that need to be addressed apart from the ones already mentioned about SAR and CEM 43ºC.

First of all and as reported in [44] the realistic head model can be improved. As it can be seen in figures 4.1 and 4.2, a truncation was made at the nose level due to the limited coverage of the original MR images. Because of this, the electric field can be higher in some tissues, although the impact on the results obtained might not be significant because the electrodes placement is relatively far from the truncation level. Secondly, the head is a complex set of several different tissues. In this project, just the scalp, skull, CSF, GM, WM, tumour and eyeballs were considered. In fact, in the high majority of the computational studies, there is only a handful of tissues considered partially because these are the most significant ones and partially because it is hard to obtain information about all the tissues present in the human head and representing them when creating the model. However, if more realism is wanted in this model some modifications that can be applied include considering the meninges between the skull and the CSF, dividing the skull in a soft bone layer (that represents the spongiosa) enclosed by two other hard layers (the compacta) [79], dividing the eyeballs in cornea, lens, retina amid others, the scalp in skin, fat and pericranium for example [79] or even consider a more realistic shape for the tumour instead of just spheres. In fact, some studies even reported that considering a layer of fat in the scalp can increase the peak temperature during an electroconvulsive treatment by a significant amount because the fat's electric conductivity is significantly lower than the scalp's [51]. Regarding the tumour, it is known that glioblastoma often has a necrotic core and a high cellularity region (the shell), but also a vasogenic edematous extracellular region [14] that was not represented in this model but its known to increase the electric field in the tumour due to its high electric conductivity and large size [80].

Regarding the electric and thermal parameters, the correct values for biological tissues at frequencies below 1 MHz are very uncertain. In fact, in the literature, values for the electric conductivity between half and twice those that were used in this project can be found in some cases (for example, for GM the electric conductivity used was 0.25 S/m but values as low as 0.15 S/m and as high as 0.50 S/m are reported [80]). There is also some degree of uncertainty

regarding the thermal parameters as well, although the range of variation is rather smaller compared to the electric ones. The study of Oliveira et. al [51] showed that for electroconvulsive therapy (frequencies around 20 and 120 Hz) when the electric and the thermal conductivities are increased it is expected a lower temperature increase of biological tissues, although this might not be true for TTFields. In addition, not all tissues have an isotropic conductivity value and thus a tensor has to be used instead of a single number. An anisotropic approach for the GM and WM values has already been shown to increase the electric field in the tumour and in the brain for TTFields therapy [80] by a maximum of 10%, while one other study showed that considering an anisotropic skull can change significantly the temperature in other tissues for an electroconvulsive treatment [79]. Also, a study regarding how these values change with the temperature should be performed because they are not constant as it was assumed. As a first approach, one way to study this dependence is considering a linear change with temperature (e.g.: for the specific heat: $c(T)=c_0(1+k_1\,\Delta T)$, where c_0 is the value for a certain reference temperature, k_1 is the temperature coefficient and ΔT the temperature difference to the reference temperature) as described in [81] and evaluate the main differences. The importance of considering this dependence was seen in the study of Janseen et. al [55] that reported a reduced relative perfusion by 13% and 33% when the skin temperature decreases by 10.1ºC and by 21.8ºC from its basal state, respectively.

In this project, several energy transfer processes were considered: conduction between tissues, convection with the environment, exchange of heat with the blood, metabolic heat generation and Joule heating. However, there is at least one more that should have been taken into consideration mainly because it directly affects the front pad that has the MSE for practically all simulations. The forehead has one of the highest sweat gland densities and a strong sweat response that helps to dissipate the heat of the head and to control brain's temperature [82] and this was not considered in the studies here presented. The impact of sweating during TTFields therapy is not reported in the literature, but it can affect how current is delivered as well as the temperature of the head and consequently change the efficacy of the treatment especially if the MSE is located in the front pad, as it happened with this model. On the other hand, energy transfer through radiation with the environment was also not accounted for. In this particular case it is possible to quantify this error. Considering the room temperature as 24ºC and the scalp's as 36.5ºC and modeling this latter as a black-body (thus emissivity ϵ=1, close to what is reported in the literature [83, 84]) equations (3.2) and (3.3) lead to:

$$F'_{conv} = 4 \times (36.5 - 24) = 50 \text{ W/m}^2$$
$$F'_{rad} = 1 \times 5.67 \times 10^{-8} \times ((36.5 + 273.15)^4 - (24 + 273.15)^4) = 79 \text{ W/m}^2$$

These values suggest that heat transfer through radiation is even higher than cooling through convection. This effect was neglected in the most Joule heating studies [51, 79] and was also ignored in this study because it was thought that it would not play such an important role without confirming it doing the necessary (simple) math first. Nonetheless, this matter is going to be target of a more in-depth analysis, but it is expected that the efficacy of Optune® increases if radiation is considered.

In all these studies, the room temperature, here assumed to be a constant, is a variable that largely affect the results obtained, as discussed previously. However, it is not an easy task to

assume where the patient will be and what will be the temperature of that place. The results show that being in a controlled place at a lower temperature (using air conditioner for example) can improve this technique efficacy. Of course that this is easier to say than done because very low temperatures can cause discomfort to the patient, especially for long periods of time. Additionally, other parameters such as the metabolic heat can also change depending on what the patient is doing, the outside temperature, etc [85].

Lastly, it is important to bear in mind that the conclusions here drawn are based on the results obtained for just one treatment day. Although it is possible to extrapolate them for several days the conclusions would most probably not be true because it is necessary to consider other factors such as the development of thermotolerance, how long do the effects last when the fields are shut down, cell death, etc.

6.6 Future work

Addressing all the limitations described above would definitely add more value and confidence to the results obtained. Of course that it is not possible to add every important detail to the model due to all the limitations already discussed, but a more in-depth study of the impact of adding some of them (like the radiation) would be very helpful. A sensitivity study with respect to the electric and thermal parameters and an investigation of the best switching time constant (instead of one second) are also important to perform alongside with an analysis of the impact of changing the threshold of 41^{o}C and the tumour position. Injecting more current in the transducers closer to the tumour and less in the ones that are further would also be interesting to do. Plus, all these conclusions are valid for this particular head model, but the results concerning damage and safety can be different for other models. In fact, in the literature, different electric fields in the tumour were obtained for different head models [80] with the same virtual tumour at the same location. Another interesting idea to investigate more in-depth is related with the computational study of Korshoej et. al [86] that showed an increased electric field of around 60% in the tumour site if a craniectomy is performed. Reducing the electric fields intensity instead of shutting them down as reported in [20] is also an idea that deserves some attention. Regarding this latter, the reduced field would have an anti-motility effect rather than anti-mitotic.

Finally, adjusting the electric fields and the arrays' position throughout the course of the treatment would also help to enhance the obtained results as described in the paper of Wenger et. al [87] where a maximum increase of 184% of the electric field in the tumour was seen compared to the standard array layout. However, there are at least two problems with this: the cost of making regular diagnostic images and regularly adapt the treatment depending on how the tumour evolves and the lack of a pipeline that can create a personalized array configurations and run the necessary simulations fast enough to make this approach feasible. Concerning this latter point, the use of simplified head models might be helpful.

Despite these conclusions it is important to validate all the results with different head models and, if possible, compare them with data from clinical trials. Of course than this can be a cumbersome task because of all the ethical and safety questions involved.

Chapter 7

Conclusion

Glioblastoma Multiforme is one of the deadliest brain diseases that is characterized by a rapid progression and a very low survival rate even with optimal treatment. Typically the patients who suffer from this condition have to be subjected to different treatment techniques each one of them responsible by a variety of side effects that are more or less understood. Up until now, only dermatitis was reported as a major consequence of TTFields. Although the concern about tissue heating due to the Joule effect is known, there is not any study that tried to quantify the thermal damage. Thus, this project intended to model how this device works in different conditions taking in consideration these limitations while, at the same time, suggesting different ways to improve it.

Despite the low survival rate of the patients who suffer from this condition, it is important to continue to study not only the best way to improve their treatment, but also how to evaluate the harm that is done when applying these electric fields for so many hours per day. Research groups are so focused on trying to maximize the electric field in the tumour that little importance was given to the consequences of tissue heating at short-medium term and how they can affect patient's comfort and safety. We hope that all these results can at least be considered as a principle of proof that more attention should be paid to the small changes that can occur and that more investigation remains to be done to evaluate their impact. One major asset in this area would be the creation of a computational pipeline that allowed not only to change the electrodes position quickly to obtain the field that leads to the best ratio between treatment efficacy and thermal harm, but also to increase the speed of the calculations. Each of these simulations took around two days just to compute while retrieving all the important data cost one extra day.

We presented the first results we obtained for a steady-state situation at the the 10th Workshop on Biomedical Engineering (Appendix A3) as a poster communication. To spread what our work group does an oral presentation was also given by one of our team members in Ciência 2018 (Appendix A4). Lastly, we also sent a report to Novocure^{TM} with the main results we got (Appendix A5).

Bibliography

[1] J. S. Young, S. J. Chmura, D. A. Wainwright, B. Yamini, K. B. Peters, and R. V. Lukas, "Management of glioblastoma in elderly patients," *Journal of the Neurological Sciences*, vol. 380, pp. 250–255, 2017.

[2] D. Blackburn, S. Sargsyan, P. N. Monk, and P. J. Shaw, "Astrocyte function and role in motor neuron disease: A future therapeutic target?" *Glia*, vol. 57, no. 12, pp. 1251–1264, 2009.

[3] R. Stupp, W. P. Mason, M. J. van den Bent, M. Weller, B. Fisher, M. J. Taphoorn, K. Belanger, A. A. Brandes, C. Marosi, U. Bogdahn, J. Curschmann, R. C. Janzer, S. K. Ludwin, T. Gorlia, A. Allgeier, D. Lacombe, J. G. Cairncross, E. Eisenhauer, and R. O. Mirimanoff, "Radiotherapy plus concomitant and adjuvant temozolomide for glioblastoma," *New England Journal of Medicine*, vol. 352, no. 10, pp. 987–996, 2005.

[4] A. A. Kanner, E. T. Wong, J. L. Villano, and Z. Ram, "Post hoc analyses of intention-to-treat population in phase III comparison of NovoTTF-100A™ system versus best physician's choice chemotherapy," *Seminars in Oncology*, vol. 41, no. 5 Suppl 6, pp. S25–S34, 2014.

[5] C. J. Farrell and S. R. Plotkin, "Genetic causes of brain tumors: neurofibromatosis, tuberous sclerosis, von hippel-lindau, and other syndromes," *Neurologic Clinics*, vol. 25, no. 4, pp. 925–946, 2007.

[6] R. M. Young, A. Jamshidi, G. Davis, and J. H. Sherman, "Current trends in the surgical management and treatment of adult glioblastoma." *Annals of Translational Medicine*, vol. 3, no. 9, pp. 121–136, 2015.

[7] "Optune® Treatment | Official Novocure Site." [Online]. Available: https://www.optune.com/

[8] E. D. Kirson, Z. Gurvich, R. Schneiderman, E. Dekel, A. Itzhaki, Y. Wasserman, R. Schatzberger, and Y. Palti, "Disruption of cancer cell replication by alternating electric fields," *Cancer Research*, vol. 64, no. 9, pp. 3288–3295, 2004.

[9] J. Lantos, R. J. Young, P. C. Miranda, C. Wenger, and E. T. Wong, "TTFields therapy: preclinical and clinical data," in *Handbook of Neuro-Oncology Neuroimaging*, 2nd ed., H. B. Newton, Ed. Academic Press, 2016, ch. 25, pp. 243–256.

[10] M. Giladi, R. S. Schneiderman, T. Voloshin, Y. Porat, M. Munster, R. Blat, S. Sherbo, Z. Bomzon, N. Urman, A. Itzhaki, S. Cahal, A. Shteingauz, A. Chaudhry, E. D. Kirson, U. Weinberg, and Y. Palti, "Mitotic spindle disruption by alternating electric fields leads to improper chromosome segregation and mitotic catastrophe in cancer cells," *Scientific Reports*, vol. 5, no. 1, p. 18046, 2016.

[11] J. A. Tuszynski, C. Wenger, D. E. Friesen, and J. Preto, "An overview of sub-cellular mechanisms involved in the action of TTFields," *International Journal of Environmental Research and Public Health*, vol. 13, no. 11, 2016.

[12] K. J. Barnum and M. J. O 'connell, "Cell cycle regulation by checkpoints," in *Cell Cycle Control: Mechanisms and Protocols*, 2nd ed., E. Noguchi and M. C. Gadaleta, Eds. Humana Press, New York, NY, 2014, vol. 1170, ch. 2, pp. 29–40.

[13] K. L. Spalding, O. Bergmann, K. Alkass, S. Bernard, H. B. Huttner, I. Westerlund, C. Vial, A. Buchholz, D. C. Mash, H. Druid, C. Jordan, I. Physics, and L. Livermore, "Dynamics of hippocampal neurogenesis in adult humans," *Cell*, vol. 153, no. 6, pp. 1219–1227, 2015.

[14] P. C. Miranda, A. Mekonnen, R. Salvador, and P. J. Basser, "Predicting the electric field distribution in the brain for the treatment of glioblastoma," *Phys Med Biol.*, vol. 59, no. 15, pp. 4137–4147, 2014.

[15] E. D. Kirson, V. Dbaly, F. Tovarys, J. Vymazal, J. F. Soustiel, A. Itzhaki, D. Mordechovich, S. Steinberg-Shapira, Z. Gurvich, R. Schneiderman, Y. Wasserman, M. Salzberg, B. Ryffel, D. Goldsher, E. Dekel, and Y. Palti, "Alternating electric fields arrest cell proliferation in animal tumor models and human brain tumors," *Proceedings of the National Academy of Sciences*, vol. 104, no. 24, pp. 10 152–10 157, 2007.

[16] M. Salzberg, E. Kirson, Y. Palti, and C. Rochlitz, "A pilot study with very low-intensity, intermediate-frequency electric fields in patients with locally advanced and/or metastatic solid tumors," *Onkologie*, vol. 31, no. 7, pp. 362–365, 2008.

[17] E. D. Kirson, R. S. Schneiderman, V. Dbalý, F. Tovaryš, J. Vymazal, A. Itzhaki, D. Mordechovich, Z. Gurvich, E. Shmueli, D. Goldsher, Y. Wasserman, and Y. Palti, "Chemotherapeutic treatment efficacy and sensitivity are increased by adjuvant alternating electric fields (TTFields)," *BioMed Central Medical Physics*, vol. 9, no. 1, pp. 1–13, 2009.

[18] R. Stupp, E. T. Wong, A. A. Kanner, D. Steinberg, H. Engelhard, V. Heidecke, E. D. Kirson, S. Taillibert, Z. Ram, J. L. Villano, N. Rainov, F. Liebermann, V. Dbaly, U. Weinberg, D. Schiff, L. Kunschner, J. Raizer, J. Honnorat, A. Sloan, M. Malkin, J. C. Landolfi, F. Payer, M. Mehdorn, R. J. Weil, S. C. Pannullo, M. Westphal, M. Smrcka, L. Chin, H. Kostron, S. Hofer, J. Bruce, R. Cosgrove, N. Paleologous, Y. Palti, P. H. Gutin, and C. Bernard, "NovoTTF-100A versus physician ' s choice chemotherapy in recurrent glioblastoma : A randomised phase III trial of a novel treatment modality," *European Journal of Cancer*, vol. 48, pp. 2192–2202, 2012.

[19] M. M. Mrugala, H. H. Engelhard, D. Dinh Tran, Y. Kew, R. Cavaliere, J. L. Villano, D. Annenelie Bota, J. Rudnick, A. Love Sumrall, J. J. Zhu, and N. Butowski, "Clinical practice experience with NovoTTF-100A™ system for glioblastoma: the patient registry dataset (PRiDe)," *Seminars in Oncology*, vol. 41, no. S6, pp. S4–S13, 2014.

[20] M. Giladi and R. Shnaiderman, "US 2017/0281934A1: Reducing motility of cancer cells using tumor treating fields (TTFields)," 2017.

[21] Y.-S. Sun, "Direct-current electric field distribution in the brain for Tumor Treating Field applications: A simulation study." *Computational and Mathematical Methods in Medicine*, no. 3829768, 2018.

[22] Q. Castellví, M. M. Ginestà, G. Capellà, and A. Ivorra, "Tumor growth delay by adjuvant alternating electric fields which appears non-thermally mediated," *Bioelectrochemistry*, vol. 105, pp. 16–24, 2015.

[23] P. Wust, B. Hildebrandt, G. Sreenivasa, B. Rau, J. Gellermann, H. Riess, R. Felix, and P. M. Schlag, "Hyperthermia in combined treatment of cancer," *The Lancet Oncology*, vol. 3, no. 8, pp. 487–97, 2002.

[24] M. Mallory, E. Gogineni, G. C. Jones, L. Greer, and C. B. Simone, "Therapeutic hyperthermia: the old, the new, and the upcoming," *Critical Reviews in Oncology/Hematology*, vol. 97, pp. 56–64, 2016.

[25] A. Valero-Cabré, J. Amengual, C. Stengel, A. Pascual-Leone, and O. A. Coubard, "Transcranial magnetic stimulation in basic and clinical neuroscience: a comprehensive review of fundamental principles and novel insights," *Neuroscience & Biobehavioral Reviews*, vol. 83, pp. 381–404, 2017.

[26] P. Minhas, V. Bansal, J. Patel, J. S. Ho, J. Diaz, A. Datta, and M. Bikson, "Electrodes for high-definition transcutaneous DC stimulation for applications in drug delivery and electrotherapy, including tDCS," *Journal of Neuroscience Methods*, vol. 190, no. 2, pp. 188–197, 2010.

[27] A. Datta, M. Elwassif, and M. Bikson, "Bio-heat transfer model of transcranial DC stimulation: Comparison of conventional pad versus ring electrode," *Proceedings of the 31st Annual International Conference of the IEEE Engineering in Medicine and Biology Society: Engineering the Future of Biomedicine, EMBC 2009*, vol. 5, pp. 670–673, 2009.

[28] F. G. Shellock and J. V. Crues, "MR procedures: biologic effects, safety, and patient care." *Radiology*, vol. 232, no. 3, pp. 635–652, 2004.

[29] Z. Wang, J. C. Lin, W. Mao, W. Liu, M. B. Smith, and C. M. Collins, "SAR and temperature: simulations and comparison to regulatory limits for MRI," *Journal of Magnetic Resonance Imaging*, vol. 26, no. 2, pp. 437–441, 2007.

[30] S. A. Sapareto and W. C. Dewey, "Thermal dose determination in cancer therapy," *International Journal of Radiation Oncology, Biology, Physics*, vol. 10, no. 6, pp. 787–800, 1984.

[31] M. W. Dewhirst, B. L. Viglianti, M. Lora-Michiels, M. Hanson, and P. J. Hoopes, "Basic principles of thermal dosimetry and thermal thresholds for tissue damage from hyperthermia," *International Journal of Hyperthermia*, vol. 19, no. 3, pp. 267–294, 2003.

[32] P. S. Yarmolenko, E. J. Moon, C. Landon, A. Manzoor, D. W. Hochman, B. L. Viglianti, and M. W. Dewhirst, "Thresholds for thermal damage to normal tissues: an update," *International Journal of Hyperthermia*, vol. 27, no. 4, pp. 320–343, 2011.

[33] C. Werner and K. Engelhard, "Pathophysiology of traumatic brain injury," *British Journal of Anaesthesia*, vol. 99, no. 1, pp. 4–9, 2007.

[34] B. S. Meldrum, "Glutamate as a neurotransmitter in the brain: review of physiology and pathology." *The Journal of Nutrition*, vol. 130, no. 4 Suppl, pp. 1007S–15S, 2000.

[35] M. Roslin, R. Henriksson, P. Bergström, U. Ungerstedt, and A. T. Bergenheim, "Baseline levels of glucose metabolites, glutamate and glycerol in malignant glioma assessed by stereotactic microdialysis," *Journal of Neuro-Oncology*, vol. 61, no. 2, pp. 151–160, 2003.

[36] N. Matsumi, K. Matsumoto, N. Mishima, E. Moriyama, T. Furuta, A. Nishimoto, and K. Taguchi, "Thermal damage threshold of brain tissue–histological study of heated normal monkey brains." *Neurologia medico-chirurgica*, vol. 34, no. 4, pp. 209–15, 1994.

[37] M. Frosini, "Changes in CSF composition during heat stress and fever in conscious rabbits," *Progress in Brain Research*, vol. 162, no. 06, pp. 449–457, 2007.

[38] W. Eric, *Science in the age of computer simulation*, 1st ed. University of Chicago Press, 2010.

[39] A. E. Anderson, B. J. Ellis, and J. A. Weiss, "Verification, validation and sensitivity studies in computational biomechanics," *Computer Methods in Biomechanics and Biomedical Engineering*, vol. 10, no. 3, pp. 171–184, 2007.

[40] S. S. Rao, *The finite element method in engineering*, 5th ed., S. S. Rao, Ed. Butterworth-Heinemann, 2004.

[41] P. C. Miranda, M. Hallett, and P. J. Basser, "The electric field induced in the brain by magnetic stimulation: A 3-D finite-element analysis of the effect of tissue heterogeneity and anisotropy," *IEEE Transactions on Biomedical Engineering*, vol. 50, no. 9, pp. 1074–1085, 2003.

[42] K. A. Werley and J. G. Gilligan, "The temperature distribution of a sphere placed in a directed uniform heat flux," *Journal of Heat Transfer*, vol. 103, pp. 399–401, 1981.

[43] V. Gerlich, K. Sulovská, and M. Zálešák, "COMSOL Multiphysics validation as simulation software for heat transfer calculation in buildings: building simulation software validation," *Measurement: Journal of the International Measurement Confederation*, vol. 46, no. 6, pp. 2003–2012, 2013.

[44] P. C. Miranda, A. Mekonnen, R. Salvador, and G. Ruffini, "The electric field in the cortex during transcranial current stimulation," *NeuroImage*, vol. 70, pp. 48–58, 2013.

[45] H. H. Pennes, "Analysis of tissue and arterial blood temperatures in the resting human forearm," *Journal of Applied Physiology*, vol. I, no. 2, pp. 5–34, 1948.

[46] O. Ley and Y. Bayazitoglu, "Effect of physiology on the temperature distribution of a layered head with external convection," *International Journal of Heat and Mass Transfer*, vol. 46, no. 17, pp. 3233–3241, 2003.

[47] T. K. Tullius and Y. Bayazitoglu, "Analysis of relaxation times on the human head using the thermal wave model," *International Journal of Heat and Mass Transfer*, vol. 67, pp. 1007–1013, 2013.

[48] A. L. Sukstanskii and D. A. Yablonskiy, "Theoretical model of temperature regulation in the brain during changes in functional activity," *Proceedings of the National Academy of Sciences*, vol. 103, no. 32, pp. 12 144–12 149, 2006.

[49] F. P. E. Janssen, G. M. Van Leeuwen, and A. A. Van Steenhoven, "Numerical simulation of scalp cooling to prevent chemotherapy-induced alopecia," *Journal of Mechanical Engineering*, vol. 51, no. 7-8, pp. 386–390, 2005.

[50] G. Pinton, M. Pernot, E. Bossy, J. F. Aubry, M. Muller, and M. Tanter, "Mechanisms of attenuation and heating dissipation of ultrasound in the skull bone: Comparison between simulation models and experiments," *Proceedings - IEEE Ultrasonics Symposium*, pp. 225–228, 2010.

[51] M. M. D. Oliveira, S. Member, P. Wen, and T. Ahfock, "Bio-heat transfer model of electroconvulsive therapy : Effect of biological properties on induced temperature variation," *38th Annual International Conference of the IEEE Engineering in Medicine and Biology Society (EMBC)*, pp. 3997–4000, 2016.

[52] O. Ley and Y. Bayazitoglu, "Brain temperature distribution during deep hypothermic circulatory arrest in humans," *Journal of Mechanics in Medicine and Biology*, vol. 4, no. 2, pp. 197–212, 2004.

[53] S. Kim, R. A. Normann, R. Harrison, and F. Solzbacher, "Preliminary study of the thermal impact of a microelectrode array implanted in the brain," *Annual International Conference of the IEEE Engineering in Medicine and Biology - Proceedings*, pp. 2986–2989, 2006.

[54] S. Fitzgerald, H. Atkins, R. Leknys, and R. Kelso, "A thermal test system for helmet cooling studies," *Proceedings*, vol. 2, no. 6, p. 272, 2018.

[55] F. E. Janssen, G. M. Van Leeuwen, and A. A. Van Steenhoven, "Modelling of temperature and perfusion during scalp cooling," *Physics in Medicine and Biology*, vol. 50, no. 17, pp. 4065–4073, 2005.

[56] G. M. Van Leeuwen, J. W. Hand, J. J. Lagendijk, D. V. Azzopardi, and A. D. Edwards, "Numerical modeling of temperature distributions within the neonatal head," *Pediatric Research*, vol. 48, no. 3, pp. 351–356, 2000.

[57] F. A. Duck, *Physical properties of tissue: A comprehensive referenc e book*. Academic Press, 1991, vol. 13, no. 5.

[58] C. W. Connor and K. Hynynen, "Patterns of thermal deposition in the skull during transcranial focused ultrasound surgery," *IEEE Transactions on Biomedical Engineering*, vol. 51, no. 10, pp. 1693–1706, 2004.

[59] C. M. Collins, W. Liu, J. Wang, R. Gruetter, J. T. Vaughan, K. Ugurbil, and M. B. Smith, "Temperature and SAR calculations for a human head within volume and surface coils at 64 and 300 MHz," *Journal of Magnetic Resonance Imaging*, vol. 19, no. 5, pp. 650–656, 2004.

[60] M. M. Elwassif, Q. Kong, M. Vazquez, and M. Bikson, "Bio-heat transfer model of deep brain stimulation induced temperature changes," *2006 International Conference of the IEEE Engineering in Medicine and Biology Society*, pp. 3580–3583, 2006.

[61] L. Zhu and C. Diao, "Theoretical simulation of temperature distribution in the brain during mild hypothermia treatment for brain injury," *Medical & Biological Engineering & Computing*, vol. 39, pp. 681–687, 2001.

[62] "Current Results - Weater and Science Facts." [Online]. Available: https://www.currentresults.com/index.php

[63] "BDF, Generalized Alpha, and Runge-Kutta Methods - 1062 - Knowledge Base." [Online]. Available: https://www.comsol.pt/support/knowledgebase/1062/

[64] G. Ruffini, F. Wendling, I. Merlet, B. Molaee-Ardekani, A. Mekonnen, R. Salvador, A. Soria-Frisch, C. Grau, S. Dunne, and P. C. Miranda, "Transcranial current brain stimulation (tCS): Models and technologies," *IEEE Transactions on Neural Systems and Rehabilitation Engineering*, vol. 21, no. 3, pp. 333–345, 2013.

[65] L. Santos, M. Martinho, R. Salvador, C. Wenger, S. R. Fernandes, G. Ruffini, and P. C. Miranda, "Evaluation of the electric field in the brain during Transcranial Direct Current stimulation : a sensitivity analysis," *Engineering in Medicine and Biology Society (EMBC), 2016 38th Annual International Conference of the IEEE*, pp. 1778–1781, 2016.

[66] M. Hallett, "Transcranial Magnetic Stimulation: A primer," *Neuron Primer*, vol. 55, no. 2, pp. 187–199, 2007.

[67] R. J. Ilmoniemi, J. Ruohonen, and J. Karhu, "Transcranial magnetic stimulation–a new tool for functional imaging of the brain," *Critical Reviews in Biomedical Engineering*, vol. 27, no. 3-5, pp. 241–284, 1999.

[68] C. Wenger, M. Giladi, Z. Bomzon, R. Salvador, P. J. Basser, and P. C. Miranda, "Modeling tumor treating fields (TTFields) application in single cells during metaphase and telophase," *Proceedings of the Annual International Conference of the IEEE Engineering in Medicine and Biology Society, EMBS*, pp. 6892–6895, 2015.

[69] F. A. C. M. Castelijns, J. Ezendam, M. A. H. E. Latijnhouwers, I. M. J. J. Van Vlijmen-Willems, P. L. J. M. Zeeuwen, P. C. M. D. E. Van Kerkhof, and P. E. J. Van Erp, "Epidermal cell kinetics by combining in situ hybridization and immunohistochemistry," *Histochemical Journal*, vol. 30, no. 12, pp. 869–877, 1998.

[70] R. P. A. Teixeira, S. J. Malik, and J. V. Hajnal, "Joint system relaxometry (JSR) and Crámer-Rao lower bound optimization of sequence parameters: A framework for enhanced precision of DESPOT T1 and T2 estimation," *Magnetic Resonance in Medicine*, vol. 79, no. 1, pp. 234–245, 2018.

[71] ICNIRP, "ICNIRP Guidelines for limiting exposure to time - varying electric, magnetic and electromagnetic fields (up to 300 GHz)," *Health Physics*, vol. 74, no. 4, pp. 494–522;, 1998.

[72] G. C. Van Rhoon, "Is CEM43^{o}C still a relevant thermal dose parameter for hyperthermia treatment monitoring?" *International Journal of Hyperthermia*, vol. 32, no. 1, pp. 50–62, 2016.

[73] H. Wang, B. Wang, K. P. Normoyle, K. Jackson, K. Spitler, M. Sharrock, C. M. Miller, C. Best, D. Llano, and R. Du, "Brain temperature and its fundamental properties: A review for clinical neuroscientists," *Frontiers in Neuroscience*, vol. 8, no. 307, pp. 1–17, 2014.

[74] B. Obermeier, R. Daneman, and R. M. Ransohoff, "Development, maintenance and disruption of the blood-brain-barrier," *Nature Medicine*, vol. 19, no. 12, pp. 1584–1596, 2013.

[75] A. Miranda, T. Cova, J. Sousa, C. Vitorino, and A. Pais, "Computational modeling in glioblastoma: From the prediction of blood-brain barrier permeability to the simulation of tumor behavior," *Future Medicinal Chemistry*, vol. 10, no. 1, pp. 121–131, 2018.

[76] O. A. C. Petroff, "GABA and glutamate in the human brain," *The Neuroscientist*, vol. 8, no. 6, pp. 562–573, 2002.

[77] J. van der Zee, "Heating the patient: A promising approach?" *Annals of Oncology*, vol. 13, no. 8, pp. 1173–1184, 2002.

[78] S. Lindquist and E. A. Craig, "The heat-shock proteins." *Annual review of genetics*, vol. 22, pp. 631–677, 1988.

[79] M. Menezes de Oliveira, P. Wen, and T. Ahfock, "Heat transfer due to electroconvulsive therapy: Influence of anisotropic thermal and electrical skull conductivity," *Computer Methods and Programs in Biomedicine*, vol. 133, pp. 71–81, 2016.

[80] C. Wenger, R. Salvador, P. J. Basser, and P. C. Miranda, "The electric field distribution in the brain during TTFields therapy and its dependence on tissue dielectric properties and anatomy: a computational study," *Physics in Medicine and Biology*, vol. 60, no. 18, pp. 7339–7357, 2015.

[81] D. Rossmann, Christian; Haemmerich, "Review of temperature dependence of thermal properties, dielectric properties, and perfusion of biological tissues at hyperthermic and ablation temperatures," *Critical Reviews in Biomedical Engineering*, vol. 42, no. 6, pp. 467–492, 2014.

[82] H. Wang, M. Kim, K. P. Normoyle, and D. Llano, "Thermal regulation of the brain-an anatomical and physiological review for clinical neuroscientists," *Frontiers in Neuroscience*, vol. 9, no. 528, pp. 1–6, 2016.

[83] J. Steketee, "Spectral emissivity of skin and pericardium," *Physics in Medicine and Biology Med. Biol.*, vol. 18, no. 5, pp. 686–694, 1973.

[84] F. J. Sanchez-Marin, S. Calixto-Carrera, and C. Villasennor-Mora, "Novel approach to assess the emissivity of the human skin," *Journal of Biomedical Optics*, vol. 14, no. 2, p. 024006, 2009.

[85] C. Gisolfi, *Nutritional needs in hot environments: Applications for military personnel in field operations*, 1st ed., B. M. Marriiott, Ed. The National Academies, 1993.

[86] A. R. Korshoej, G. B. Saturnino, L. K. Rasmussen, G. Von Oettingen, J. C. H. Sørensen, and A. Thielscher, "Enhancing predicted efficacy of tumor treating fields therapy of glioblastoma using targeted surgical craniectomy: a computer modeling study," *PLoS ONE*, vol. 11, no. 10, pp. 1–25, 2016.

[87] C. Wenger, R. Salvador, P. J. Basser, and P. C. Miranda, "Improving tumor treating fields treatment efficacy in patients with glioblastoma using personalized array layouts," *International Journal of Radiation Oncology Biology Physics*, vol. 94, no. 5, pp. 1137–1143, 2016.

Appendix

A1. COMSOL validation tests: additional information

Table A1: Additional information regarding COMSOL validation tests.

Test	Mesh	DoF (internal)	Elements	Average Element Quality	Computation time	Notes
1	Coarse	531 (462)	Tethrahedral: 244; Triangular: 180; Edge: 48; Vertex: 8	0.172	< 10 s	3D Stationary
	Normal	1573 (814)	Tethrahedral: 865; Triangular: 336; Edge: 68; Vertex: 8	0.745	< 10 s	
	Fine	2629 (1110)	Tethrahedral: 1616; Triangular: 476; Edge: 76; Vertex: 8	0.777	< 10 s	
2	Coarse	531 (462)	Tethrahedral: 244; Triangular: 180; Edge: 48; Vertex: 8	0.187	< 1 min	3D Time dependent
	Normal	1524 (814)	Tethrahedral: 865; Triangular: 336; Edge: 68; Vertex: 8	0.738	< 1 min	
	Fine	2671 (1110)	Tethrahedral: 1616; Triangular: 476; Edge: 76; Vertex: 8	0.772	< 1 min	
3	Coarse	4043 (1080)	Tethrahedral: 2656; Triangular: 464; Edge: 72; Vertex: 6	0.163	< 1 min	3D Time dependent
	Normal	12334 (1904)	Tethrahedral: 8569; Triangular: 852 Edge: 96; Vertex: 6	0.779	< 1 min	
	Fine	23645 (2888)	Tethrahedral: 16684; Triangular: 1320; Edge: 120; Vertex: 6	0.772	< 2 min	
4	Coarse	271 (56)	Triangular: 122; Edge: 26; Vertex: 4	0.968	< 10 s	2D axisymmetric Time dependent
	Normal	589 (84)	Traingular: 274; Edge: 40; Vertex: 4	0.972	< 10 s	
	Fine	915 (104)	Triangular: 432; Edge: 50; Vertex: 4	0.971	< 10 s	

Notes: Solver used for all tests: PARDISO. Relative tolerance: Test 1: 0.01; Tests 2,3 and 4: 0.001.

A2. Additional figures

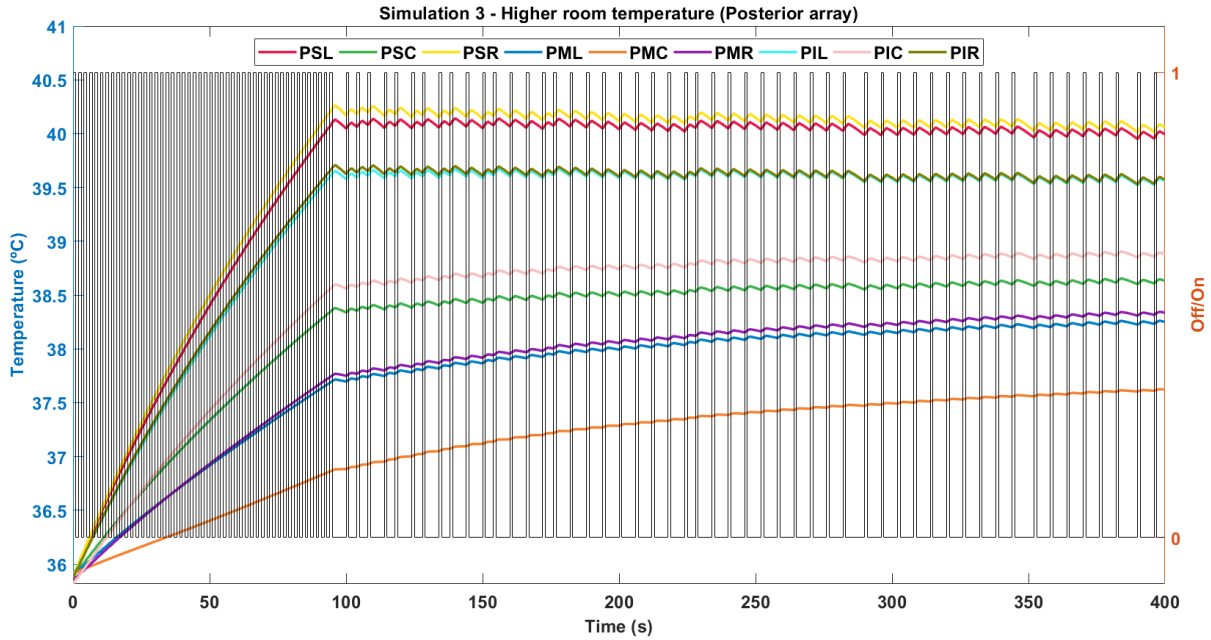

Figure A1: Temperature variation as a function of time for the posterior array when the room temperature is 27.3^{o}C (Simulation 3). In this plot when the device is on (1 in the right y-axis) it means that the current is being injected in the AP direction. Transducers naming is the same as used before.

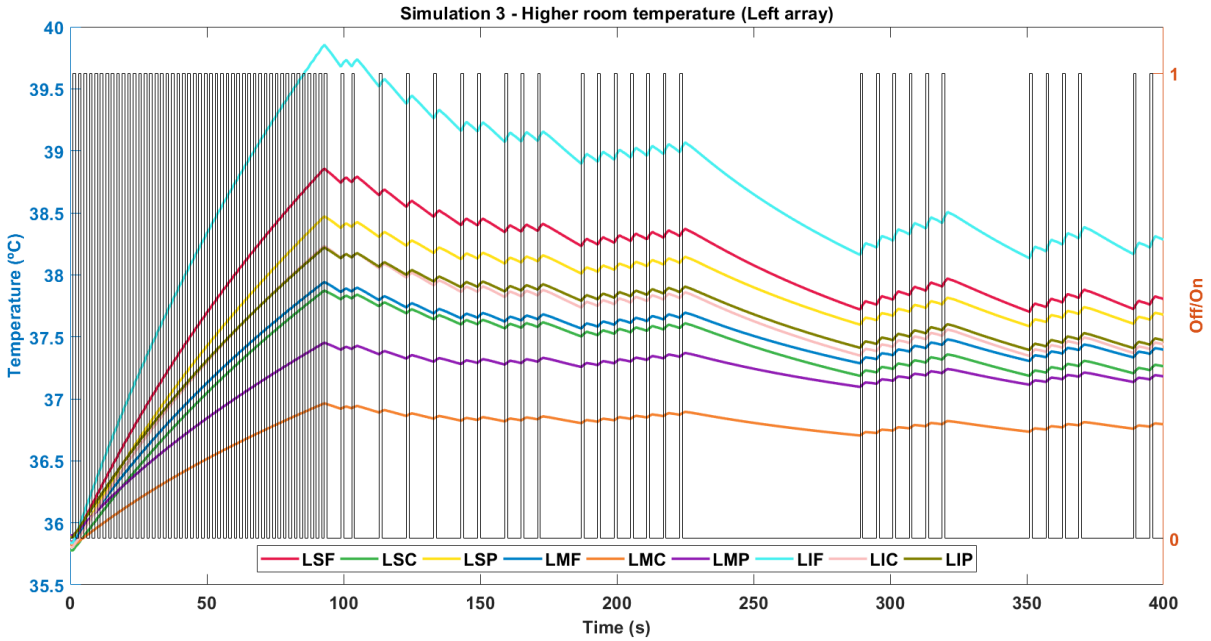

Figure A2: Temperature variation as a function of time for the left array when the room temperature is 27.3^{o}C (Simulation 3). In this plot when the device is on (1 in the right y-axis) it means that the current is being injected in the LR direction. Transducers naming is the same as used before.

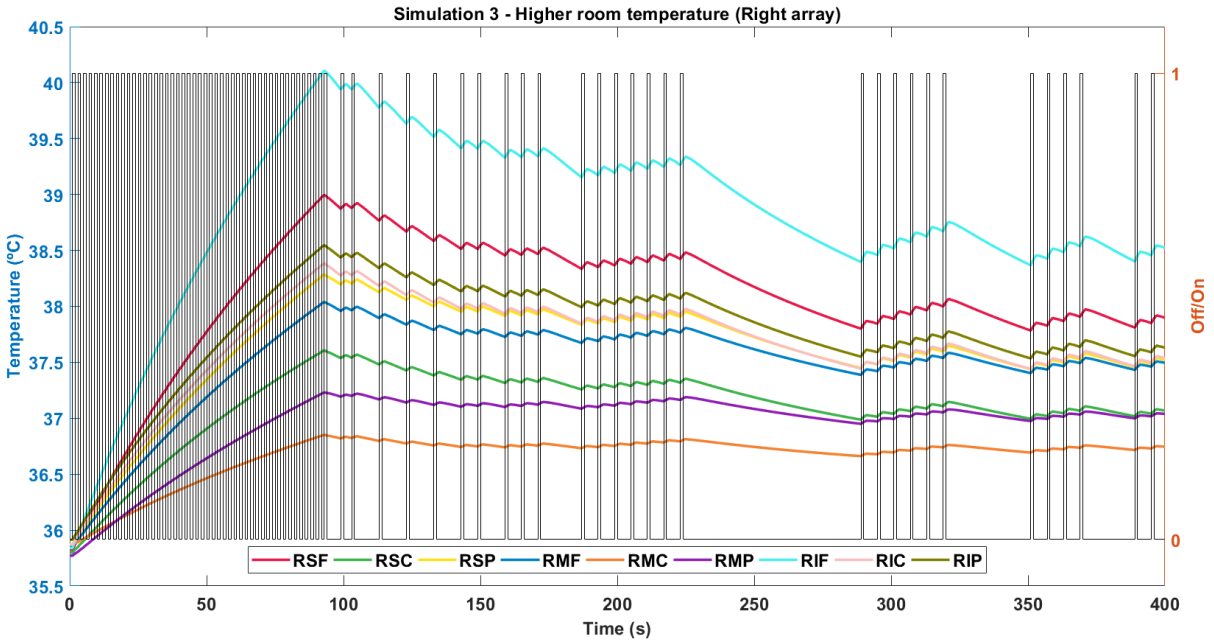

Figure A3: Temperature variation as a function of time for the right array when the room temperature is 27.3^{o}C (Simulation 3). In this plot when the device is on (1 in the right y-axis) it means that the current is being injected in the LR direction. Transducers naming is the same as used before.

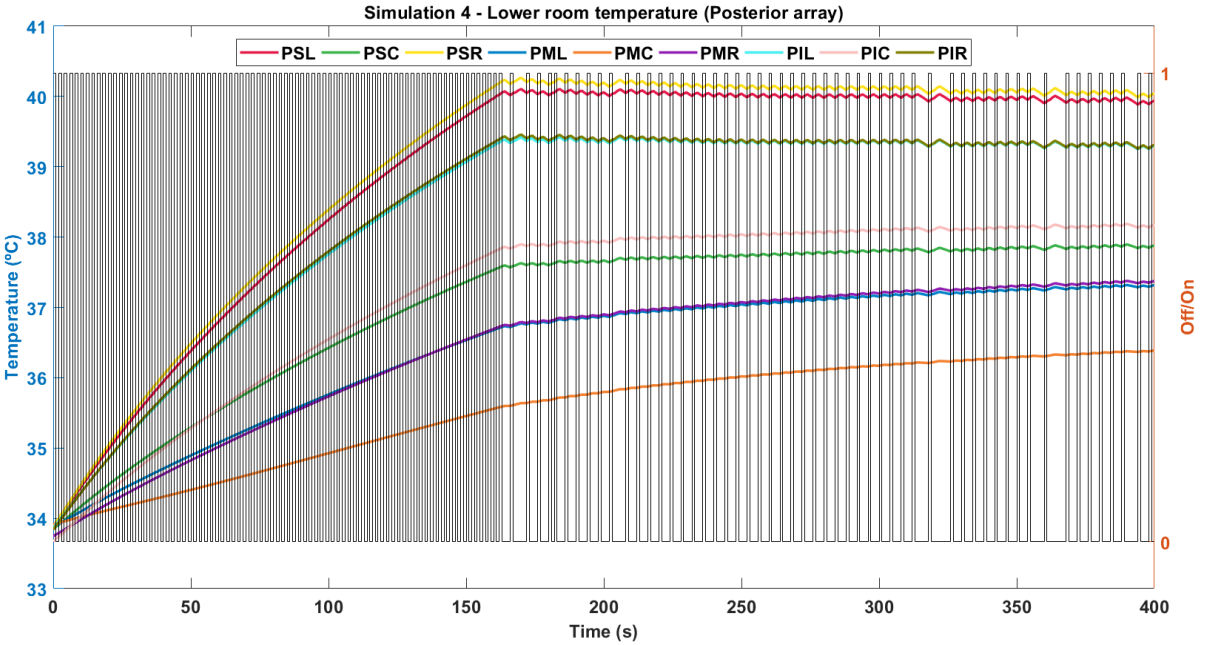

Figure A4: Temperature variation as a function of time for the posterior array when the room temperature is 7.9^{o}C (Simulation 4). In this plot when the device is on (1 in the right y-axis) it means that the current is being injected in the AP direction. Transducers naming is the same as used before.

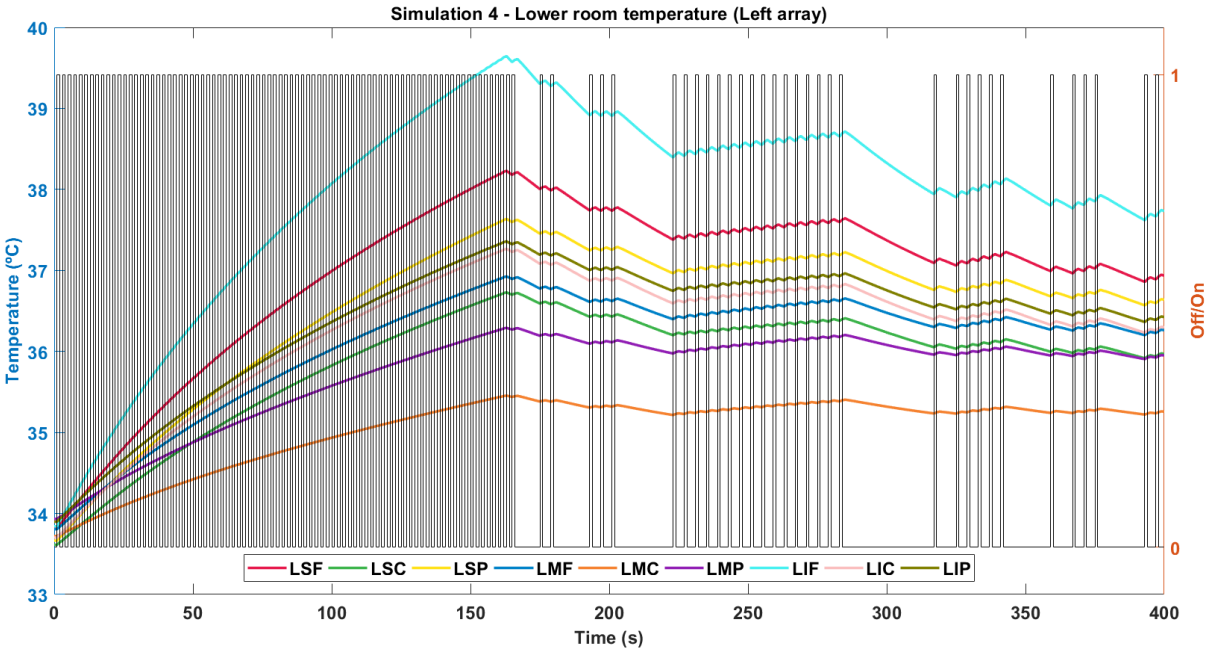

Figure A5: Temperature variation as a function of time for the left array when the room temperature is 7.9^{o}C (Simulation 4). In this plot when the device is on (1 in the right y-axis) it means that the current is being injected in the LR direction. Transducers naming is the same as used before.

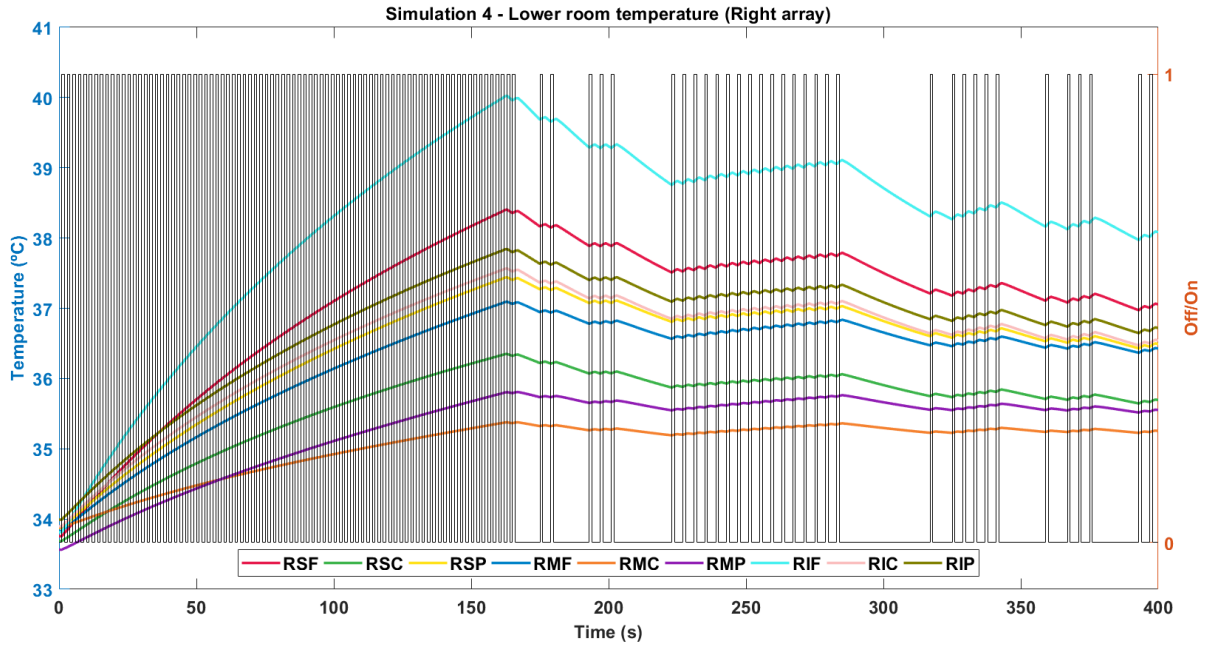

Figure A6: Temperature variation as a function of time for the right array when the room temperature is 7.9^{o}C (Simulation 4). In this plot when the device is on (1 in the right y-axis) it means that the current is being injected in the LR direction. Transducers naming is the same as used before.

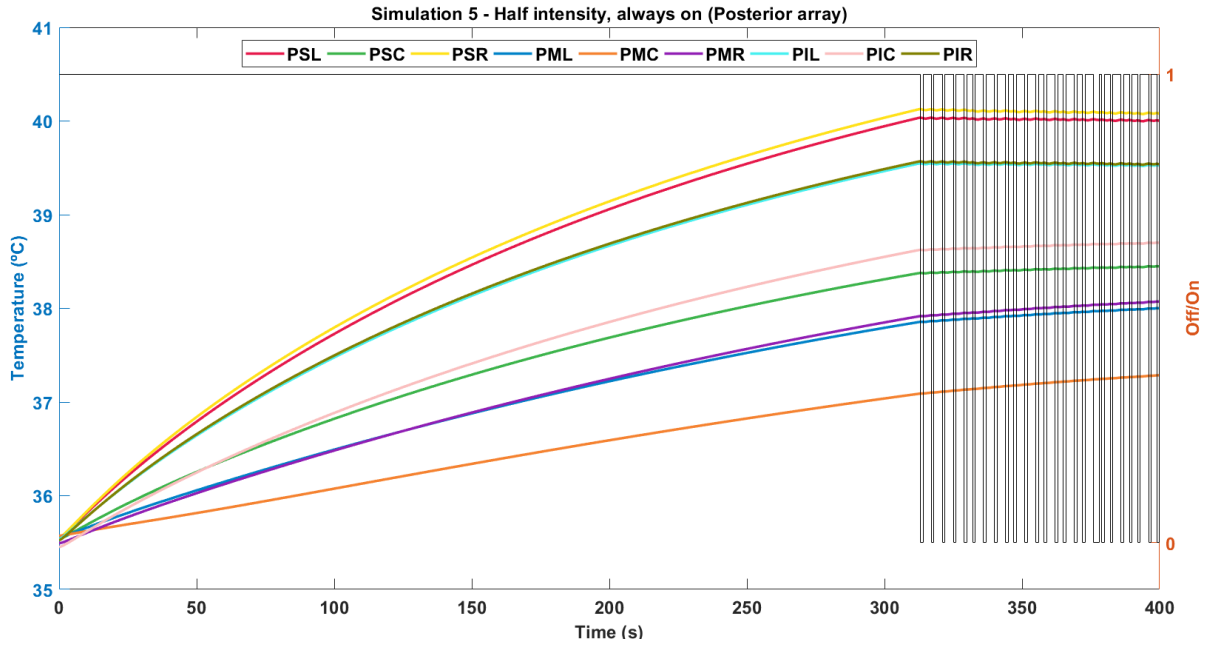

Figure A7: Temperature variation as a function of time for the posterior array when both configurations are applied at the same time but with half the current injected (Simulation 5). In this plot when the device is on (1 in the right y-axis) it means that the current is being injected in the AP direction. Transducers naming is the same as used before.

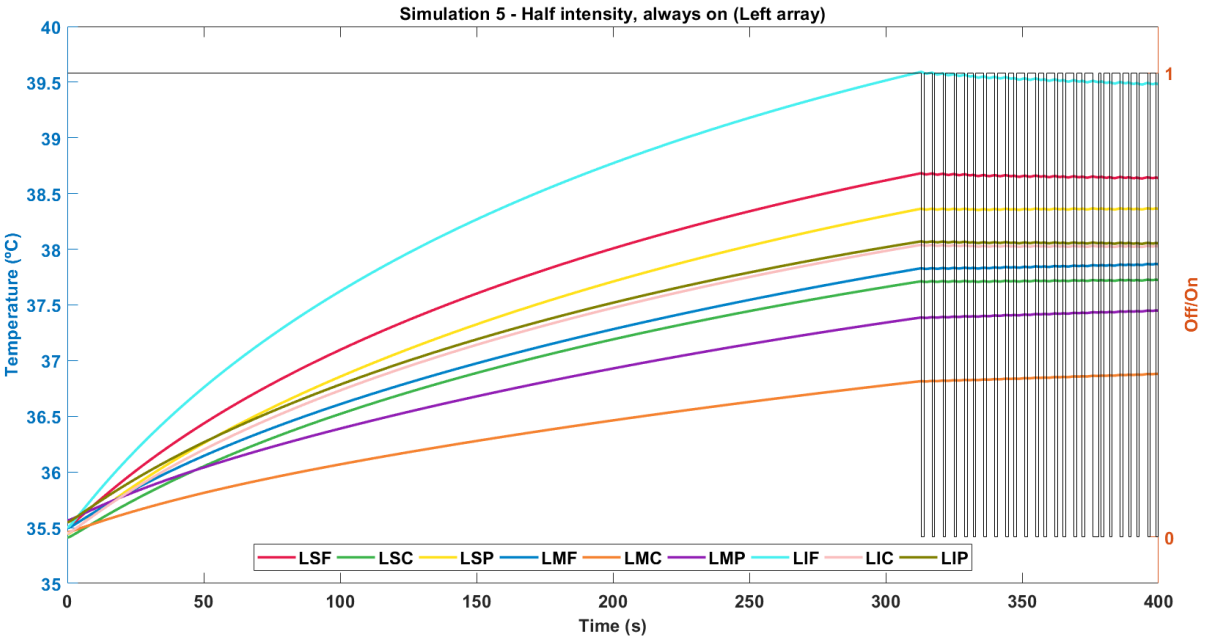

Figure A8: Temperature variation as a function of time for the left array when both configurations are applied at the same time but with half the current injected (Simulation 5). In this plot when the device is on (1 in the right y-axis) it means that the current is being injected in the LR direction. Transducers naming is the same as used before.

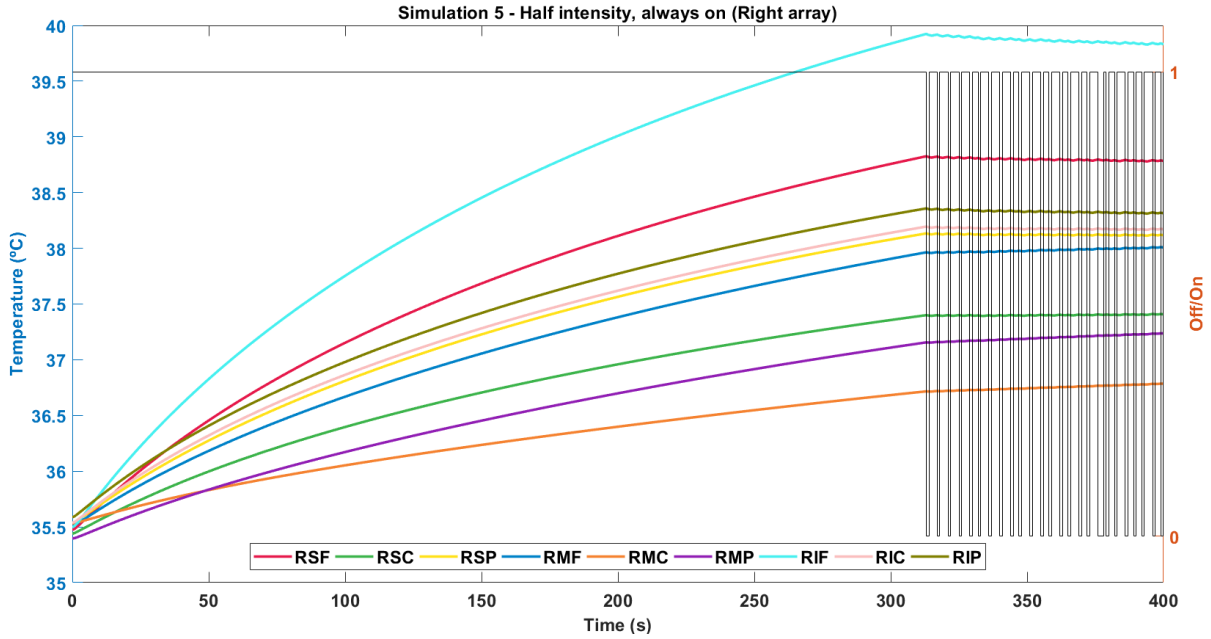

Figure A9: Temperature variation as a function of time for the right array when both configurations are applied at the same time but with half the current injected (Simulation 5). In this plot when the device is on (1 in the right y-axis) it means that the current is being injected in the LR direction. Transducers naming is the same as used before.

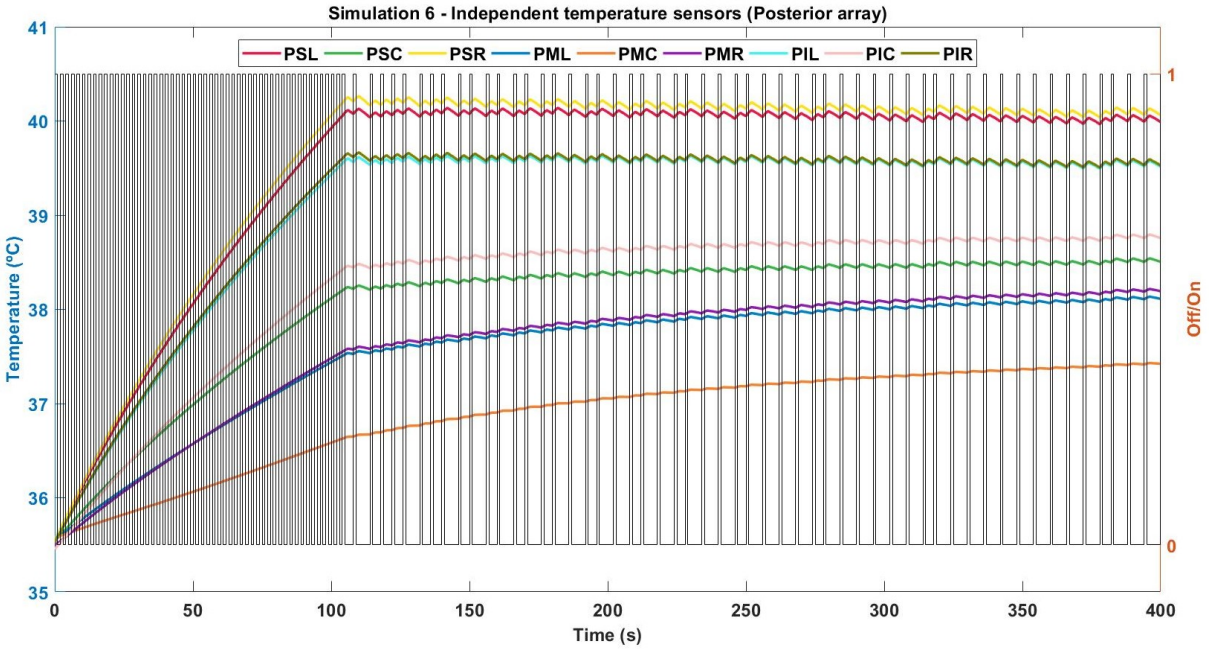

Figure A10: Temperature variation as a function of time for the posterior array when independent temperature sensors are used (Simulation 6). In this plot when the device is on (1 in the right y-axis) it means that the current is being injected in the AP direction. Transducers naming is the same as used before.

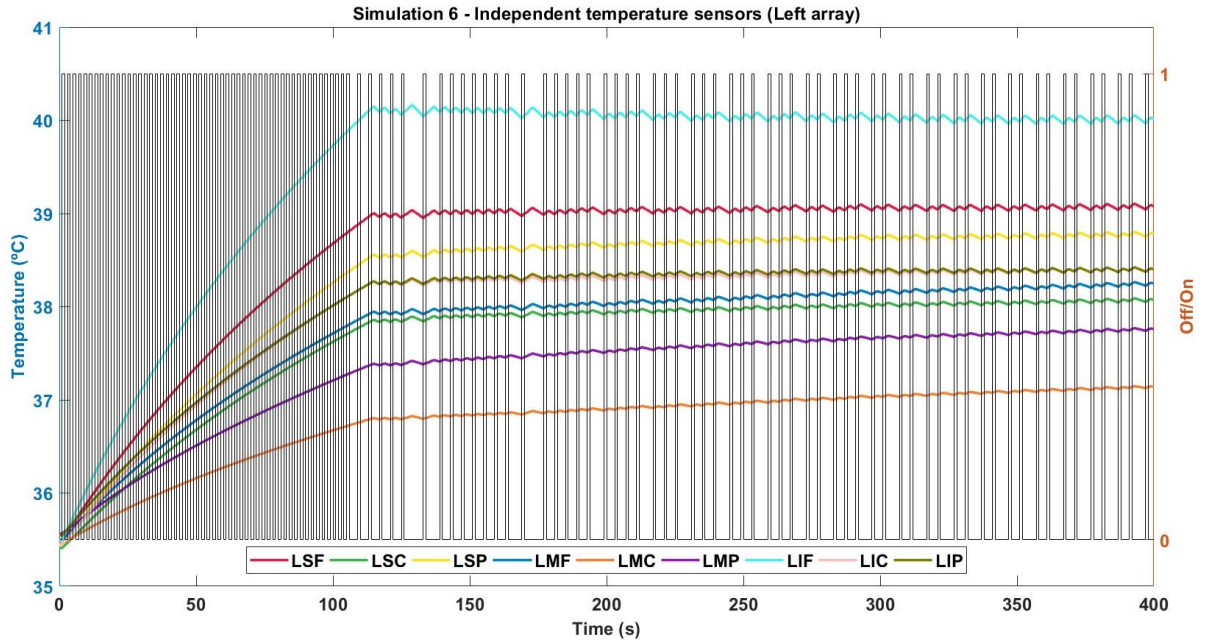

Figure A11: Temperature variation as a function of time for the left array when independent temperature sensors are used (Simulation 6). In this plot when the device is on (1 in the right y-axis) it means that the current is being injected in the LR direction. Transducers naming is the same as used before.

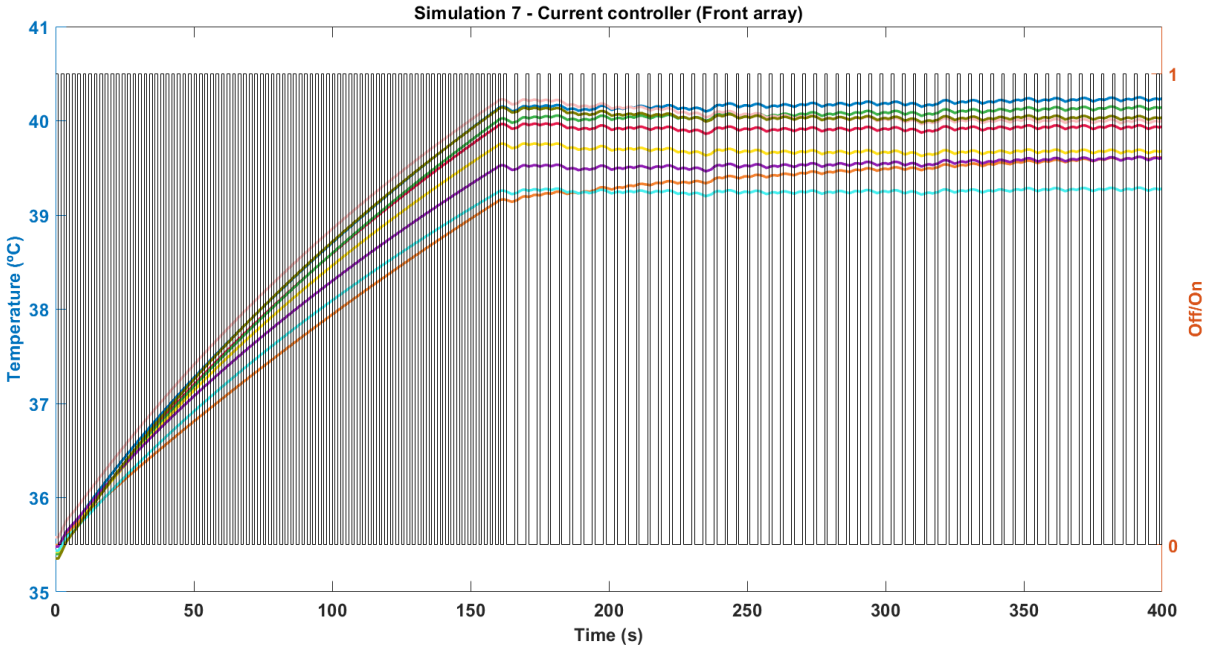

Figure A12: Temperature variation as a function of time for the front array when current is controlled at a array level (Simulation 7). In this plot when the device is on (1 in the right y-axis) it means that the current is being injected in the AP direction. Transducers naming is the same as used before.

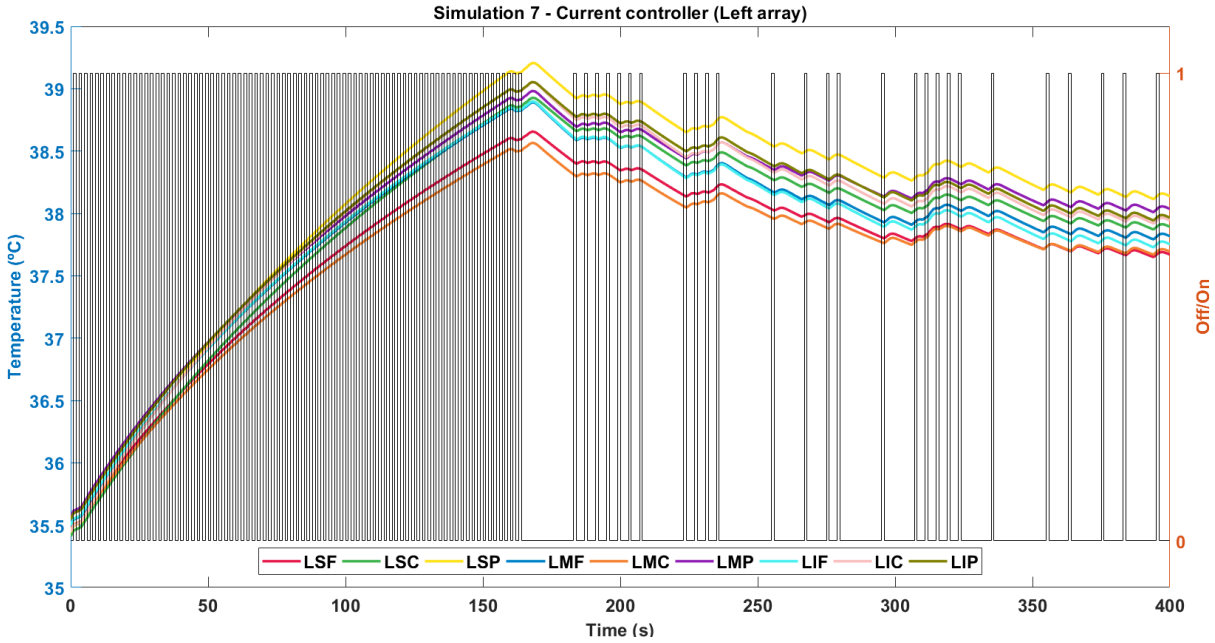

Figure A13: Temperature variation as a function of time for the left array when current is controlled at a array level (Simulation 7). In this plot when the device is on (1 in the right y-axis) it means that the current is being injected in the AP direction. Transducers naming is the same as used before.

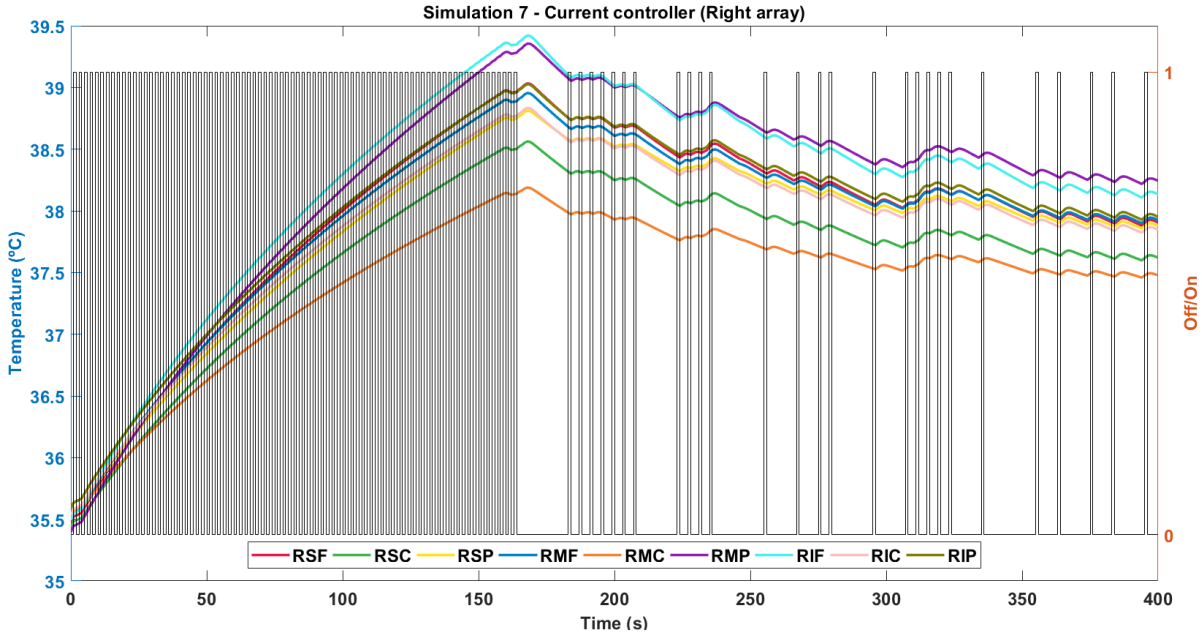

Figure A14: Temperature variation as a function of time for the right array when current is controlled at a array level (Simulation 7). In this plot when the device is on (1 in the right y-axis) it means that the current is being injected in the LR direction. Transducers naming is the same as used before.

A3. 10th Workshop on Biomedical Engineering Abstract

10th WORKSHOP ON BIOMEDICAL ENGINEERING
Faculty of Sciences of the University of Lisbon, Portugal,
14th of April, 2018

Head tissue heating during TTFields therapy: a computational study

Authors: Nichal Gentilal[1], Ricardo Salvador[2] and Pedro Cavaleiro Miranda[1]
Affiliations: [1]Instítuto de Biofísica e Engenheira Biomédica, Faculdade de Ciências, Universidade de Lisboa, 1749-016 Lisboa, Portugal; [2]Neuroelectrics, Barcelona, Espanha.

Keywords: Tissue heating; tumor treating fields (TTFields); Glioblastoma multiforme (GBM)

Abstract:

Tumor Treating Fields (TTFields) is the most recent modality for the treatment of glioblastoma multiforme (GBM). Approved in 2011 for the treatment of patients who had recurrence and in 2015 for newly-diagnosed patients, TTFields consist on the application of an electric field with an intensity of 1-3 V/cm and a frequency between 100-300 kHz. When applied continuously, these fields can affect tumour cells mitosis during metaphase and cytokinesis by interfering with the orientation of the microtubules and with the formation of the cleavage furrow.
The device used to deliver these fields is called Optune (https://www.optune.com) and is produced by Novocure (https://www.novocure.com/). In order to increase treatment outcome, these fields are applied in the Left-Right (LR) and Anterior-Posterior (AP) directions alternatively. So far, the only problems reported regarding this technique are skin dermatitis underneath the regions where the electrodes are placed, which can be easily treated using topical corticosteroids. However, there are still some issues that were not yet been addressed in detail. It is known that Optune shuts down every time the scalp temperature reaches 39.5ºC to avoid skin injuries. However, the results we obtained performing simulations using COMSOL in a realistic head model indicate that, in a steady-state situation, which should be reached within minutes, scalp's temperature can reach values greater than 45 ºC in the LR direction and greater than 50 ºC in the AP direction.
In practice, Optune alternates between the LR and the AP transducer pairs every 1 s. We are current undertaking time-transient studies to investigate tissue heating as a function of the frequency at which Optune alternates between field directions. The aim is to optimize this parameter to minimize tissue heating. Although there are uncertainties that can influence the results, such as biological tissues electrical and thermal conductivities, we hope that the results we obtained so far and the ones that we are currently working on can help to increase our understanding regarding head tissue heating and to improve glioblastoma treatment using Optune.

A4. Ciência 2018 Abstract

Non-Invasive Brain and Spinal Cord Stimulation:

optimizing Electric-field delivery for clinical applications

Sofia Rita Fernandes, Amparo Callejon, Nichal Gentilal, Pedro Cavaleiro Miranda

Non-invasive electrical stimulation of the brain and spinal cord is a promising therapeutic application for dysfunctions and diseases of the central nervous system, with thousands of research papers published over the past three decades, combining knowledge from the scientific, clinical and technical communities.

Medical devices for non-invasive electrical stimulation are current sources that can deliver in the mA range, independently of the load impedance. The current passes through electrodes placed over the regions to be stimulated, and generate electric fields in the nervous system, altering the resting membrane potential to inhibit or facilitate neuronal responses. A similar application is also found in the treatment of Glioblastoma Multiforme. Instead of neuromodulating neuronal responses, higher electric fields will be generated to disrupt tumor cell mitosis and consequent development.

Most of the clinical trials and experimental studies published so far on the therapeutic use of electric currents are on transcranial direct current stimulation (tDCS), transcutaneous spinal direct current stimulation (tsDCS) and Tumor Treating Fields (TTFields). A better understanding of how the electric field distributes in the brain and spinal cord, and how it interacts with the central nervous system is necessary to optimize electric field delivery at the clinical target, thereby increasing the efficacy and reducing the variability of its outcome. As in vivo measurements of the electric field in humans are impractical, we have developed computational models, based on realistic human phantoms of the head and vertebral column, to investigate the effect on the electric field distribution in the cerebral and spinal nervous tissue of parameters such as: electrode size and position, tissue conductivity, tissue heating and anatomical characteristics.

Our results illustrate the impact of the complexity of tissue geometry on the electric field distribution and the importance of the position of the electrodes relative to the target in the cortex or spinal cord. The simulations also provide information about the direction of the electric field in the GM and WM, which may be relevant for neuronal stimulation since the effect of the electric field on individual neurons is known to be directional.

Anatomic features, such as skull thickness in tDCS and in TTFields and CSF narrowing in tDCS and tsDCS, were observed to influence local electric field maxima position. The next step is to build personalized models to determine the electrode positions that optimize the electric field at the target, and to avoid local maxima for safety reasons.

Future research should also be to combine electric field models with neuronal models of brain and spinal circuits. These models would then have to be validated through experimental clinical studies.

A5. Report for Novocure™

Report

Aim: Describing the main findings regarding how Optune works considering its thermal limitations and suggesting ways to work them around.

Summary: The temperature increase during TTFields therapy is due to the Joule effect. To avoid skin burns, Optune shuts down everytime an electrode's temperature reaches 41ºC. However, if the fields are not applied GBM is not being treated. Up until now, there are no studies regarding the efficacy of this technique nor an evaluation of the thermal damage that it may cause in biological tissues. This brief report quantifies this damage and the electric safety using the CEM 43ºC and SAR metrics, respectively. It is important to note that these metrics may not be appropriate to evaluate TTFields.

Methods: We used the same realistic head model described in [1]. The tissues segmented were the scalp, skull, CSF, WM, GM and the eyeballs. A virtual lesion to mimic a glioblastoma was created and the transducers arrays were placed as realistically as possible to represent Optune. The same electric properties used in [1] were considered and the thermal ones were obtained after an extensive literature review.

Results: We considered that Optune shuts down when the average temperature of any electrode reached 40.4ºC because this corresponds to having around 5% of the electrode's volume at 41ºC. This 5% were considered as the volume occupied by the temperature sensor. Figures 1 to 4 show the temperature variation of every electrode throughout time. Each transducer is named as a three-letter combination: the first represents the array (Front, Posterior, Left, Right), the second represents the row within the array (Superior, Middle, Inferior) and the third the position within the row (Front, Posterior, Left, Right, Central). As it can be seen, just one electrode controls the switching of the whole device. In this case, it is the electrode that is at the front pad (F), superior row (S) and left position (L), which is also the one where the highest current is injected.

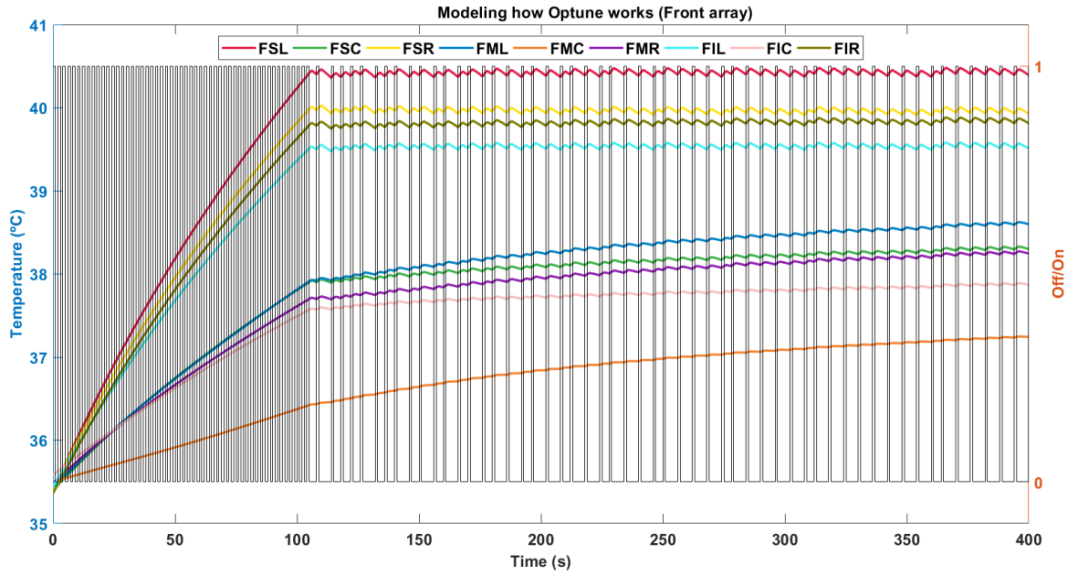

Figure 1 – Average temperature variation of each transducer (Front array). As it can be seen the temperature (left y-axis) never increases above 40.4ºC. It is the electrode FSL that controls if the device is on (1 in the right y-axis) or off (0 in the right y-axis). In this plot when the device is on it means that the current is being injected in the AP direction.

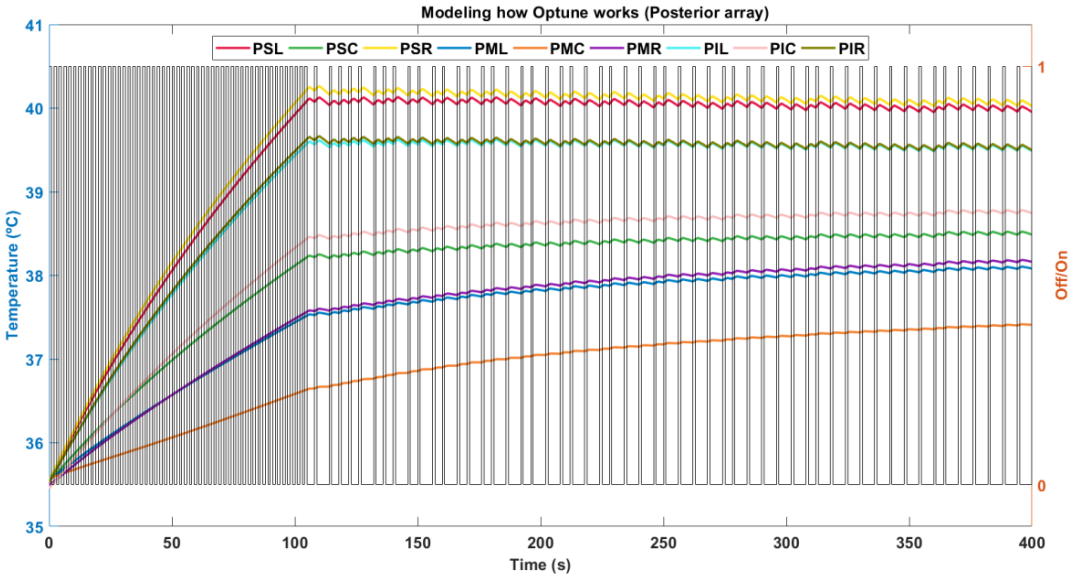

Figure 2- Average temperature variation of each transducer (Posterior array). As it can be seen the temperature (left y-axis) never increases above 40.4ºC. In this plot when the device is on it means that the current is being injected in the AP direction.

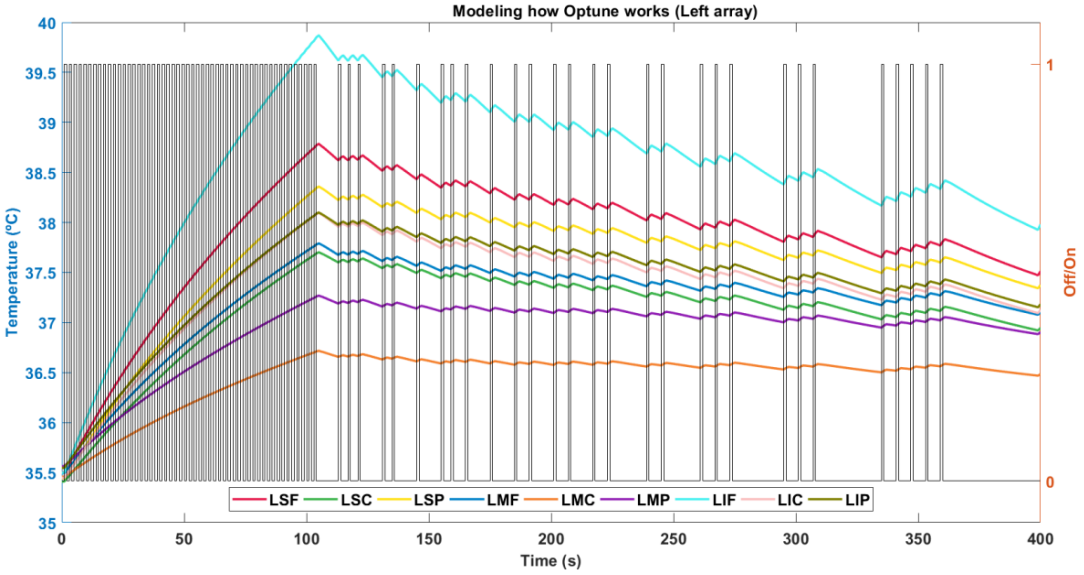

Figure 3 - Average temperature variation of each transducer (Left array). As it can be seen the temperature (left y-axis) never increases above 40.4ºC. In this plot when the device is on it means that the current is being injected in the LR direction.

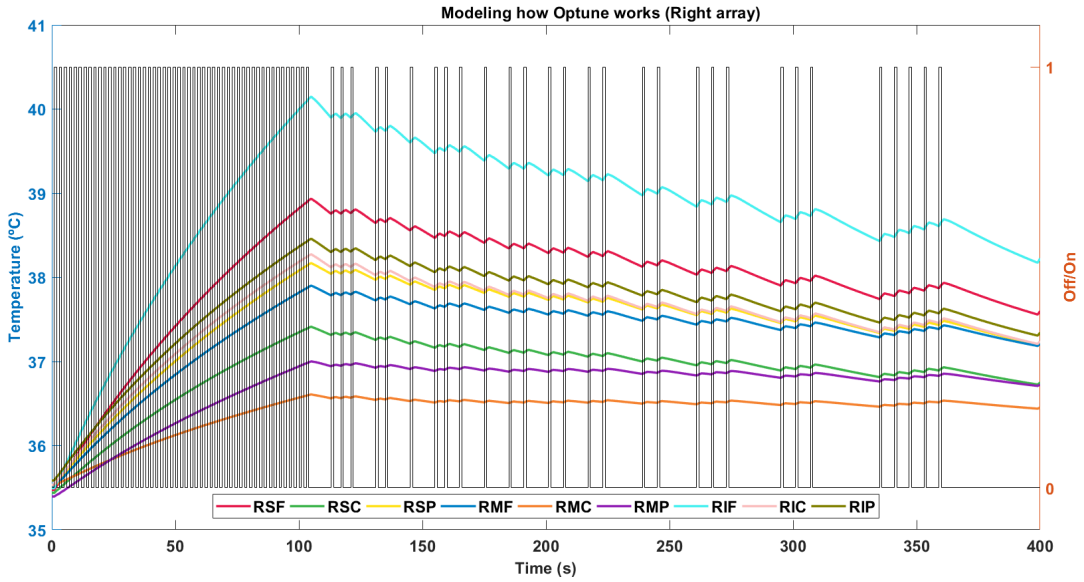

Figure 4 - Average temperature variation of each transducer (Right array). As it can be seen the temperature (left y-axis) never increases above 40.4ºC. In this plot when the device is on it means that the current is being injected in the LR direction.

These results show that, after the first shutdown, the AP fields were applied during 37% of the maximum time they could have been, while this value decreases to 20% for the LR configuration. Overall, Optune is being used to treat the tumour around 31% of the time. A deeper analysis shows that it is the LR field the one who contributes the most to the treatment because the electric field produced by this configuration reaches 1 V/cm in 72% of the tumour volume, while for the AP this value is just 13%. The duty cycle could be increased by allowing the LR configuration to continue switching on and off until one electrode in this array reaches the temperature threshold.

The SAR values according to how the FDA measures it gave 4.3 W/kg (limit: 3.2 W/kg). Following the IEC logic, we obtained 27.1 W/kg (limit: 20 W/kg). TTFields surpassing the thresholds was already expected because the electric fields are the basis of the treatment and the time they are applied should be maximized. Regarding tissues temperature, figure 5 shows the average temperature of each tissue.

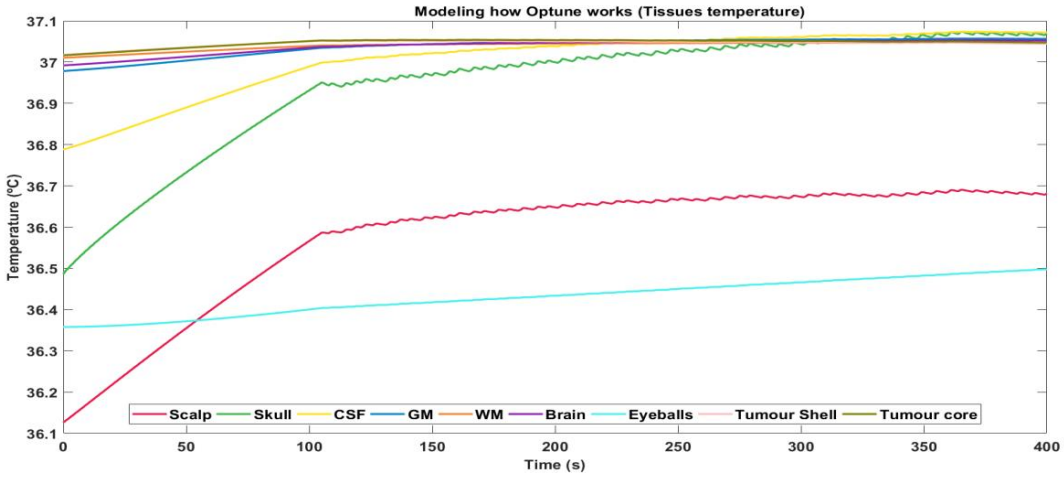

Figure 5 - Average tissue temperature. The scalp's starts as the lowest because it is in contact with the environment that is at 24ºC.

To evaluate the thermal damage two CEM 43ºC for each tissue were calculated: one for the whole volume and one considering a cylinder defined by the most significant electrode (the one that controls Optune). These quantities are summarised in table I for one treatment day.

Table I - CEM 43ºC values for each biological tissue considering one treatment day (18 hours). When a value is not reported it means that the cylinder does not pass by that tissue. All values are in minutes.

	Scalp	Skull	CSF	GM	WM	Tumour	Eyeballs
Volume average	0.17	0.29	0.29	0.29	0.28	0.28	0.13
Cylinder average	12.6	3.47	0.45	0.33	0.29	--	--

According to the thresholds presented in [2,3] thermal damage might occur only for the scalp and the brain (GM+WM). For the first only acute and minor damage is expected (small burns for example), while for the brain an increase in the blood-brain permeability, a change in the cerebral blood flow and in the concentrations of GABA, glutamate and glycine is likely to happen. It is important to note that these results are only for one treatment day (18 hours). Whether the effects of the temperature are additive considering several days or not have to be studied.

Suggestions: Other simulations were done to test different hypotheses. We obtained an increased application time of the fields for three different cases: 1) if the room temperature is lower; 2) if Optune shuts down the current only for the configuration that reaches 41ºC instead of shutting down both configurations and 3) if the current is controlled at the electrode level (i.e., each transducer gets 100 mA) instead than at the array level (i.e., the array gets 900 mA, but distributed unequally through all the electrodes).

Limitations: This study did not consider heat transfer through sweating nor heat looses via radiation. This latter is likely to be as important as convection. These limitations and other new hypotheses are being considered in new tests that we are perfoming. Additionally, the SAR and CEM 43ºC metrics were developed for hyperthermia treatments and the thresholds for TTFields may be different.

References:

[1] P. C. Miranda, A. Mekonnen, R. Salvador, and P. J. Basser, _Predicting the electric field distribution in the brain for the treatment of glioblastoma, Phys Med Biol., vol. 59, no. 15, pp. 4137-4147, 2014.

[2] M. W. Dewhirst, B. L. Viglianti, M. Lora-Michiels, M. Hanson, and P. J. Hoopes, Basic principles of thermal dosimetry and thermal thresholds for tissue damage from hyperthermia, International Journal of Hyperthermia, vol. 19, no. 3, pp. 267-294, 2003.

[3] P. S. Yarmolenko, E. J. Moon, C. Landon, A. Manzoor, D. W. Hochman, B. L. Viglianti, and M. W. Dewhirst, Thresholds for thermal damage to normal tissues: an update, International Journal of Hyperthermia, vol. 27, no. 4, pp. 320-343, 2011.